AN ABSTRACT OF THE DISSERTATION OF

Martin. H. Schroth for the degree of Doctor of Philosophy in Civil Engineering presented on February 2, 1996. Title: Multiphase Flow in Homogeneous and Bedded Porous Media.

Abstract approved: Redacted for Privacy

Jonathan D. Istok

Use of well-characterized porous media can improve the efficiency of laboratory subsurface hydrologic studies. We present a comprehensive set of hydrological properties for commercially-available silica sands. Four different sand grades were characterized for physical properties, chemical composition, water retention, three-phase saturation-pressure relationships, saturated and unsaturated hydraulic conductivity. Sand properties included narrow particle size distribution, high chemical purity and low organic matter content. Water retention curves featured well-defined air entry pressures. (in press, *Soil Science Society of America Journal*).

Predicting light nonaqueous-phase liquid (LNAPL) movement in heterogeneous subsurface environments is critical for designing effective remediation schemes. To develop a method for predicting the shape and extent of LNAPL lenses in the capillary fringe of the vadose zone, two-dimensional experiments were performed in a glass chamber (50 cm x 60 cm x 0.95 cm) using characterized silica sands and two LNAPLs (Soltrol® 220, Duoprime® 55 Mineral Oil). LNAPLs were released in water-wetted sands to simulate a point-source discharge above a water table. Light transmission was used to delineate the changing LNAPL lens boundary during infiltration. At equilibrium, no zone above the capillary fringe remained at NAPL saturations higher than the residual saturation. A previously published model was tested. Discrepancies between measured and predicted lens thicknesses were found when model equations were modified to a fully explicit form. (published in *Journal of Contaminant Hydrology*).

To investigate LNAPL movement in the vicinity of sloping textural interfaces, two-dimensional experiments were conducted in the glass chamber using two sand grades (12/20 and 30/40 sieve sizes) to create fine-over-coarse interfaces. Soltrol® 220 was released at the sand surface under constant water irrigation, simulating a point-source discharge. Light transmission was used to observe water and LNAPL flow paths. LNAPL movement strongly depended on the water saturation in the fine layer above the interface. Extensive lateral spreading of LNAPL along the interface was observed in most cases. These experiments demonstrated the critical role water saturation plays in determining LNAPL disposition in heterogeneous vadose environments. (submitted to *Water Resources Research*).

Multiphase Flow in Homogeneous and Bedded Porous Media

by

Martin H. Schroth

A DISSERTATION

submitted to

Oregon State University

In partial fulfillment of
the requirements for the
degree of

Doctor of Philosophy

Completed February 2, 1996
Commencement June 1996

Doctor of Philosophy dissertation of Martin H. Schroth presented on February 2, 1996.

APPROVED:

Redacted for Privacy

Major Professor, representing Civil Engineering

Redacted for Privacy

Chair of Department of Civil Engineering

Redacted for Privacy

Dean of Graduate School

I understand that my dissertation will become part of the permanent collection of Oregon State University libraries. My signature below authorizes release of my thesis to any reader upon request.

Redacted for Privacy

Martin H. Schroth, Author

ACKNOWLEDGMENTS

I would like to express my sincere gratitude towards my Major Advisor, Dr. Jack Istok. Jack was a great Advisor, and he gave much of his time and effort to direct me towards accomplishing my goals. Whenever I needed advice and/or encouragement, Jack was there to show me the way and to make me feel better. His enthusiasm for science will always be an inspiration to me.

I would also like to sincerely thank my Minor Advisor, Dr. John Selker. As Principal Investigator of the research project, he provided outstanding support for me over the years of my studies. John was always there when I needed him. Whenever I walked into his office and told him about a new problem (and I did frequently!), he instantly came up with new ideas to keep us going.

Thanks go to my committee members Dr. John Baham, Dr. Jon Kimerling, and Dr. Lew Semprini for their helpful discussions and for donating their time towards this research. Special thanks to Lew Semprini, who provided me with an opportunity to conduct exciting experiments for a class term project, which eventually led to a scientific publication (chapter 3).

Many thanks go to Dr. Bob Lenhard, Sultan Qaboos University, Sultanate of Oman. Bob donated his time and effort while serving on my committee. He not only sponsored a fellowship for me at Pacific Northwest National Laboratory through Associated Western Universities (AWU), but he also taught me a great deal about multiphase flow.

Many thanks also to Drs. Mart Oostrom and Mark White, Pacific Northwest National Laboratory. Without the help of Mart and Mark, I would have been overwhelmed by the task of numerically modeling multiphase flow processes. Their unselfish help and collegiality was unparalleled and greatly appreciated.

Special thanks to my friend and former colleague Stephen Ahearn for the good times we had working together. Thanks to Joan Istok, who drafted many drawings in this dissertation. Thanks also to Bob Schnekenburger for his efforts in maintaining the

computer workstations, and to Aaron Burkhardt, Darren Lerner, and Zichao Yu for their help. Thanks to all my other friends and colleagues who helped me along the way.

This research project was funded by the U.S. Department of Energy (DOE), under the Subsurface Science Program, under DOE contract # DE-FG06-92ER61523.

CONTRIBUTION OF AUTHORS

Dr. Jonathan D. Istok, my Major Advisor, provided much guidance and direction and donated much of his time towards this dissertation work, and is a co-author on all three manuscripts that make up this dissertation.

Dr. John S. Selker, my Minor Advisor and research project Principal Investigator, also provided much guidance, help and time towards this body of work, and is also a co-author on all three manuscripts.

Stephen J. Ahearn helped conducting many of the experiments described in chapters 2 and 3 of this dissertation. He is also a co-author on these two manuscripts.

TABLE OF CONTENTS

TABLE OF CONTENTS (Continued)

TABLE OF CONTENTS (Continued)

LIST OF FIGURES

LIST OF FIGURES (Continued)

LIST OF FIGURES (Continued)

Figure Page

LIST OF TABLES

Dedicated to

Traudl and Lucia

for their love, support, patience,
and for making my life better every day.

Multiphase Flow in Homogeneous and Bedded Porous Media

1. INTRODUCTION

Contamination of soil and aquifer systems by light nonaqueous-phase liquids (LNAPLs) has become a wide-spread problem. Fuel spills and leaks from commercial and domestic underground storage facilities are examples of LNAPL releases which typically occur near the soil surface in the vadose zone. Improved knowledge of LNAPL transport mechanisms in the subsurface is required for correct risk assessment and remediation design. Unfortunately, the understanding of LNAPL movement in the subsurface, particularly in heterogeneous vadose environments, is still incomplete.

Countless experiments are being conducted to study the movement of NAPLs and other aqueous-phase contaminants in subsurface environments. Fluid flow and solute transport problems frequently involve complex physical, chemical and biological processes. Laboratory experiments in physical models, columns and chambers are often conducted to limit scientific studies to the investigation of specific phenomena.

The selection of porous media is an important initial step for conducting laboratory subsurface hydrologic experiments. Availability, sometimes in large quantities, of low cost porous media with well-defined physical, chemical and biological properties is highly desirable. In addition, the porous media should be representative of the natural environment.

Knowledge of basic hydrologic properties is required to interpret experimental results. Obtaining these properties often requires specialized equipment and techniques which can be time consuming and expensive. For many applications, the use of previously characterized media may be desirable. However, for such media to be reliable, it must possess high batch to batch consistency and uniformity in the desired properties. Commercial processing is usually required to produce this level of consistency and uniformity.

The primary objective in chapter 2 was to present a comprehensive set of hydrologically relevant properties for commercially-available silica sands so that the media could be employed by the broad scientific community. In addition, we wanted to verify that the four grades of sand characterized were hydrodynamically similar in the sense of Miller and Miller (1956). Finally, we wanted to develop a more accurate approach to analyzing water retention data obtained in retention cells for coarse, uniform textured soils.

Prediction of NAPL movement in porous media requires constitutive conductivity-saturation-pressure (K-S-P) relationships in three-phase air-NAPL-water systems. A model that includes the effects of hysteresis and non-wetting fluid entrapment was developed by Parker and Lenhard (1987) and Lenhard and Parker (1987). Lenhard (1992) verified an amended version of the model by comparing model predictions with three-phase air-NAPL-water saturation-pressure measurements and concluded that neglecting hysteresis could lead to erroneous predictions of fluid movement in the subsurface. He demonstrated the importance of tracking the location of fluid interfaces within the pore space to correctly predict S-P relationships. Recently, Ostendorf et al. (1993) applied the constitutive theory successfully to model field data from a gasoline spill site. Essaid et al. (1993) investigated the fluid distribution at a crude oil spill site and concluded that including hysteresis and oil entrapment was essential for predicting large-scale features of the oil body. Nevertheless, the uncertainty of estimated values of field parameters led to considerable discrepancies between observed and predicted oil distributions in their study. Farr et al. (1990) and Lenhard and Parker (1990) investigated methods to estimate free LNAPL volumes in soils from fluid levels in monitoring wells. Both concluded that free LNAPL volumes cannot be inferred directly from fluid levels in monitoring wells or from soil LNAPL thicknesses (Lenhard and Parker, 1990) without consideration of porous media properties.

Several researchers have investigated NAPL infiltration in the vadose zone. Cary et al. (1989b) used hydrocarbon oils of different viscosities in column infiltration experiments to show that NAPL infiltration was predictable using classical non-hysteretic soil-water relationships and NAPL physical properties. Other one-dimensional

infiltration experiments were conducted by Eckberg and Sunada (1984) and Abdul (1988). Abdul (1988) speculated that NAPL would fully penetrate the capillary fringe and at equilibrium form "pancake-shaped" lenses. Pantazidou and Sitar (1993) conducted two-dimensional NAPL infiltration experiments in sands and developed a set of equations to predict vertical equilibrium dimensions of LNAPL lenses emplaced in the vadose zone. In their model, they simplified the actual pore geometry of the sand by assuming that NAPL advance and drainage was dictated by the sizes of pore necks and pore bodies, each of which could be identified with a characteristic diameter.

The overall objective in chapter 3 was to evaluate the equilibrium NAPL lens geometry and position with respect to the capillary fringe. In addition, possible changes of interfacial tensions as a function of time and their influence on NAPL emplacement in the vadose zone were investigated. Finally, we wanted to test the applicability of the vertical lens equilibrium model (Pantazidou and Sitar, 1993) to a set of different NAPL-porous media combinations.

A basic element of vadose zone heterogeneity exists when a layer of fine-grained porous medium overlays coarse-grained porous medium and the textural interface between the two layers is inclined. These fine-over-coarse sloping textural interfaces, frequently encountered in bedded sedimentary deposits, may form capillary barriers. At a capillary barrier, infiltrating water is held in the fine-grained layer by capillary forces and is diverted downdip, parallel to the textural interface. As streamlines of infiltrating water converge near the textural interface, the water saturation in the fine-grained layer above the interface increases until water breakthrough occurs into the underlying coarse layer.

Several researchers have investigated NAPL movement in heterogeneous subsurface environments. Cary et al. (1994) conducted NAPL infiltration and redistribution experiments in one-dimensional vertical columns packed with horizontal layers of soils of different texture. The authors observed effects of layering on the distribution of water and NAPL, and their experiments provided useful information for the verification of a predictive model for immiscible fluid flow. Unfortunately, the one-dimensional character of the experiments, i.e. the enforced fluid flow perpendicular to textural interfaces, severely limited a more general analysis of the influence of

heterogeneity on immiscible fluid flow. Pantazidou and Sitar (1993) conducted two-dimensional NAPL infiltration experiments in unsaturated homogeneous as well as heterogeneous (layered) sand packs. They found that NAPL movement was strongly dependent on the number and horizontal continuity of layers and that in general more lateral spreading of NAPL occurred in layered than in homogeneous sand packs. However, they did not analyze NAPL flow behavior at fine-over-coarse textural interfaces in detail, and no comparison between NAPL and water flow at these interfaces was provided. In addition, hysteretic effects on NAPL and water flow in the vicinity of textural interfaces have not been addressed.

The main objective in chapter 4 was to study LNAPL movement in the vicinity of sloping textural interfaces that form capillary barriers. In particular, we wanted to determine if the LNAPL movement in the vicinity of capillary barriers depends on the water saturation in the fine-grained layer above the interface. In addition, we wanted to determine if LNAPL and water exhibit parallel flow paths in the vicinity of capillary barriers and whether hysteresis plays an important role for the LNAPL flow pattern. Finally, we wanted to compare our experimental findings to flow predictions based upon multiphase and capillary barrier flow theory.

2. CHARACTERIZATION OF MILLER-SIMILAR SILICA SANDS FOR LABORATORY HYDROLOGIC STUDIES

M. H. Schroth, S. J. Ahearn, J. S. Selker and J. D. Istok

Departments of Bioresource and Civil Engineering
Oregon State University, Corvallis, OR 97331

in press
Soil Science Society of America Journal
February 1996

2.1 Abstract

The use of well-characterized porous media can simplify and improve the efficiency of laboratory subsurface flow and transport experiments. The objective of this study was to present a comprehensive set of hydrologically relevant properties for a unique set of commercially-available silica sands. Features of sands selected for characterization included high sphericity, high batch to batch consistency, Miller-similarity, and availability in large quantities. Samples of four different sand grades (12/20, 20/30, 30/40 and 40/50 sieve sizes) were characterized for physical properties, chemical composition, water retention, three-phase air-NAPL-water saturation-pressure relationships for water and a model NAPL, Soltrol® 220, and saturated and unsaturated hydraulic conductivity. Properties common to all sand grades included high chemical purity and low organic matter content. Water retention curves featured well-defined air entry pressures and the Miller-similarity of the media was demonstrated for both static and dynamic properties. During water retention measurements, we determined that the common assumption of a uniform vertical water content distribution in retention cells can result in significant errors in uniform porous media. A numerical correction procedure was developed and successfully applied to correct fitted water retention curve parameters, illustrating that potential errors of up to 70% in volumetric water content are made without proper analysis. The characterization data for the four sand grades presented here should facilitate their use in a wide range of laboratory flow and transport studies.

2.2 Introduction

Fluid flow and solute transport are critical processes related to contamination, remediation and conservation of soil and groundwater resources. Countless experiments are being conducted to study the movement of single fluid phases, i.e. water, nonaqueous phase liquids (NAPLs) and gases, multiple fluid phases and contaminants in subsurface environments. Fluid flow and solute transport problems frequently involve complex

physical, chemical and biological processes. Laboratory experiments in physical models, chambers and columns are often conducted to limit scientific studies to the investigation of specific phenomena.

The selection of porous media is an important initial step for conducting laboratory subsurface hydrologic experiments. Availability, sometimes in large quantities, low cost, and well-defined physical, chemical and biological properties are desired features of porous media. In addition, the porous media should be representative of the natural environment.

To interpret experimental results, knowledge of basic hydrologic properties is required. Obtaining these properties often requires specialized equipment and techniques which can be time consuming and expensive. For many applications, the use of previously characterized media may be desirable. However, for previously characterized media to be reliable, it must possess high batch to batch consistency and uniformity in the desired properties. Therefore, commercial processing is usually required to produce this level of consistency and uniformity.

The primary objective of this study was to present a comprehensive set of hydrologically relevant properties for commercially-available silica sands so that the media could be employed by the broad scientific community. In addition, we wanted to verify that the four grades of sand characterized were hydrodynamically similar in the sense of Miller and Miller (1956). Finally, we wanted to develop a more accurate approach to interpreting water retention data obtained in retention cells for coarse, uniform textured porous media.

2.3 Materials and Methods

2.3.1 *Porous Media and Liquids*

The porous media selected for characterization were four grades of silica sand (12/20, 20/30, 30/40 and 40/50 sieve sizes), available in large quantities from Unimin Corporation[1], Le Sueur, MN, under the trade name "Accusand®."[1] Accusand grades were obtained prewashed (with water) and presieved by the manufacturer. Prior to conducting characterization experiments, all Accusand grades were rinsed with distilled water to remove fine dusts generated in transit. The Accusand grades were then oven dried at 50 °C. No further treatment was employed.

Liquids used for the characterization of Accusand grades were distilled water and Soltrol® 220[1], hereafter referred to as Soltrol, a light nonaqueous phase liquid (LNAPL) manufactured by Phillips Petroleum Company[1], Bartlesville, OK. Soltrol is a mixture of branched C_{13} to C_{17} alkanes with a specific gravity of 0.81. Its components can be found in a variety of petrochemical products, e.g. diesel fuel. Negligible water solubility, very low volatility at room temperature as well as a low health hazard are reasons for the extensive use of Soltrol as a model NAPL in multiphase flow studies (e.g., Cary et al., 1994; Lenhard, 1992).

2.3.2 *Physical and Chemical Characterization*

Sieve analyses and determination of sphericity for four Accusand grades were performed by the manufacturer using standard methods (ASTM, 1987; API, 1986). Particle densities were measured in our laboratory by helium pycnometry (Ayral et al.,

[1] Reference to trade names or companies is made for information purposes only and does not imply endorsement by Oregon State University or the US-DOE.

1992) using an ACCUPYC Model 1330 pycnometer (Micromeritics Instr. Corp., Norcross, GA).

The cation exchange capacities for the four Accusand grades were determined by extraction (Page et al., 1982) and Inductively Coupled Plasma Atomic Absorption Spectrophotometry (ICP/AAS) (U.S. EPA, 1986). Total iron (Fe), total cadmium (Cd), total copper (Cu), total lead (Pb), total manganese (Mn) and total zinc (Zn) contents were determined by HNO_3 digestion and ICP/AAS (U.S. EPA, 1986). Iron oxide (Fe_2O_3) content was determined by extraction (Page et al., 1982) and ICP/AAS (U.S. EPA, 1986). Organic carbon content was determined from sand samples pre-treated with H_3PO_4 using a Nitrogen-Carbon-Sulfur (NCS) analyzer (Artiola, 1990).

2.3.3 *Water Retention Measurements*

Water retention data were obtained using a three-phase retention cell as described by Lenhard and Parker (1988). The retention cell consisted of four acrylic rings joined together with silicone sealant (Fig. 2.1a). Four ceramic rings were glued to the inside of the retention cell's acrylic rings. Two of the ceramic rings (the "NAPL rings") were chemically treated with chlorotrimethylsilane to render them hydrophobic to conduct only NAPL (Lenhard, 1992). The other two rings (the "water rings") were not treated and were used to conduct water. Fittings connected to cavities behind the ceramic rings allowed free liquid movement into and out of the retention cell. Plastic tubing was used to connect the water and NAPL rings to pressure transducers, burets, and vacuum/pressure regulators. In this manner, water and NAPL volumes and pressures could be measured independently. The pressure transducers were kept in a fixed position relative to the retention cell throughout the measurements.

Prior to conducting water retention measurements, the water pressure transducer was calibrated with the free water surface elevation set to the upper sand surface (Fig. 2.1a). All subsequent pressure measurements were thus made in reference to this location. To conduct water retention measurements, the porous media was packed by

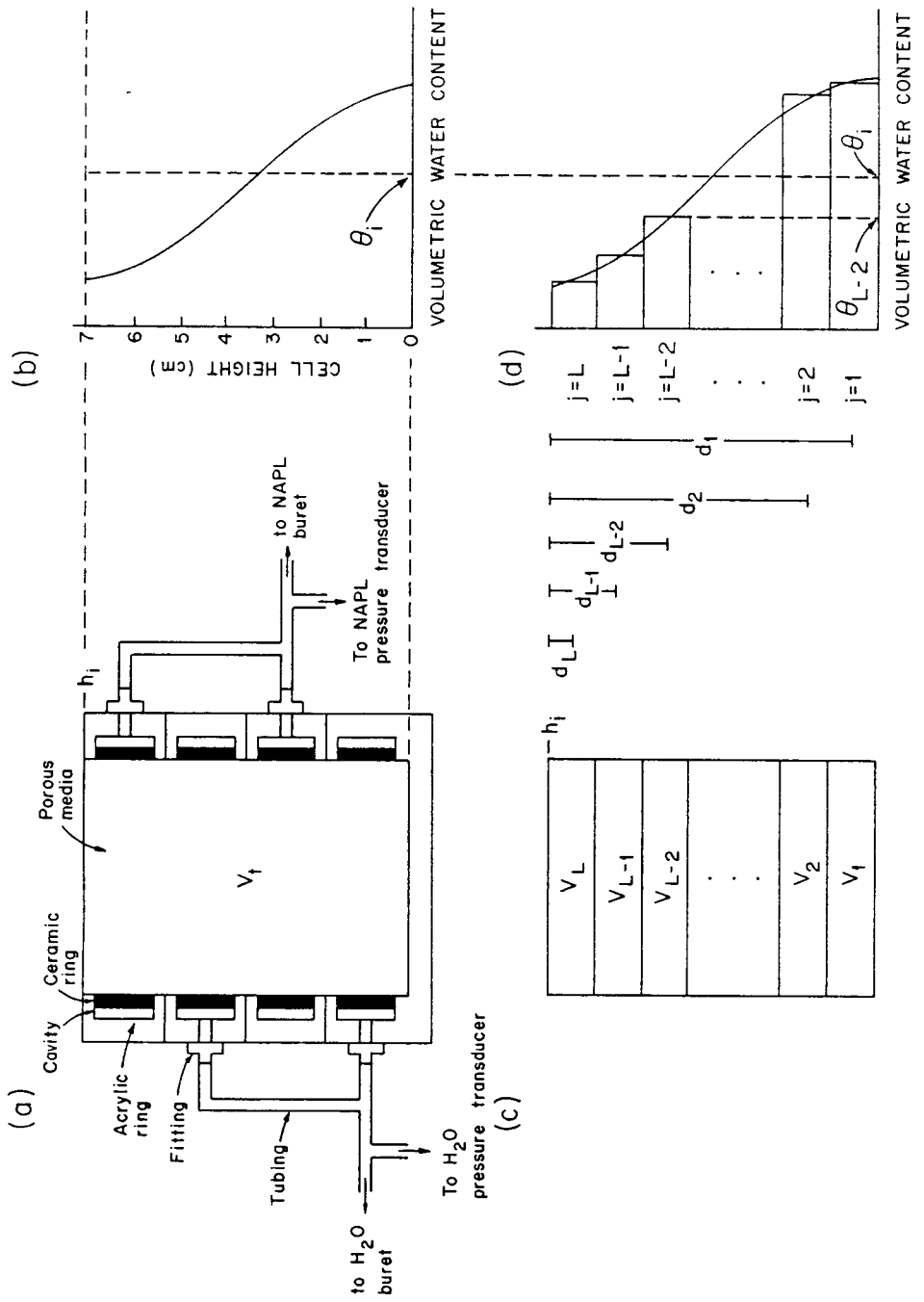

Figure 2.1 Experimental apparatus and numerical correction for water retention measurements: (a) retention cell, (b) actual water content distribution and commonly assumed water content (eq.[1]), (c) numerical subdivision of retention cell, (d) approximated water content distribution using numerical correction method.

pouring sand into the retention cell under water while continuously stirring to establish an initial condition of complete (100%) water saturation. Water was subsequently drained from the porous media by applying an external vacuum to the water rings; the volume of water drained was determined using a buret. Measurements of capillary pressure head as a function of the cumulative volume of water drained were recorded when all flow from the cell had ceased. During water retention measurements, the tubing to the NAPL rings was clamped off.

For each cumulative increment of water drained from the porous media $V_{w,i}$, the corresponding volumetric water content θ_i of the porous media was computed using:

$$\theta_i = (V_t \phi - V_{w,i}) / V_t \qquad [1]$$

where V_t is the total volume of the retention cell (Fig. 2.1a), ϕ is the porosity of the packed sand, and subscript i = 1 to K, where K represents the total number of observations. To test the Miller similarity of the media, the water retention data (θ_i, h_i) were scaled by multiplying measured capillary pressure head values (h_i) by media scaling factors, f_M (Miller and Miller, 1956):

$$h_i^* = f_M \, h_i \qquad [2]$$

where h_i^* is the scaled capillary pressure head, and the subscript M represents the four Accusand grades. The media scaling factors were computed using the effective particle diameters d_{50} for each sand grade. Using the effective particle diameter for the 20/30 sand ($d_{50,\,20/30}$) as a reference:

$$f_M = d_{50,\,M} / d_{50,\,20/30} \qquad [3]$$

Effective particle diameters were determined from the particle size distributions; fifty percent by weight of the particles have diameters smaller than d_{50}.

The water retention data were fit to the widely used van Genuchten model (van Genuchten, 1980):

$$\Theta = \left[\frac{1}{1+(\alpha h)^n}\right]^m \qquad [4]$$

where α and n are fitting parameters, $m = 1 - 1/n$, the capillary pressure head h is assumed to be positive, and Θ is the effective water saturation, defined as:

$$\Theta = (\theta - \theta_{ir}) / (\theta_s - \theta_{ir}) \qquad [5]$$

where θ_{ir} is the irreducible volumetric water content and θ_s is the saturated volumetric water content. Eq. [4] and [5] can be combined to obtain a functional relationship between θ and h (van Genuchten, 1980). To fit eq. [4] to our experimental data ($V_{w,i}$, h_i), we combined eq. [1], [4] and [5] to obtain:

$$\hat{V}_{w,i} = V_t \left[\phi - \left[\frac{1}{1+(\alpha h_i)^n}\right]^m (\theta_s - \theta_{ir}) - \theta_{ir} \right] \qquad [6]$$

where $\hat{V}_{w,i}$ is the predicted value of $V_{w,i}$. The advantage of writing eq. [6] in terms of $V_{w,i}$ rather than θ_i will become apparent shortly. The parameters α and n were obtained by fitting eq. [6] to the experimental water retention data ($V_{w,i}$, h_i) using a non-linear least squares routine, minimizing the sum of the squared differences between measured and predicted cumulative volumes of water removed from the cell:

$$\min \left[\sum_{i=1}^{K} \left(V_{w,i} - \hat{V}_{w,i} \right)^2 \right] \qquad [7]$$

2.3.4 *Corrections to Water Retention Data*

Using eq. [1] to compute θ_i from $V_{w,i}$ implies the assumption that the volumetric water content is vertically uniform throughout the porous media. However, vertical variation in capillary pressure head within the retention cell create a non-uniform vertical distribution of volumetric water content (Fig. 2.1b). While the assumption of vertically uniform distribution of volumetric water content within the cell is reasonable for many soils, for porous media with extremely narrow particle size distributions, such as the Accusand grades used here, it can create significant errors in the analysis of experimental water retention data. To retroactively compensate for these errors, we developed a numerical technique, based on the van Genuchten (1980) retention model (eq. [4]), to correct fitted water retention curve parameters to account for non-uniform vertical water content distributions during water retention experiments. A more general computational procedure to correct multiphase fluid capillary pressure - saturation data was recently proposed by Liu and Dane (1995). To obtain corrected retention parameters, they used the Brooks-Corey (1964) function in their computational procedure, with $\Theta = (h_d / h)^{\lambda}$ for $h \geq h_d$, and $\Theta = 1$ for $h < h_d$, where h_d is the displacement capillary pressure head and λ is a fitting parameter.

In our approach, the retention cell is imagined to be subdivided into a set of L horizontal layers (Fig. 2.1c). Layer j has a total volume V_j, so that

$$\sum_{j=1}^{L} V_j = V_t \qquad [8]$$

The capillary pressure head for any layer can be directly calculated from the measured capillary pressure head h_i and the vertical distance d_j between the top surface of the retention cell (the reference point for h_i in our experiments) and the center of the layer (Fig. 2.1c). Similar to eq. [6], the cumulative water volume removed from the cell can be predicted by summing the predicted cumulative water volumes removed from each layer $\hat{V}_{w,j}$, using:

$$\hat{V}_{w,i} = \sum_{j=1}^{L} \hat{V}_{w,j} = V_t \sum_{j=1}^{L} \left[\phi - \left[\frac{1}{1+[\alpha (h_i - d_j)]^n} \right]^m (\theta_s - \theta_{ir}) - \theta_{ir} \right] \quad \text{for } h_i - d_j > 0 \quad [9a]$$

$$\hat{V}_{w,j} = 0 \quad \text{for } h_i - d_j \leq 0 \quad [9b]$$

Eq. [9] was fit to the experimental water retention data using a non-linear least squares routine to obtain improved estimates for α and n by minimizing the sum of the squared differences between measured and predicted cumulative volumes of water removed from the cell (eq. [7]).

2.3.5 *Air-NAPL-Water Saturation-Pressure Measurements*

Three-phase air-NAPL-water saturation-pressure (S-P) characterization was performed using Soltrol as NAPL and distilled water as the aqueous phase employing the method of Lenhard (1992). S-P measurements were performed in the three-phase retention cell (Fig. 2.1a) with both water and NAPL rings unclamped. Prior to conducting the experiments, both water and NAPL pressure transducers were calibrated with the respective free liquid surface set to the upper sand surface. All subsequent water and NAPL capillary pressure head measurements were thus made in reference to that location (Fig. 2.1a). Porous media packing was conducted in the same fashion as for water retention measurements. Three-phase S-P data were obtained from simultaneous measurements of water and NAPL capillary pressure heads as a function of cumulative volumes of water and NAPL drained from or imbibed into the porous media.

At the beginning of each experiment, water was drained from the porous media by increasing the external vacuum connected to the water rings. Once the porous media was drained to a water saturation $S_w \approx 0.10$, where $S_w = \theta / \phi$, a wetting sequence was initiated by lowering the applied vacuum incrementally and allowing water to imbibe into the

porous media. At a water saturation $S_w \approx 0.55$, a known volume of NAPL was imbibed through the NAPL rings, thus changing the system from a two-phase air-water to a three-phase air-NAPL-water system. Thereafter, another draining sequence was initiated by allowing water to drain from the porous media. Finally, water was again allowed to imbibe into the porous media until the porous media was apparently liquid-saturated, i.e. free NAPL started to become visible at the surface of the retention cell. Fitted three-phase S-P model parameters (Lenhard, 1992) were obtained from measured S-P data using a non-linear least squares routine.

2.3.6 *Saturated and Unsaturated Hydraulic Conductivity Measurements*

One-dimensional column experiments were performed in triplicate to measure saturated and unsaturated hydraulic conductivities for each Accusand grade. The experimental device consisted of a vertical brass column (75 cm high x 5.4 cm inside diameter), equipped with 8 tensiometers spaced 10 cm apart along the column length. Wire screens (200 mesh) were used to retain the sand at each end of the column. The column was packed by pouring air-dry sand into the upper end of the column through a funnel containing a set of coarse sieves to randomize the particle motion. The funnel and column were electrically grounded during packing to reduce electrostatic charges on the sand particles in order to facilitate a more homogeneous packing. Porosities were computed for each packing from the mass of sand utilized, the particle density and the total column volume. The column was then flushed with CO_2 gas followed by slow water saturation from the lower end to minimize gas entrapment in the porous media during the initial water imbibition. Since CO_2 gas has a higher water solubility than air, any initially entrapped CO_2 gas was assumed to dissolve in the aqueous phase, thus creating an initial condition of complete water saturation within the porous media.

Measurements of saturated hydraulic conductivity were performed during upward flow using the constant head method (Klute and Dirksen, 1986). The water flow rate into the lower end of the column was controlled with a pump; the upper end of the column

was maintained at a constant head by an overflow reservoir. For each packing, measurements of capillary pressure head were performed at three different flow rates. Values of saturated hydraulic conductivity, K_{sat}, were computed using Darcy's law for all pairs of adjacent tensiometers from measured capillary pressure heads, known tensiometer elevations and the water flow rates. Average K_{sat} values were computed for each flow rate, giving a total of nine K_{sat} values per Accusand grade.

To test the Miller-similarity of the four Accusand grades for K_{sat}, scaling was performed by dividing average K_{sat} values by their squared effective particle diameter (Miller and Miller, 1956):

$$K^{*}_{sat,M} = K_{sat,M} / (d_{50,M})^2 \qquad [10]$$

where K^{*}_{sat} is the scaled average saturated hydraulic conductivity.

Measurements of unsaturated hydraulic conductivity were conducted immediately following K_{sat} measurements using the steady-state flux control method (Klute and Dirksen, 1986). After completion of K_{sat} measurements, the flow through the column was reversed by connecting the pump to the upper end of the column and the constant head reservoir to the lower end of the column. The column remained fully water saturated during this procedure. To insure controlled flow conditions at the column bottom, the free water surface of the constant head reservoir was kept slightly above the outlet port. Downward flow was initiated at a flow rate previously calculated to be sufficient to maintain complete water saturation. The flow rate was then reduced in a series of steps. For each step, measurements of capillary pressure head and water flow rate were conducted when measured capillary pressure heads appeared constant. Using Darcy's law, values of unsaturated hydraulic conductivities, K_{unsat}, were computed for adjacent tensiometers from measured capillary pressure head values, known tensiometer elevations and measured water flow rates. Relative hydraulic conductivities, K_{rel}, were computed for each Accusand grade using:

$$K_{rel,M}(h) = K_{unsat,M}(h) / K_{sat,M} \qquad [11]$$

Computed K_{rel} values were assigned to the average capillary pressure head values for each pair of adjacent tensiometers.

2.4 Results and Discussion

2.4.1 *Physical and Chemical Characterization*

The four Accusand grades are classified as medium to fine sands (ASTM, 1990). The highly uniform character of the four Accusand grades is exhibited by their narrow particle size distributions (Fig. 2.2). To assess the batch to batch consistency of the sands, we computed averages and standard deviations of effective particle diameters (d_{50}) and uniformity coefficients (d_{60}/d_{10}, where 60 % and 10 % by weight of particles have diameters smaller than d_{60} and d_{10}, respectively) from sieve analyses conducted by the manufacturer over a period of three years. The small standard deviations for effective particle diameters and uniformity coefficients (< 3% of the mean in both cases) indicate a high batch to batch consistency for all four Accusand grades (Tab. 2.1). Particle densities are similar to that of pure quartz. The high sphericity of the Accusand grades increases experimental reproducibility by minimizing porosity variations between consecutive packings. All Accusand grades consisted essentially of quartz with only trace levels of metals (Tab. 2.1); low organic matter content and small cation exchange capacity were additional features common to all four grades of Accusand.

2.4.2 *Water Retention Measurements*

As a result of their narrow particle size distributions, measured water retention curves featured well defined air entry pressures (Fig. 2.3). The close agreement of the scaled capillary heads to the unscaled 20/30 Accusand water retention curve

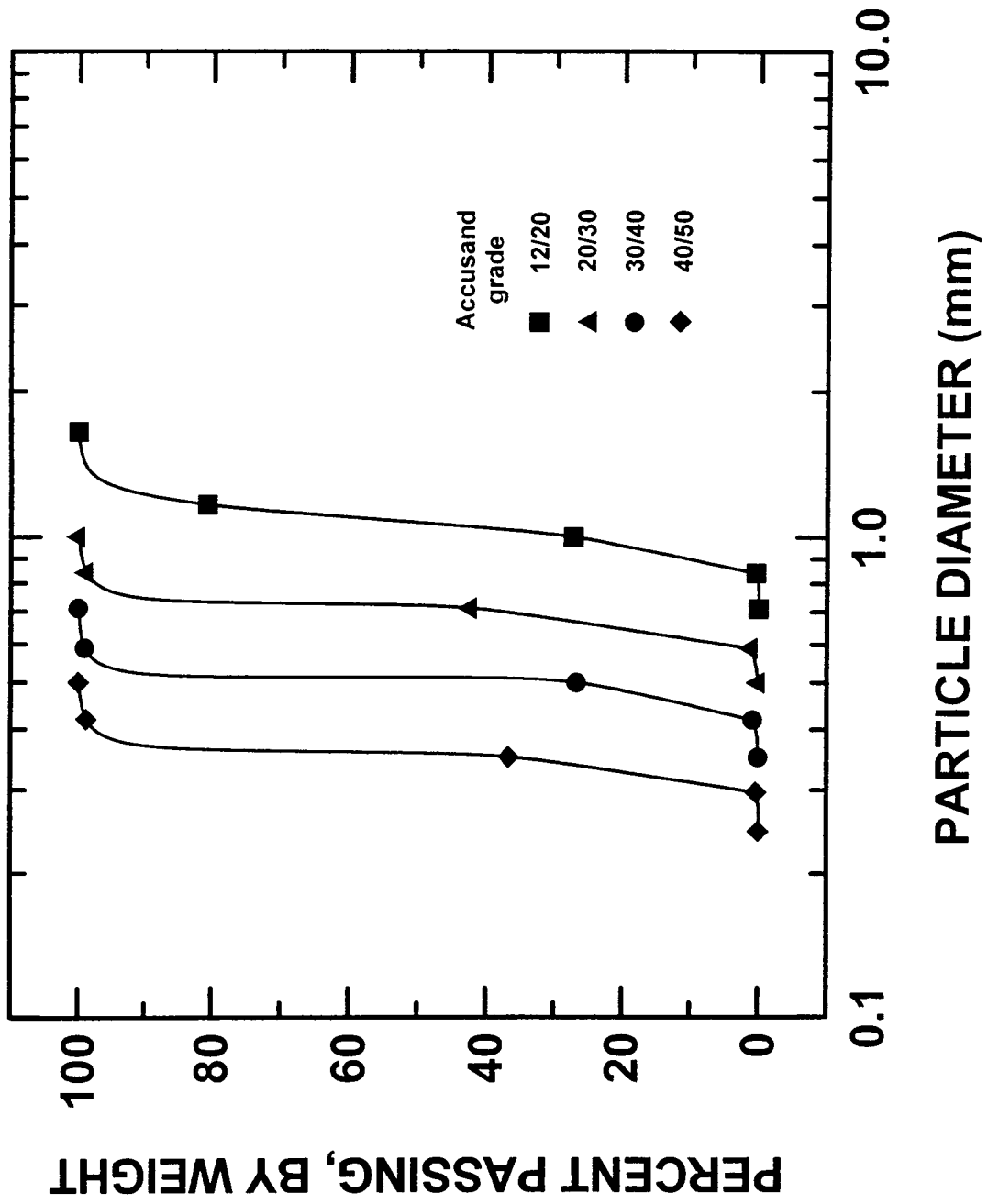

Figure 2.2 Particle size distribution for four Accusand® grades.

Table 2.1 Physical properties and chemical analyses for four Accusand® grades.

		Accusand grade			
		12/20	20/30	30/40	40/50
Physical Properties					
Particle diameter d_{50}†(mm)		1.105±0.014	0.713±0.023	0.532±0.003	0.359±0.010
Uniformity coeff. d_{60}/d_{10}†		1.231±0.043	1.190±0.028	1.207±0.008	1.200±0.018
Particle sphericity		0.9	0.9	0.9	0.9
Particle density	(Mg/m^3)	2.665	2.664	2.665	2.663
Chemical Analyses					
Cation Exchange Capacity (CEC)	($cmol_c/kg$)	0.60	0.57	0.62	0.67
Total Iron	(%)	0.931	0.764	0.765	0.558
Iron Oxides	(%)	0.036	0.029	0.034	0.030
Organic Carbon	(%)	0.03	0.04	0.03	0.03
Total Cadmium	(mg/kg)	< 7.0	< 7.0	< 7.0	< 7.0
Total Copper	(mg/kg)	< 14.0	< 14.0	< 14.0	< 14.0
Total Lead	(mg/kg)	< 5.0	< 5.0	< 5.0	< 5.0
Total Manganese	(mg/kg)	51.6	43.6	40.3	34.1
Total Zinc	(mg/kg)	9.95	6.98	7.1	6.18

† Averages and standard deviations. Total number of sieve analyses were 19 for 12/20, 170 for 20/30, 9 for 30/40, and 4 for 40/50 sand.

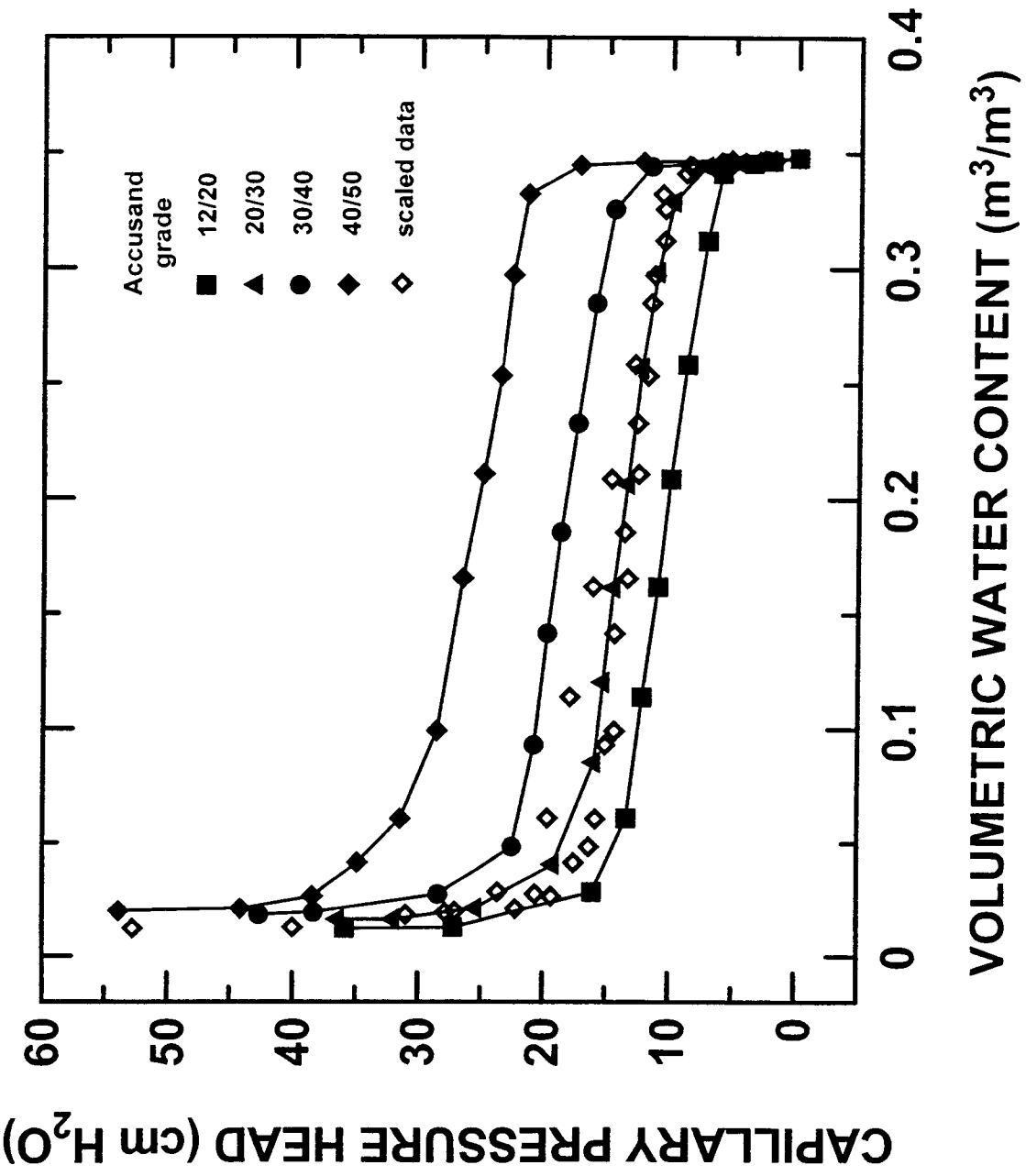

Figure 2.3 Water retention data (main drainage curves) for four Accusand® grades. Closed symbols show actual data, solid lines connect consecutive data points, and open symbols represent scaled data.

demonstrated the Miller similarity of the Accusand grades. Good agreement was found between measured water retention curves and fitted van Genuchten retention functions for all four Accusand grades (Tab. 2.2), with coefficients of multiple determination $R^2 > 0.99$ in all cases.

2.4.3 *Corrections to Water Retention Data*

Fitting parameters α and n obtained with eq. [6] and [9] were significantly different (Tab. 2.2), i.e. larger values of α and n were obtained when our numerical correction technique (eq. [9]) was employed. The values of α and n obtained with eq. [9], and hence the shape of the fitted water retention curves, depended on the number of layers used to subdivide the retention cell (Fig. 2.4). Fitted values of α and n increased

Table 2.2 Uncorrected and corrected van Genuchten and corrected Brooks-Corey fitting parameters of water retention data (main drainage curves) for four Accusand® grades.

			van Genuchten				Brooks - Corey	
			uncorrected		corrected†		corrected†	
Accusand grade	θ_s	θ_{ir}	α	n	α	n	h_d	λ
	—— m^3/m^3 ——		cm^{-1}		cm^{-1}		cm	
12/20	0.348	0.012	0.100	6.54	0.151	7.35	5.42	3.94
20/30	0.348	0.016	0.0744	8.47	0.0995	10.57	8.66	5.57
30/40	0.348	0.018	0.0552	10.54	0.0679	13.10	13.03	6.91
40/50	0.348	0.020	0.0392	11.58	0.0453	12.18	19.37	6.17

† corrected for non-uniform water content distribution using 14 layer subdivision.

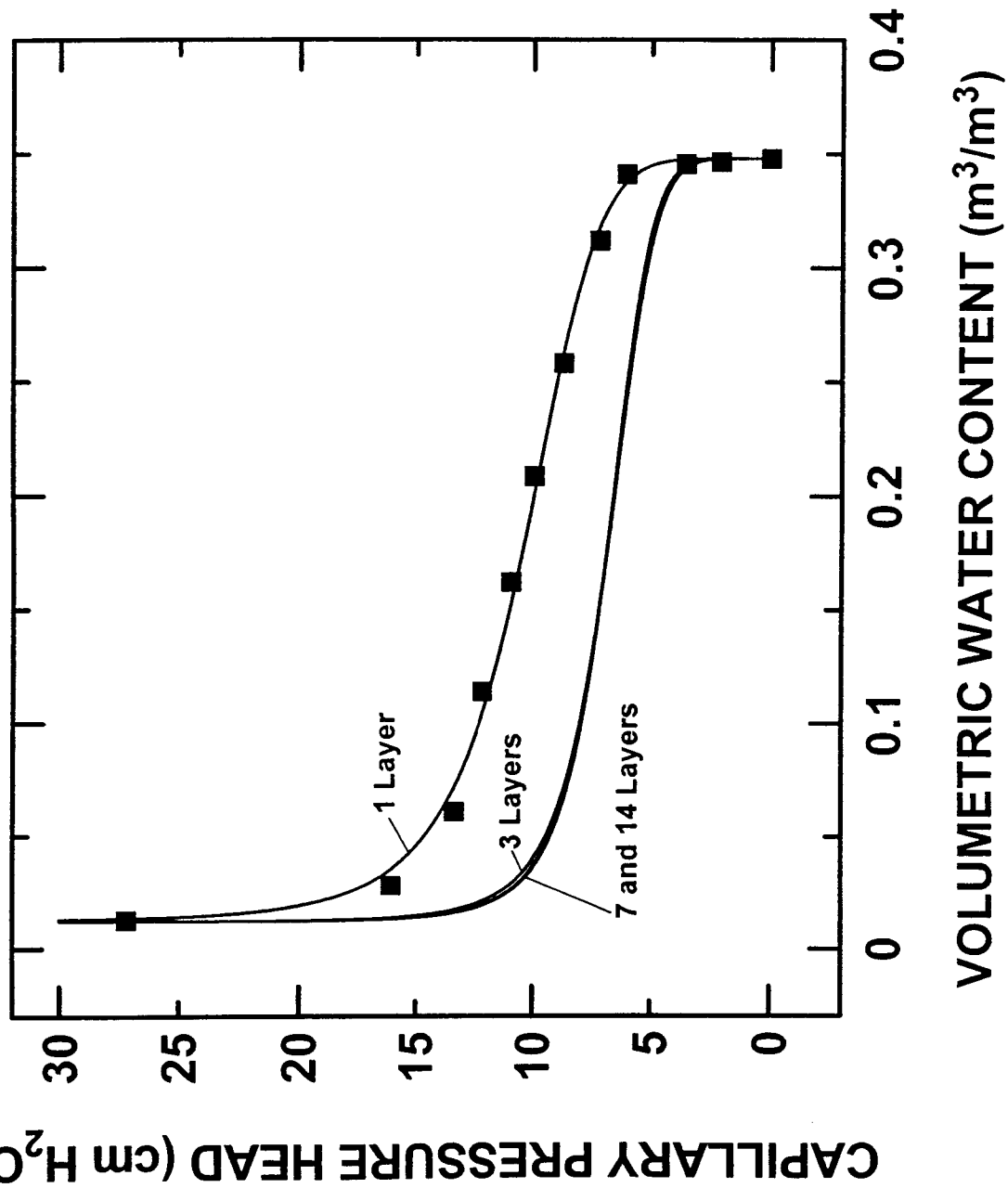

Figure 2.4 Effect of numerical correction procedure on fitted Accusand® 12/20 water retention function. Closed symbols show measured data, solid lines show fitted van Genuchten retention functions for subdivision into different numbers of layers.

as the number of layers increased. Significant differences in α and n existed between the uncorrected (L = 1) fit and the correction with 3 layers. Small differences in α and n were observed for L = 3 to 7, and negligible differences in α and n existed for L = 7 to 14, resulting in fitted water retention curves which were graphically indiscernible (Fig. 2.4). Since the correction method could be easily implemented on a standard computer spreadsheet, a higher resolution was chosen for the data presented in this study (14 layers), equivalent to 0.5 cm thick layers (Tab. 2.2).

Large differences between uncorrected and corrected fitting parameters illustrated the importance of the correction for modeling water retention curves for these sands. When employing eq. [4] and [5] to predict θ from h, errors in volumetric water content as high as 70% could result from using uncorrected fitting parameters (Fig. 2.4). However, the magnitude of these errors will depend on the height of the retention cell, i.e. they decrease with decreasing cell height, and the porous media pore size distribution. Smaller errors can be expected in less uniform porous media. Note that these errors are not restricted to the retention cell used in our experiments, but also apply to water retention experiments conducted using standard Tempe cells (Klute, 1986). The basic approach for the numerical correction employed in this study can be modified for use with alternate retention functions, e.g. the Brooks-Corey function (Brooks and Corey, 1964). Corrected Brooks-Corey fitting parameters for the four Accusand grades are provided in Tab. 2.2.

2.4.4 *Air-NAPL-Water Saturation-Pressure Measurements*

Three-phase S-P model parameters (Lenhard, 1992; Parker and Lenhard, 1987) for water and Soltrol were obtained using the three-phase S-P data. An example of S-P data for Accusand 30/40 is shown in Fig. 2.5. Water saturation S_w, and total liquid saturation S_t, with $S_t = S_w + S_o$, where S_o is the NAPL saturation ("o" stands for "oil" and is commonly used in lieu of NAPL), were plotted against scaled capillary pressure heads, measured on a water-height equivalent basis. Scaling of capillary pressure heads was

(a)

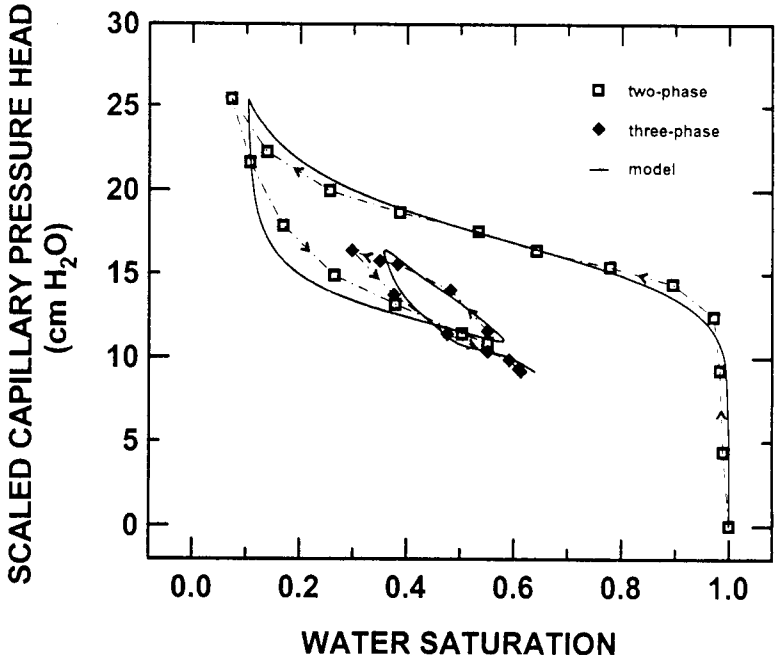

(b)

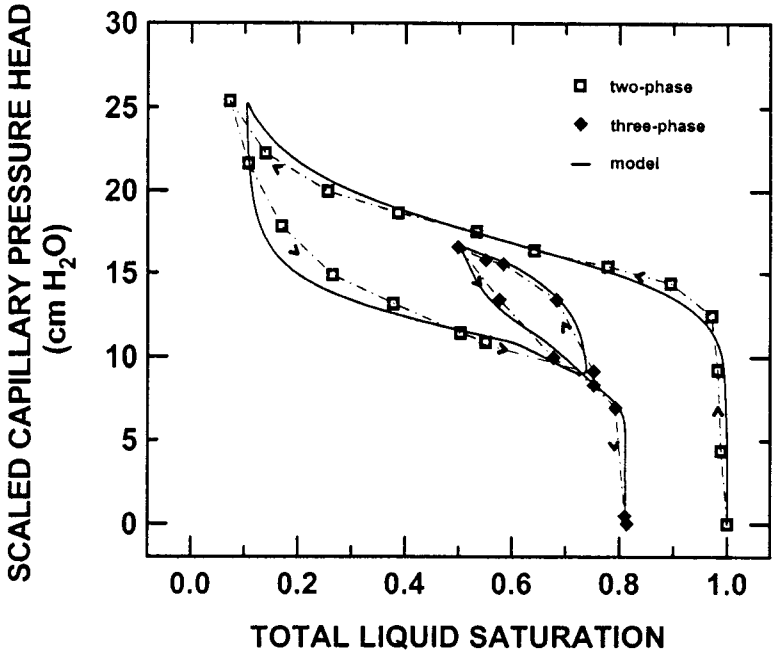

Figure 2.5 Three-phase air-NAPL-water saturation-pressure (S-P) data for Accusand® 30/40 using Soltrol® 220: (a) water S-P data, (b) total liquid S-P data. Open squares represent saturations in two-phase air-water system, closed diamonds represent saturations in three-phase air-NAPL-water system, arrows indicate saturation path, and solid lines show model (Lenhard, 1992) prediction.

conducted by multiplying air-NAPL capillary pressure heads with the air-NAPL scaling factor, β_{ao}, and NAPL-water capillary pressure heads with the NAPL-water scaling factor, β_{ow} (Tab. 2.3). It is due to this scaling of capillary pressure heads that three-phase S-P data appear as a smooth continuation of two-phase S-P data. Other fitted model parameters obtained included van Genuchten (1980) retention parameters α_d, α_i and n, where α_d and α_i were modified parameters associated with the main drainage and main imbibition branches, respectively. Following investigations of Kool and Parker (1987), n was assumed constant for drainage and imbibition branches. In addition, the maximum residual air saturation associated with the main air-water imbibition branch, $S_{ar}(aw)$, the maximum residual air saturation associated with the main air-NAPL imbibition branch, $S_{ar}(ao)$, and the maximum residual NAPL saturation associated with the main NAPL-water imbibition branch, $S_{or}(ow)$, were obtained using the inverse of an algorithm proposed by Land (1968) to determine entrapped non-wetting fluid saturations. Increasing fluid wettability in the order air<NAPL<water was assumed for our experiments. Good agreement between experimental data and fitted model was observed for all four Accusand grades, indicated by high R^2 (Tab. 2.3).

Similar to water retention data, three-phase S-P data were analyzed assuming vertically uniform fluid saturation distributions. No numerical correction during fitting was attempted to correct three-phase model parameters for conditions of vertical non-uniform fluid saturation distributions and no rigorous analysis of parameter sensitivity to errors in interpreting S-P data in this manner is given here. By similarity to water retention measurements, it is reasonable to assume that water retention parameters (α_d, α_i, n) are significantly affected by these errors (Tab. 2.3). Scaling factors (β_{ao}, β_{ow}) may be more robust because measurements of NAPL and water capillary pressure heads were made relative to the same reference point (h_i, Fig. 2.1). Residual non-wetting fluid saturations ($S_{ar}(aw)$, $S_{ar}(ao)$, $S_{or}(ow)$) were determined from fluid drainage and imbibition sequences (Lenhard, 1992). Identical scaled capillary pressure heads existed at start and end points of these sequences, rendering these parameters more robust to errors due to non-uniform vertical saturation distributions.

Table 2.3 Three-phase air-NAPL-water model parameters for four Accusand® grades obtained from saturation-pressure data using distilled water and Soltrol® 220 as NAPL.

Accusand grade	θ_s	θ_{ir}	uncorrected† α_d	uncorrected† α_i	uncorrected† n	corrected‡ α_d	corrected‡ α_i	corrected‡ n	β_{ao}	β_{ow}	$S_{ar}(aw)$	$S_{ar}(ao)$	$S_{or}(ow)$	R^2§
	— cm^3/cm^3 —		—— cm^{-1} ——			—— cm^{-1} ——								
12/20	0.348	0.012	0.105	0.144	6.75	0.151	0.217	7.35	2.38	1.76	0.08	0.17	0.16	0.98
20/30	0.348	0.016	0.0787	0.117	8.07	0.0995	0.156	10.57	2.21	1.60	0.11	0.11	0.15	0.98
30/40	0.348	0.018	0.0584	0.0880	8.35	0.0679	0.108	13.10	2.20	1.82	0.11	0.16	0.17	0.99
40/50	0.348	0.020	0.0421	0.0714	9.34	0.0453	0.0825	12.18	2.17	1.62	0.10	0.10	0.12	0.93

† not corrected for non-uniform fluid saturation distribution, ‡ corrected parameters recommended for modeling purposes, § coefficient of multiple determination for uncorrected fit.

Corrected water retention parameters α and n obtained for two-phase air-water systems (Tab. 2.2) were directly employed as corrections for parameters α_d and n in Tab. 2.3. To obtain corrected values of α_i for each Accusand grade (Tab. 2.3), we multiplied the uncorrected values of α_i by the ratio of $\alpha_{corrected} / \alpha_{uncorrected}$ (Tab. 2.2). Based on our findings for fitted water retention curves (Fig. 2.4), we recommend the use of corrected water retention parameters for three-phase fluid flow modeling purposes (Tab. 2.3).

2.4.5 *Saturated and Unsaturated Hydraulic Conductivity Measurements*

Measured saturated hydraulic conductivities (K_{sat}) exhibited good reproducibility, indicated by small standard deviations (Tab. 2.4). However, consistent packing of the experimental device (to similar porous media porosities) was required to obtain such reproducibility. Porosities in our experiments ranged from 0.33 to 0.35. Measured K_{sat} values for four Accusand grades (Tab. 2.4) agreed well with typical K_{sat} values for uniform sands (Bear, 1972). In preliminary experiments, we obtained porosities of

Table 2.4 Average saturated hydraulic conductivities (K_{sat}) and scaled saturated hydraulic conductivities (K^*_{sat}) for four Accusand® grades.

Accusand grade	K_{sat}		
	x	SD	K^*_{sat}
	cm/min	cm/min	cm/min
12/20	30.2	1.00	24.7
20/30	15.0	0.31	29.5
30/40	8.9	0.31	31.4
40/50	4.3	0.11	33.4

approximately 0.40 (funnel and column were not electrically grounded during packing) and K_{sat} values measured were larger by nearly a factor of 2 compared to the values reported in Tab. 2.4. This illustrates that it is critically important to achieve similar porosities in experimental devices when employing the data presented in this study.

Scaling of average K_{sat} values also illustrated the Miller-similarity of the four Accusand grades (Tab. 2.4). Although a slight trend existed in the scaled data (K^*_{sat}) for the four Accusand grades, an average K^*_{sat} value for the four Accusand grades of 29.9 cm/min was computed with a standard deviation of only 3.80 cm/min.

Abrupt changes in K_{rel}, computed from K_{unsat} and K_{sat} measurements (eq. [11]), were observed within a narrow range of applied capillary pressure heads (Fig. 2.6). We tested the agreement between computed K_{rel} data and values predicted by the van Genuchten-Mualem model (van Genuchten, 1980):

$$K_{rel}(h) = \frac{\left(1-(\alpha h)^{n-1}\,[1+(\alpha h)^n]^{-m}\right)^2}{[1+(\alpha h)^n]^{m/2}} \qquad [12]$$

with $m = 1 - 1/n$, using corrected water retention parameters α and n (Tab. 2.2) as input parameters in eq. [12]. The shapes of the predicted relative conductivity functions reproduced those obtained experimentally (Fig. 2.6). However, a shift of 1.5 cm - 2.5 cm in capillary pressure head existed on average between model predictions and computed K_{rel} data. This led to discrepancies between computed and predicted K_{rel} values up to approximately one order of magnitude (Fig. 2.6). The observed shift in capillary pressure head may be due to experimental error in obtaining averaged capillary pressure head data, the assumption that capillary pressure head varied linearly between tensiometers, and the high sensitivity of K_{rel} to small changes in capillary pressure head. In addition, porosities in hydraulic conductivity experiments were slightly smaller on average (0.33 to 0.35) than in water retention experiments. Thus, parameters α and n determined from water retention experiments may not have exactly reflected experimental conditions during hydraulic conductivity measurements, i.e. water retention of the porous media was slightly under-predicted during hydraulic conductivity

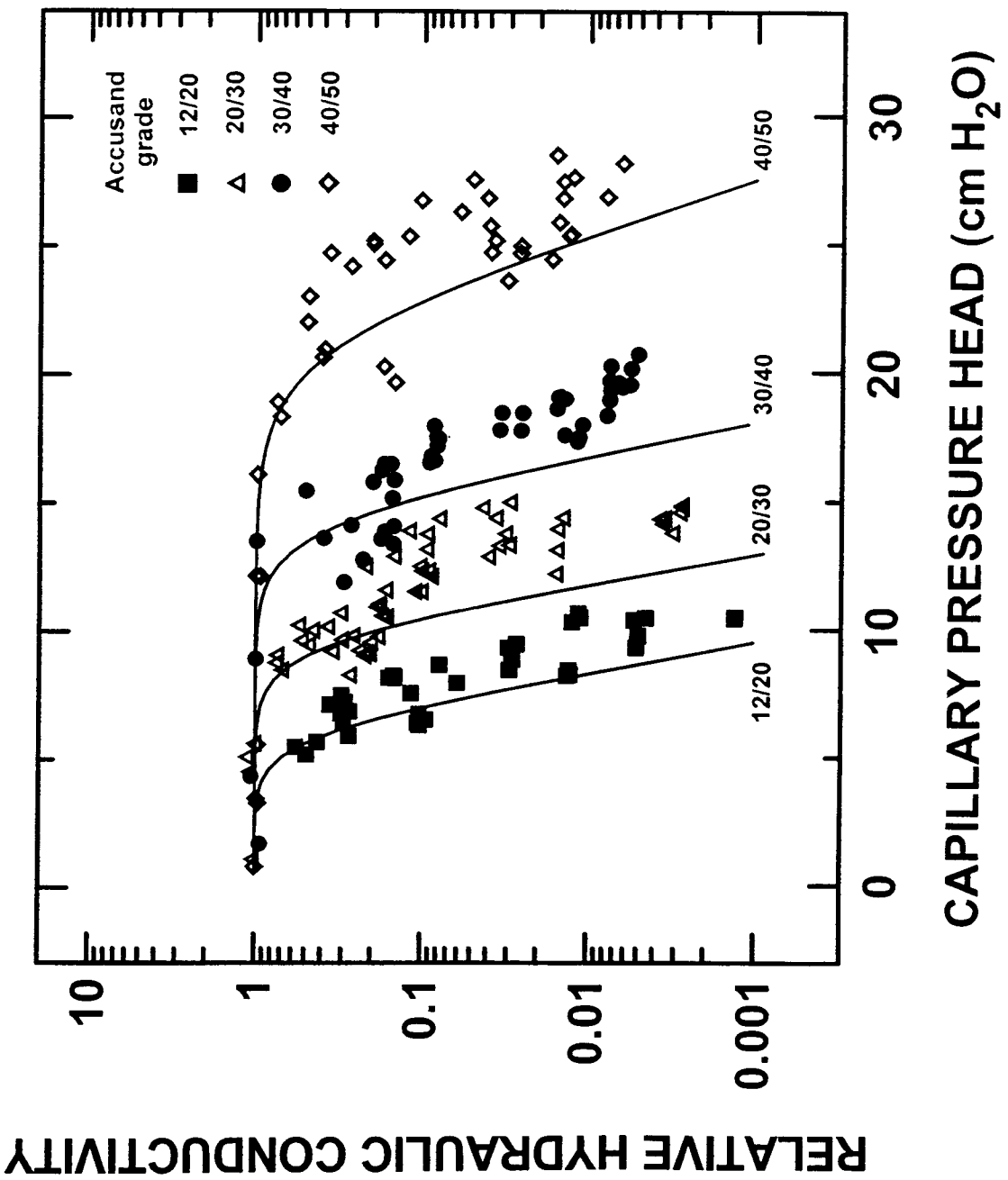

Figure 2.6 Relative hydraulic conductivities (K_{rel}) for four Accusand® grades. Symbols represent measured data, solid lines represent predicted values of K_{rel} using the van Genuchten - Mualem model (eq. [12]) and corrected water retention parameters α and n (Tab. 2.2).

measurements, and may be responsible for under-predicting experimentally determined K_{rel} data for any given capillary pressure head (Fig. 2.6). Nonetheless, the van Genuchten-Mualem model (van Genuchten, 1980) appears adequate for predicting the unsaturated hydraulic conductivities of the media for numerical modeling applications, provided that modeled packing densities match those of our water retention experiments.

When uncorrected water retention parameters (Tab. 2.2) where used in eq. [12] to predict K_{rel} (data not shown), poor agreement between computed and predicted values of K_{rel} was observed. The predictive models of van Genuchten-Burdine (van Genuchten, 1980), Brooks-Corey-Burdine (Brooks and Corey,1964), and Gardner (Gardner, 1958) did not exhibit improved agreement with the computed K_{rel} data (data not shown).

2.5 **Conclusions**

We presented a comprehensive set of hydrologically relevant parameters for four commercially-available silica sands. The sands featured narrow particle size distributions and were found very amenable to Miller-scaling for both hydrostatic (water retention) and hydrodynamic (saturated hydraulic conductivity) parameters.

Parameterization of water retention data for four Accusand grades was obtained by fitting a general equation (van Genuchten, 1980) to the experimental data. A numerical correction procedure was outlined to be used during the fitting of the general equation to compensate for an interpretation error in the experimental water retention data due to a commonly made assumption. The error resulted from non-uniform vertical distributions of volumetric water content due to hydrostatic pressure differences in the experimental device. This numerical correction procedure is not restricted to the water retention function used in this study, but may be applied to a variety of functional forms.

Three-phase S-P model parameters (Lenhard, 1992) were obtained for a widely used model NAPL. Similar to water retention data, three-phase S-P data were analyzed implying the assumption of vertically uniform fluid saturation distributions. Numerical correction of three-phase model parameters for errors in interpretation of S-P data was

limited to water retention parameters, and was conducted by employing previously corrected two-phase water retention data. To rigorously assess the influence of these errors on all three-phase model parameters, a more specific analysis is required.

Reasonable agreement was found between measured and predicted values of relative hydraulic conductivity using corrected water retention fitting parameters in the van Genuchten-Mualem model (van Genuchten, 1980). Poor agreement for uncorrected parameters indicated the importance of the numerical correction procedure for the porous media used in this study.

The four Accusand grades appear to be a suitable set of media for a broad range of flow and transport studies due to their well-defined hydrologic properties, high batch to batch consistency, availability in large quantities, chemical purity, as well as their Miller-similarity.

2.6 Acknowledgements

This work was funded by the U.S. Department of Energy (DOE) under contract # DE - FG06-92-ER61523 under the Subsurface Science Program. The authors would like to thank Dr. Robert J. Lenhard, Sultan Qaboos University, Sultanate of Oman, for valuable technical and material assistance. We would also like to thank Dr. Raina M. Miller, University of Arizona, for conducting the chemical analyses on the media. Thanks also to Jenny Curtis, U.S. Geological Survey, who performed the helium pycnometer measurements of particle density and to Darren Lerner for helping conduct the conductivity measurements.

2.7 References

API, 1986. Recommended practices for testing sand used in gravel packing operations (API RP - 58). 1st ed. American Petroleum Institute, Washington, D.C.

Artiola, J.F. 1990. Determination of carbon, nitrogen, and sulfur in soils, sediments, and wastes: a comparative study. Intern. J. Environ. Anal. Chem., 41: 159-171.

ASTM, 1987. Standard Specification for Wire-Cloth Sieves for Testing Purposes (ASTM E11 - 87). In 1993 Annual book of ASTM standards, Vol. 14.02, American Society of Testing Materials, Philadelphia, PA., 13-16.

ASTM, 1990. Standard Test Method for Particle-Size Analysis of Soils (ASTM D 422 - 63 (Reapproved 1990)). In 1993 Annual book of ASTM standards, Vol. 04.08, American Society of Testing Materials, Philadelphia, PA., 93-99.

Ayral, A., J. Phalippou, and T. Woignier. 1992. Skeletal density of silica aerogels determined by helium pycnometry. J. Materials Sci., 27: 1166-1170.

Bear, J., 1972. Dynamics of Fluids in Porous Media. Dover, New York, NY.

Brooks, R.H., and A.T. Corey, 1964. Hydraulic properties of porous media. Hydrology paper No. 3, Colorado State University, Fort Collins, CO. 27 pp.

Cary , J.W., C.S. Simmons, and J.F. McBride, 1994. Infiltration and redistribution of organic liquids in layered porous media. Soil Sci. Soc. Am. J., 58: 704-711.

Gardner, W.R., 1958. Some steady-state solutions of the unsaturated moisture flow equation with application to evaporation from a water table. Soil Sci., 85: 244-249.

Klute, A., 1986. Water retention: laboratory methods. In: A. Klute (ed.), Methods of Soil Analysis: Part 1. Physical and Mineralogical Methods. ASA (Am. Soc. Agron.), Madison, WI, ASA monogr. No. 9, 2nd ed., 635-662.

Klute, A. and C. Dirksen, 1986. Hydraulic conductivity and diffusivity: laboratory methods. In: A. Klute (ed.), Methods of Soil Analysis: Part 1. Physical and Mineralogical Methods. ASA (Am. Soc. Agron.), Madison, WI, ASA monogr. No. 9, 2nd ed., 687-734.

Kool, J.B., and J.C. Parker, 1987. Development and evaluation of closed-form expressions for hysteretic soil hydraulic properties. Water Resour. Res., 23: 105-114.

Lenhard, R.J., 1992. Measurement and modeling of three-phase saturation-pressure hysteresis. Journal of Contamin. Hydrol., 9: 243-269.

Lenhard, R.J., and J.C. Parker. 1988. Experimental validation of the theory of extending two-phase saturation-pressure relations to three-fluid phase systems for monotonic drainage paths. Water Resour. Res., 24: 373-380.

Miller, E.E., and R.D. Miller, 1956. Physical theory for capillary flow phenomena. J. Appl. Phys., 27: 324-332.

Page, A.L., R.H. Miller, and D.R. Keeney. 1982. Methods of Soil Analysis: Part 2. Chemical and Microbiological Properties. ASA (Am. Soc. Agron.), Madison, WI. ASA monogr. No. 9, 2nd ed., 1159p.

Parker, J.C., and R.J. Lenhard, 1987. A model for hysteretic constitutive relations governing multiphase flow, 1. Saturation-pressure relations. Water Resour. Res., 23: 2187-2196.

U.S. EPA. 1986. Method EPA 6010 in: Methods of Analysis of Hazardous Solid Wastes. SW-846. Third Ed. U.S. Environmental Protection Agency, Office of Solid Waste. Washington, DC, 20460.

van Genuchten, M. Th., 1980. A closed-form equation for predicting the hydraulic conductivity of unsaturated soils. Soil Sci. Soc. Am. J., 44: 892-898.

3. GEOMETRY AND POSITION OF LIGHT NONAQUEOUS-PHASE LIQUID LENSES IN WATER-WETTED POROUS MEDIA

M.H. Schroth, J.D. Istok, S.J. Ahearn, J.S. Selker

Departments of Civil and Bioresource Engineering
Oregon State University, Corvallis, OR 97331

Published in
Journal of Contaminant Hydrology, 19, 269-287, 1995

3.1 Abstract

Predicting the movement of LNAPLs (Light Nonaqueous Phase Liquids) in the subsurface environment is critical for the design of effective remediatory action. The objective of this study was to develop a method for predicting the shape and extent of LNAPL lenses in the capillary fringe of the vadose zone. Two-dimensional experiments were performed in a glass chamber (50 cm x 60 cm x 0.95 cm) using four Miller-similar silica sands (12/20, 20/30, 30/40 and 40/50 sieve sizes) and two LNAPLs (Soltrol® 220 and Duoprime® 55 Mineral Oil). LNAPLs were released in water-wetted sands to simulate a point-source discharge above a water table. Observation of light transmission was used to delineate the changing LNAPL lens boundary during infiltration until equilibrium was established. At equilibrium, no zone above the capillary fringe remained at a NAPL saturation higher than the residual saturation. A previously published model for predicting vertical lens dimensions was tested and good agreement was found between measured and predicted lens thicknesses when the time dependent nature of LNAPL-water interfacial tensions was considered. Less agreement between measured and predicted lens thicknesses was found when model equations were modified to a fully explicit, predictive form. Observed spatial variability in the emplacement of LNAPLs in the capillary fringe, compounded by the strong time dependence of a key variable, limits the use of the model as a predictive tool, but provides important insight into the low precision in prediction which is attainable even if a more complete model was developed. The results provide a means to better understand LNAPL behavior in the subsurface environment.

3.2 Introduction

The contamination of soils and aquifers by nonaqueous phase liquids (NAPLs) is a wide spread problem. Gasoline spilled from leaking underground storage tanks is an

example of a light nonaqueous phase liquid (LNAPL) that poses severe contamination problems to the vadose zone and underlying saturated zone. A great deal of recent research has been directed toward helping understand the behavior of NAPLs released into the subsurface.

Prediction of NAPL movement in porous media requires constitutive conductivity-saturation-pressure (K-S-P) relationships in three-phase air-NAPL-water systems. A model that includes the effects of hysteresis and non-wetting fluid entrapment was developed by Parker and Lenhard (1987) and Lenhard and Parker (1987). Lenhard (1992) verified an amended version of the model by comparing model predictions with three-phase air-NAPL-water saturation-pressure measurements and concluded that neglecting hysteresis could lead to erroneous predictions of fluid movement in the subsurface. He demonstrated the importance of tracking the location of fluid interfaces within the pore space to correctly predict S-P relationships. Recently, Ostendorf et al. (1993) applied the constitutive theory successfully to model field data from a gasoline spill site. Essaid et al. (1993) investigated the fluid distribution at a crude oil spill site and concluded that including hysteresis and oil entrapment was essential for predicting large-scale features of the oil body. Nevertheless, the uncertainty of estimated values of field parameters led to considerable discrepancies between observed and predicted oil distributions in their study. Farr et al. (1990) and Lenhard and Parker (1990) investigated methods to estimate free LNAPL volumes in soils from fluid levels in monitoring wells. Both concluded that free LNAPL volumes cannot be inferred directly from fluid levels in monitoring wells or from soil LNAPL thicknesses (Lenhard and Parker, 1990) without consideration of porous media properties.

Several researchers have investigated NAPL infiltration in the vadose zone. Cary et al. (1989b) used hydrocarbon oils of different viscosities in column infiltration experiments to show that NAPL infiltration was predictable using classical non-hysteretic soil-water relationships and NAPL physical properties. Other one-dimensional infiltration experiments were conducted by Eckberg and Sunada (1984) and Abdul (1988). Abdul (1988) speculated that NAPL would fully penetrate the capillary fringe and at equilibrium form "pancake-shaped" lenses.

Pantazidou and Sitar (1993) conducted two-dimensional NAPL infiltration experiments in sands and developed a set of equations to predict vertical equilibrium dimensions of LNAPL lenses emplaced in the vadose zone. In their model, they simplified the actual pore geometry of the sand by assuming that NAPL advance and drainage was dictated by the sizes of pore necks and pore bodies, each of which could be identified with a characteristic diameter. They considered a lens with curved upper and lower boundaries (Fig. 3.1). To compute the vertical dimensions T and L, Pantazidou and Sitar (1993) wrote equations for the balance of forces acting at three points on the lens boundaries. Point 1, located on the lens upper boundary, was assumed to be governed by an air-NAPL interface. Because NAPL is a more wetting fluid than air and drains from the pores, this interface should be located in pore necks. The capillary pressure at point 1 can therefore be expressed as:

$$P_{c1} = P_{a1} - P_{o1} = 4\ \sigma_{ao} / d_n \qquad [1]$$

where P_{c1} is the capillary pressure, P_{a1} is the air pressure, P_{o1} is the NAPL pressure ("o" stands for "oil" and is commonly used in formulae to refer to NAPL), σ_{ao} is the air-NAPL interfacial tension and d_n is the pore neck diameter. Point 2, located on the lens lower boundary at the top of the capillary fringe, was assumed to be governed by a NAPL-water interface. Because water is a more wetting fluid than NAPL and drains from the pores, this interface should also be located in pore necks. The capillary pressure at point 2 can thus be expressed as:

$$P_{c2} = P_{o2} - P_{w2} = 4\ \sigma_{ow} / d_n \qquad [2]$$

where P_{c2} is the capillary pressure, P_{o2} is the NAPL pressure, P_{w2} is the water pressure and σ_{ow} is the NAPL-water interfacial tension. At equilibrium, the difference in NAPL pressures between points 1 and 2 is given by the static NAPL pressure distribution. If gage pressures are used so that $P_{a1} = 0$, equations 1 and 2 can be combined to give:

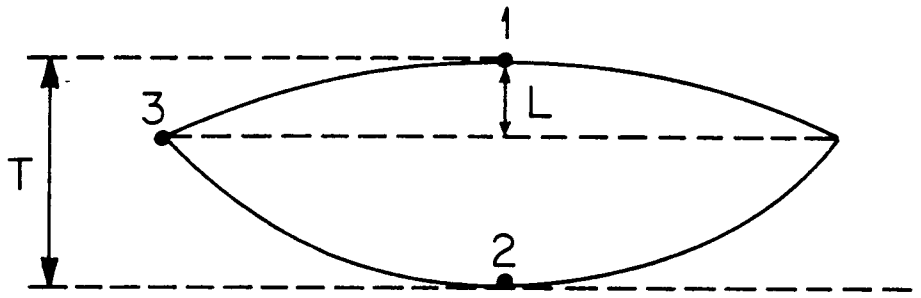

Figure 3.1 Schematic of LNAPL lens, as presented by Pantazidou and Sitar (1993).

$$P_{o2} - P_{o1} = \frac{4\sigma_{ow}}{d_n} + \frac{4\sigma_{ao}}{d_n} + P_{w2} = \rho_o g T \qquad [3]$$

where ρ_o is the NAPL density, g is the constant of gravitational acceleration and T is the maximum vertical thickness of the NAPL lens (Fig. 3.1). Noting that $P_{w2} = \rho_w g h_w$, where ρ_w is the density of water and h_w is the height of point 2 above the water table, allows us to solve eq. 3 for T:

$$T = \frac{1}{\rho_o g}\left[\frac{4(\sigma_{ow} + \sigma_{ao})}{d_n} - \rho_w g h_w\right] \qquad [4]$$

Pantazidou and Sitar (1993) derived a similar equation for the distance L (Fig. 3.1). Assuming that point 3, located at the outer edge of the lens, is governed by an air-NAPL interface where NAPL is imbibing into pores so that the interface is located in pore bodies, they obtained the following equation:

$$L = \frac{4\sigma_{ao}}{\rho_o g}\left[\frac{1}{d_n} - \frac{1}{d_b}\right] \qquad [5]$$

where d_b is the pore body diameter. This result is a contradiction to the findings of Abdul (1988), who predicted that NAPLs form lenses in the capillary fringe with horizontal upper boundaries.

At this point, the concept of NAPL lenses in porous media needs some clarification. Although not explicitly stated in the development of eqs. 4 and 5, NAPL lenses in porous media may not be entirely saturated with NAPL, but can contain substantial amounts of water and some air within their confines. Thus, NAPL lenses in porous media bear only superficial resemblance to NAPL lenses on a free water surface in the absence of porous media, e.g. in a beaker of water. In addition, simplifying assumptions were made in the development of eqs. 4 and 5 by identifying air-NAPL, NAPL-water and air-NAPL interfaces as the governing interfaces at points 1, 2 and 3 in Fig. 3.1, respectively. In a more complete analysis, three-phase air-NAPL-water S-P relations would be considered at all three locations.

To use equations 4 and 5 to predict vertical NAPL lens dimensions, several parameters have to be determined. A variety of methods and protocols have been used to obtain interfacial tension values. Pantazidou and Sitar (1993) used values (for kerosene) previously published by the U.S. Coast Guard (1984). Cary et al. (1989b) measured interfacial tensions for their NAPLs using a standard test method (ASTM, 1993). Lenhard (1992) measured interfacial tensions after prolonged NAPL-water contact. Adamson (1982) showed that measured values of air-water and air-NAPL interfacial tensions changed with time due to mutual saturation of the two liquids in one another. The pore neck and body diameters can be estimated from particle size data. Ng et al. (1978) recommended using $d_n = 0.42\ d_p$ for a random packing of spherical particles, where d_p is the particle diameter. Pantazidou and Sitar (1993) fitted d_n and d_b to obtain the closest correspondence of eqs. 4 and 5 to their experimental data, finding good agreement with the value for d_n recommended by Ng et al. (1978).

The overall objective of this study was to evaluate the equilibrium NAPL lens geometry and position with respect to the capillary fringe. In addition, possible changes of interfacial tensions as a function of time and their influence on NAPL emplacement in the vadose zone were investigated. Finally, we wanted to test the applicability of the

vertical lens equilibrium model (Pantazidou and Sitar, 1993) to a set of different NAPL-porous media combinations.

3.3 Materials and Methods

3.3.1 *Fluid and Porous Media Properties*

The geometry and position of LNAPL lenses emplaced in a capillary water fringe was studied using two different NAPLs, Soltrol® 220, hereafter referred to as Soltrol, and Duoprime® 55 Mineral Oil, hereafter referred to as Duoprime. Both NAPLs were in part selected because of their negligible solubility in water and their very low volatility at room temperature as well as for their low health hazard. Soltrol is a mixture of branched C_{13} to C_{17} alkanes manufactured by Phillips Petroleum Co., Bartlesville, Oklahoma, that has been widely used to study NAPL behavior (e.g. Cary et al., 1989b; Lenhard, 1992). Its components can be found in a variety of petrochemical products, e.g. diesel fuel. The specific gravity of Soltrol is 0.81. Duoprime is a food grade mineral oil manufactured by Lyondell Petrochemical Company, Houston, Texas. Fields of application for this product include pharmaceutics and food processing. The specific gravity of Duoprime is 0.86. Distilled water was used as the aqueous phase in the NAPL emplacement experiments.

For better delineation between water and NAPLs during the experiments, both NAPLs were dyed prior to usage by adding 0.01% by weight of Sudan® III. Sudan III is a fat stain of bright red color and is virtually insoluble in water. It is manufactured by Matheson, Coleman and Bell, Manufacturing Chemists, Norwood, Ohio.

Air-water, air-NAPL and NAPL-water interfacial tensions were measured by the ring method. In this method, a ring of precisely known circumference is submersed in the fluid with larger density, and slowly raised through the interface. Interfacial tensions are determined from the force applied on the ring at the moment when the interfacial surface

is broken. NAPL-water interfacial tensions were measured using ASTM (1993), in which the measurement is conducted one minute after the interface is created.

Interfacial tensions were also measured for both NAPLs as a function of the time of NAPL-water interfacial contact. To measure the time dependent NAPL-water interfacial tensions, the ring was first immersed in water and then the NAPL was added to create the interface. Interfacial tension was measured by raising the ring at the specified time. To measure the time dependent air-NAPL and air-water interfacial tensions, a syringe needle was submersed in the water prior to the addition of the NAPL. At specified times samples were withdrawn from both liquids, placed in clean containers, and the respective interfacial tensions measured. Interfacial tension measurements were carried out using both distilled water and "pore water" (distilled water which was previously in prolonged contact with the porous medium).

Experiments were conducted using four different grades of silica sands (Accusand® 12/20, 20/30, 30/40, and 40/50 sieve sizes), manufactured by Unimin Corporation, Le Sueur, Minnesota. Features common to these sands include high chemical purity, very low organic matter content ($\leq$ 0.04 %), and high sphericity. All four sands were obtained prewashed (with water) and presieved by the manufacturer. No further treatment was employed. The particle size distributions, as provided by the manufacturer, are shown in Fig. 3.2. Water characteristic curves for all four media were determined using a Tempe cell with a hanging water column (Klute, 1986).

3.3.2 *Two-Dimensional Chamber Experimental Procedures*

Two-dimensional chamber experiments were conducted to investigate the equilibrium geometry and position of infiltrating NAPL lenses above the water table in water-wetted porous media. Experiments were conducted in random order for 8 sand-NAPL pairs in triplicate. The experimental chamber consisted of two glass sheets (50 cm wide x 60 cm high), separated by a 0.95 cm thick acrylic spacer, which also contained a manifold along the lower boundary for introducing CO_2 gas and water into the chamber

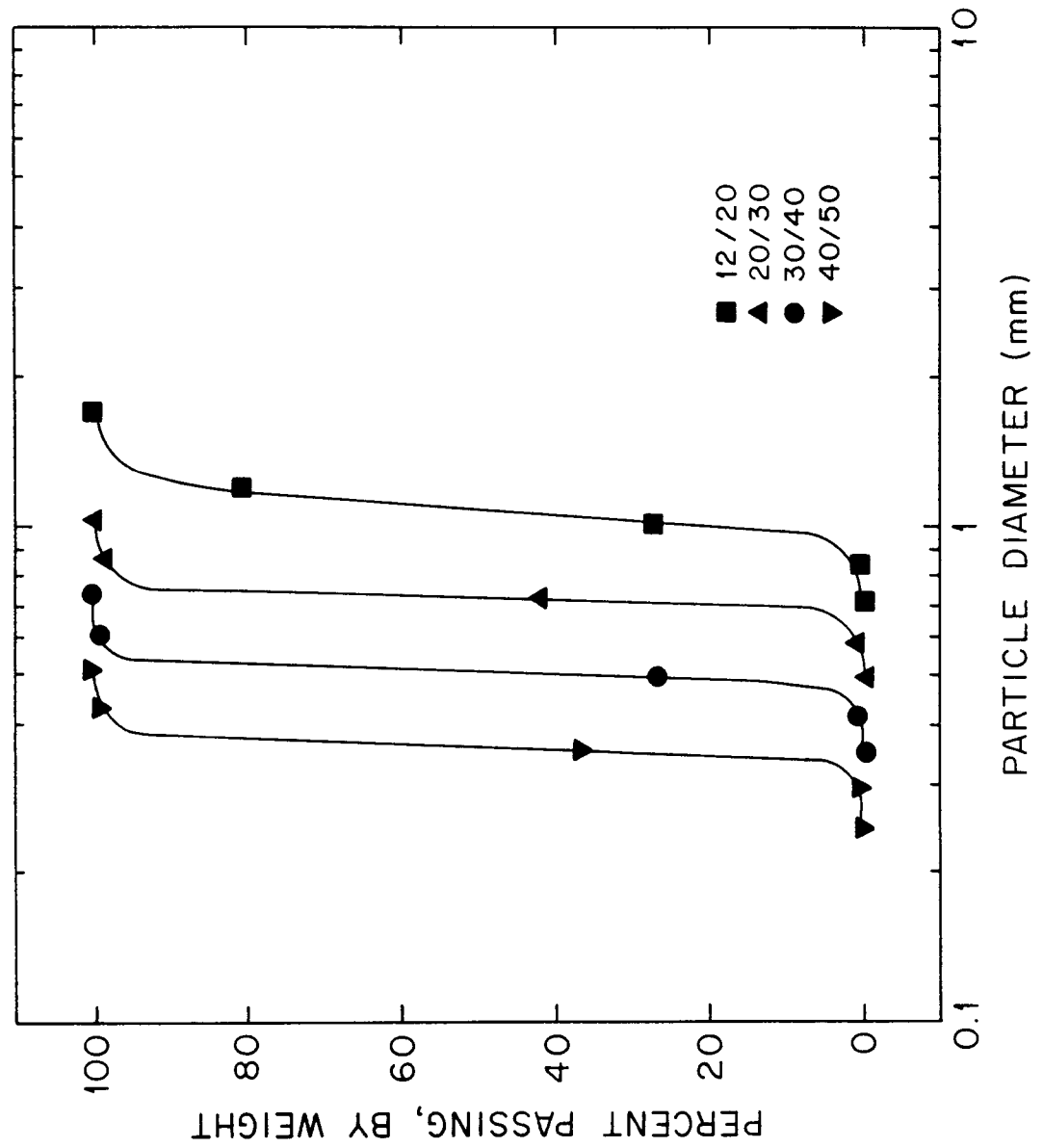

Figure 3.2 Particle size distribution for four sands used in NAPL emplacement experiments.

(Fig. 3.3). The spacer was sealed to the glass using silicone vacuum grease. The chamber was packed with air-dry sand using a prismatic funnel that fit the full width of the chamber. This funnel contained a series of coarse sieves which randomized particle motion as the sand fell into the chamber to generate a homogeneous packing. The chamber packing was conducted in one continuous pouring to prevent local gradations in particle size, which were observed to form when particle flow was interrupted during packing. The mass of sand and the packing height were recorded for each experiment and used to calculate the average porosity.

The sand packed chamber was first flushed with CO_2 gas from below through the manifold to replace the air in the pore space with CO_2. The sand was then slowly water-saturated from below by connecting the manifold to a water reservoir. Flushing with CO_2, which has a higher solubility in water than air, and water-saturating the sand from below were employed to minimize the amount of air entrapment during water imbibition. Any small quantity of initially trapped CO_2 was assumed to dissolve in the water. Visual observation showed no visible gas bubbles in the sand following saturation.

After saturating the sand pack, the water reservoir was lowered and water was allowed to monotonically drain, creating a capillary fringe approximately 20 cm below the sand surface. At least 5 hours were allowed for drainage of water prior to the addition of NAPL.

Once the equilibrated capillary fringe was established, a syringe was used to release 20 ml of NAPL into a small (approximately 1 cm^3) depression excavated in the center of the upper surface of the sand pack. For the experiments with Soltrol and Accusand 12/20, only 10 ml of NAPL were released. The released volumes were predetermined to assure that the developing NAPL lenses would not reach the edges of the chamber and form a preferential flow path along the acrylic spacers. The rate of NAPL release was adjusted such that NAPL would remain slightly ponded in the sand depression during infiltration but always remain within the local depression. After completion of the NAPL release, the top of the chamber was covered with plastic wrap to minimize water evaporation. Small holes were punched in the plastic wrap to insure that the air inside the chamber remained at atmospheric pressure during NAPL infiltration.

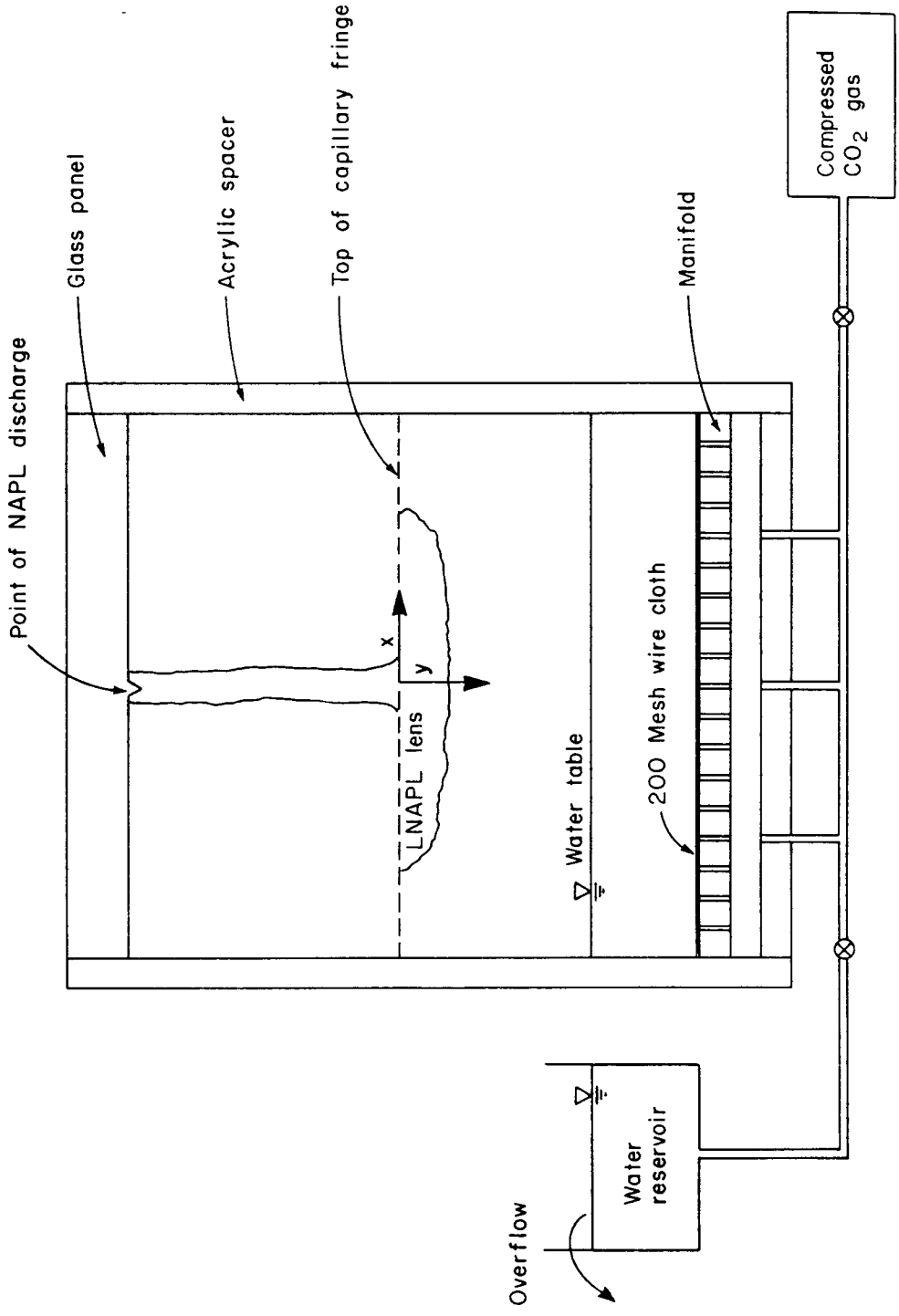

Figure 3.3 Two-dimensional chamber used in NAPL emplacement experiments.

Light transmission was used to delineate the location of the boundary of the NAPL lens. A light source was placed behind the experimental chamber and a plastic film was taped to the front glass panel. The location of the lens boundary was recorded manually by tracing the outline of the NAPL lens on the plastic film. The ambient room temperature was kept constant throughout the experiments at 23 °C. No increase in fluid temperatures due to heat generated by the light source was observed.

Following the NAPL release, the experiments were allowed to continue until no further change in the position of the NAPL lens could be visually observed. Selected experiments were continued for up to 68 hours. No significant changes in the position of the NAPL lenses were observed between 16 and 68 hours, and 16 hours was adopted as the operational definition of equilibrium. The final equilibrium position and shape of the lens was recorded on the plastic film and was subsequently digitized to obtain coordinates (see x-y coordinate system in Fig. 3.3), vertical thickness, perimeter length and cross-sectional area of the lens in the capillary fringe.

After recording the final NAPL lens position, the experimental chamber was disassembled and thoroughly cleaned with soap and window cleaner, followed by rinses with ethanol and then acetone.

3.4 **Results and Discussion**

3.4.1 *Porous Media Characteristic Curves*

For the main drainage water characteristic curves of the four sands (Fig. 3.4), the capillary head, sometimes referred to as matric or suction potential and defined here on a water-height equivalent basis, is plotted against the effective water saturation, S_{eff}:

$$S_{eff} = (S - S_m) / (1 - S_m) \qquad [6]$$

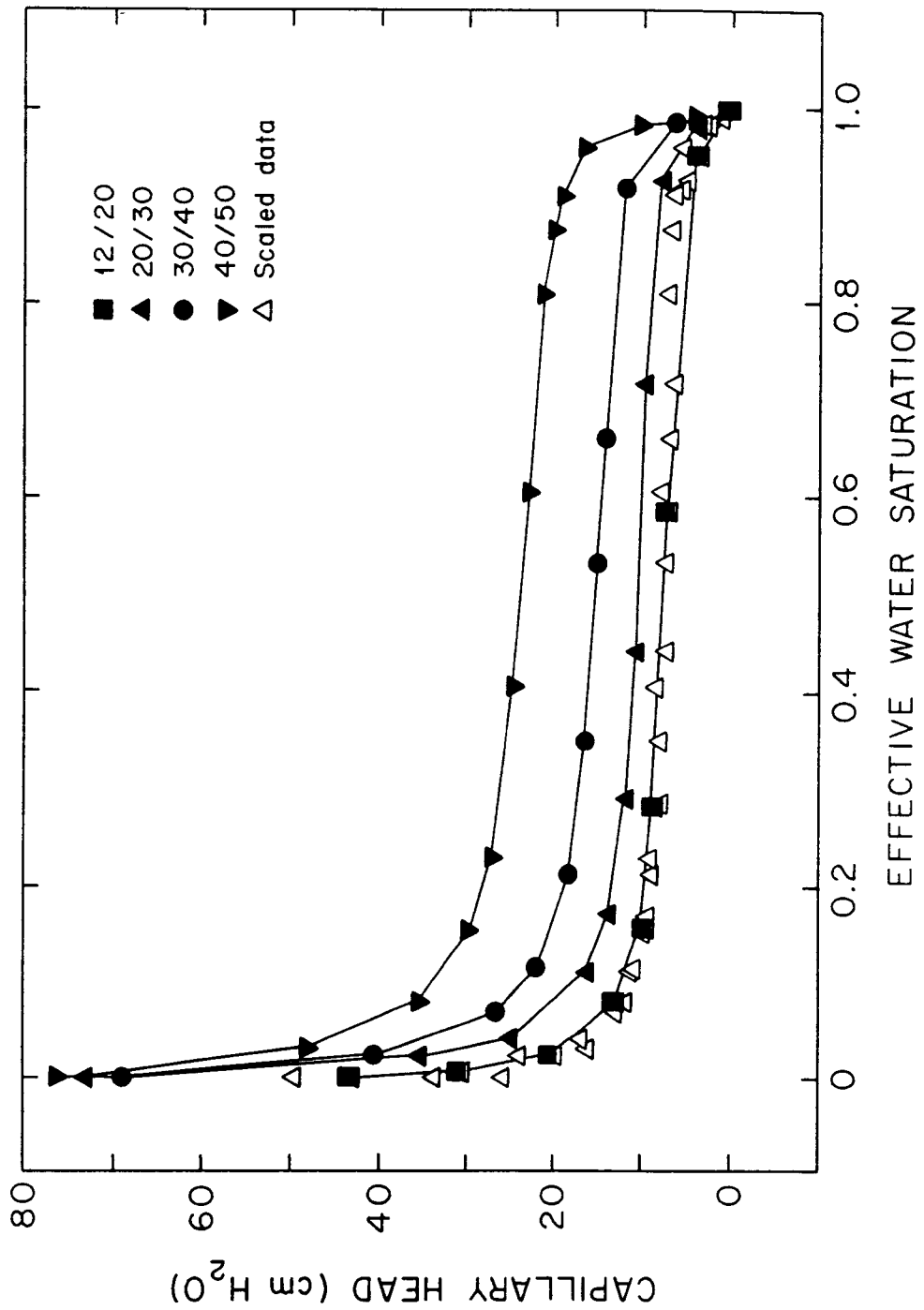

Figure 3.4 Water characteristic curves for four sands. Closed symbols represent the original data points, open symbols show the scaled capillary heads.

where S is the water saturation and S_m is the irreducible water saturation. Plotting S_{eff} instead of S allows for better comparison between experiments because it effectively normalizes the water saturation data for the slightly varying porosities (0.34 to 0.38) and irreducible water saturations (0.02 to 0.06) for the four sands in the Tempe cells. All four sands had well defined air entry pressures due to their narrow particle size distributions. This is demonstrated by the abrupt changes in effective water saturation that occurred for values of capillary head from approximately 6 cm to 30 cm (Fig. 3.4).

Scaling of the characteristic curves (Fig. 3.4) was achieved by multiplying measured capillary head values by media scaling factors, f_i :

$$h^*_i = f_i \, h_i \qquad [7]$$

where h^* is the scaled capillary head, h is the unscaled capillary head and subscript i represents the four different sands. Media scaling factors (Miller and Miller, 1956) were computed using the d_{50} particle diameters of the four sands as their media characteristic length. Particle diameters (d_{50}) employed were 1.072 mm for 12/20 sand, 0.729 mm for 20/30 sand, 0.529 mm for 30/40 sand, and 0.366 mm for 40/50 sand. The capillary heads were scaled relative to the 12/20 sand using:

$$f_i = d_{50\,i} / d_{50\,12/20} \qquad [8]$$

The Miller similarity of the four sands is illustrated by the excellent fit of the scaled capillary heads to the unscaled 12/20 sand water characteristic curve (Fig. 3.4).

3.4.2 *Fluid Interfacial Tensions*

A difference in measured interfacial tensions existed when pore water was substituted for distilled water in the respective fluid pairs (Tab. 3.1). Although the sands were of high chemical purity, low organic matter content and were obtained prewashed,

distilled water in contact with the sands was mildly contaminated by fines rendering the pore water slightly turbid. This mild contamination caused the decrease in measured air-pore water interfacial tension compared to the air-distilled water interfacial tension. For the correct interpretation of NAPL emplacement experiments, interfacial tension data obtained with pore water need to be applied, since water will always be contaminated during NAPL emplacement experiments due to the extended contact with the sand. The spreading coefficients (c_{sp}), calculated in Tab. 3.1 from:

$$c_{sp} = \sigma_{aw} - (\sigma_{ao} + \sigma_{ow}) \qquad [9]$$

indicate that Soltrol was initially slightly spreading ($c_{sp} > 0$), whereas Duoprime was non-spreading.

No changes in air-water and air-NAPL interfacial tensions were observed as a function of NAPL-water contact time for the two NAPLs used (data not shown). This is different from results presented by Adamson (1982), who reported changes in air-water and air-NAPL interfacial tension values for benzene and water which were in prolonged contact with each other. He attributed the observed changes to the process of mutual saturation of the two liquids. The NAPL-water pairs used in this study, however, had a

Table 3.1 Fluid interfacial tension data obtained using ASTM (1993).

Fluid	air	distilled water	pore water	spreading coefficient in pore water (c_{sp})
	(mN/meter)			
distilled water	72.1	---	---	---
pore water	71.3	---	---	---
*Soltrol® 220	25.9	47.7	44.8	0.6
*Duoprime® 55	30.1	49.0	45.1	-3.9

* with 0.01% by weight of Sudan® III dye.

negligible mutual solubility. Hence, air-water and air-NAPL interfacial tension values remained unaffected by prolonged NAPL-water contact. On the other hand, in all cases NAPL-water interfacial tensions decreased rapidly for the first 15 to 20 hours and approached an equilibrium value after approximately 60 to 70 hours (Fig. 3.5). Using a non-linear least square routine, the data were fitted with exponential functions of the form:

$$\sigma_{ow} = a + b\,exp\,(-c\,t) \qquad [10]$$

where a, b, and c are fitting parameters and t represents the time of interfacial aging. Parameter a represents the equilibrium interfacial tension value, the sum of $(a + b)$ represents the initial (theoretical) interfacial tension value, and c represents the interfacial tension time dependence. Faster changes of NAPL-water interfacial tension with time were measured for Soltrol, with fitted values for c about twice as high as for Duoprime (Tab. 3.2).

For both NAPLs, the change of NAPL-water interfacial tension with time was measured for two different NAPL-pore water ratios. Assuming that the change of interfacial tension with time is due to a contamination effect at the NAPL-pore water interface, different NAPL-pore water ratios should have no effect on interfacial tension measurements, thus data of different ratios should coincide. Measurements of interfacial tension as a function of time for Soltrol indicated such behavior. Minor discrepancies between measurements for different Soltrol-pore water ratios may be caused by varying interfacial contact areas between the NAPL and pore water in our experimental apparatus (approximately 31.7 cm^2 for 1:2 ratio, 42.6 cm^2 for 1:4 ratio). Measurements of interfacial tension as a function of time for Duoprime, however, showed more pronounced discrepancies between the two different NAPL-pore water ratios. No attempt will be made here to explain this phenomenon, since it is not within the scope of this paper to discuss in detail surface chemistry effects leading to the observed behavior. However, it is important to recognize the complexity of changes of NAPL-water interfacial tension as a function of time. They may be of particular importance to

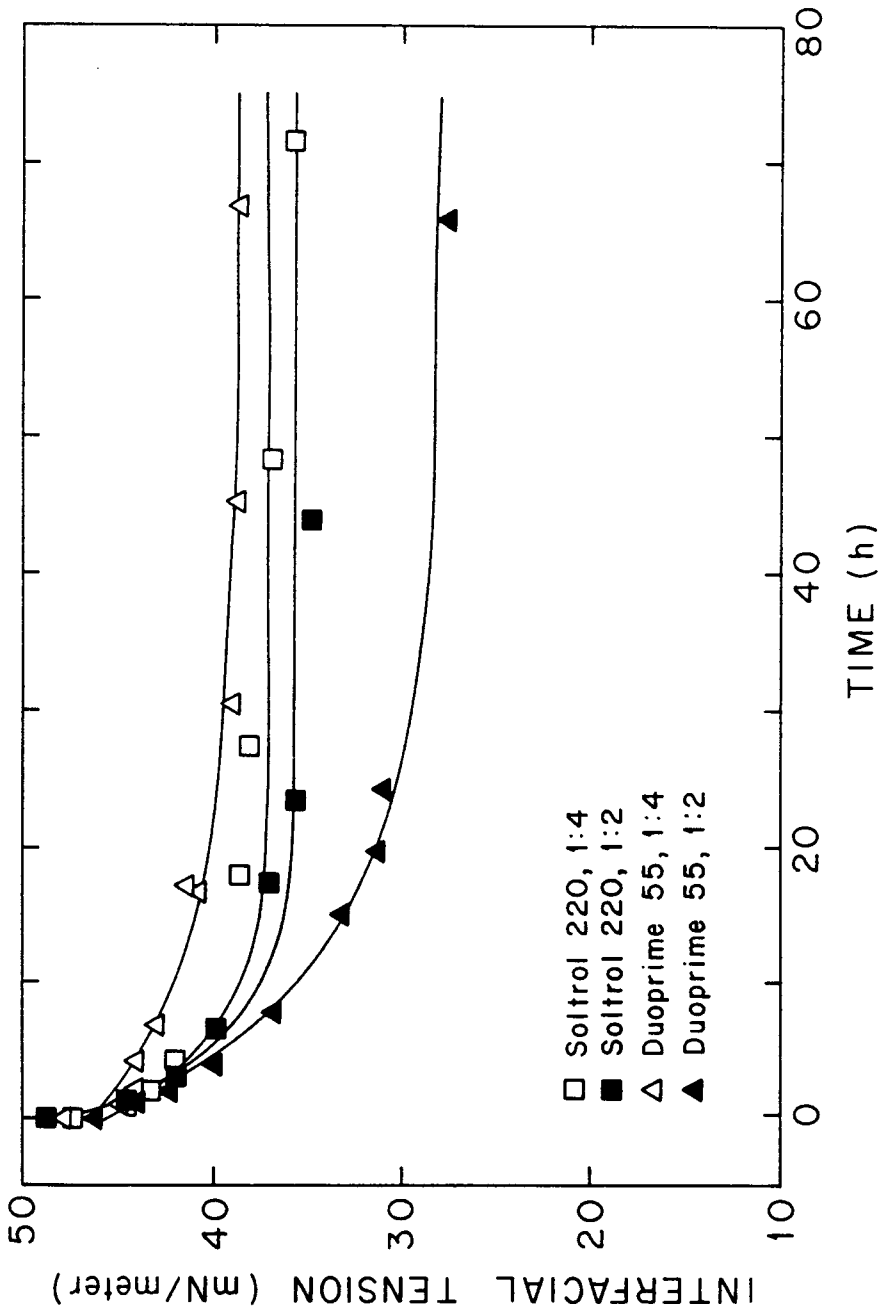

Figure 3.5 NAPL-pore water interfacial tension time dependence for Soltrol® 220 and Duoprime® 55.

Table 3.2 Best fit parameters for exponential model (eq. 10) for interfacial tension time dependence (n is the number of data points, r^2 is the coefficient of determination).

NAPL*	NAPL : water volume ratio	a (mN/meter)	b (mN/meter)	c (h^{-1})	n	r^2
Soltrol® 220	1:4	37.18	9.66	0.185	8	0.96
Soltrol® 220	1:2	35.66	12.50	0.193	7	0.98
Duoprime® 55	1:4	38.70	7.71	0.077	10	0.94
Duoprime® 55	1:2	28.09	17.56	0.084	9	0.99

* with 0.01% by weight of Sudan® III dye.

laboratory studies with similar experimental time frames. The potential significance of this effect upon NAPL lens emplacement will be demonstrated.

Similar experiments were conducted using distilled water instead of pore water and NAPLs containing no dye. The results (not shown) were similar to those in Fig. 3.5, thus eliminating the possibility that pore water composition or dye-NAPL interactions caused the observed time dependence.

3.4.3 *Two-Dimensional Chamber Experimental Observations*

The development of the capillary fringe was visually observed while the water table was lowered by draining the chamber. Areas of higher water saturation within the sands could be clearly delineated from areas of lower water saturation by the sharp change in brightness of the transmitted light. The capillary fringe was visible as a distinct wet-dry boundary. In all experiments, the height of the capillary fringe relative to the water table correlated well with capillary heads applied during measurements of the

respective characteristic curves at points where the maximum change in effective saturation occurred ($0.40 \leq S_{eff} \leq 0.70$, Fig. 3.4).

In this context, the usage of the term capillary fringe needs some explanation. Abdul (1988), as well as Pantazidou and Sitar (1993), defined the capillary fringe as the zone above a water table, in which the effective saturation is very close to 1.0. In addition, Pantazidou and Sitar (1993) defined a "visible wet-dry boundary" above the capillary fringe. For the experiments presented here, we use the term capillary fringe to describe the zone between the water table and the wet-dry boundary, which we visibly observed. This approach appears particularly reasonable for the uniform sands utilized in our experiments and agrees with the description of the term capillary fringe given by Bear (1972).

In general, homogeneous sand packing of the chamber was achieved. The average porosity obtained for all four sands was 0.341 ± 0.007. Homogeneous packing was confirmed by the formation of smooth horizontal capillary fringes due to uniform pore size distributions. Minor edge effects occurred in the vicinity of the acrylic spacers, indicated by a more wavy capillary fringe in these zones. However, they were of no significance to the NAPL emplacement experiments.

More difficulties were encountered when finer sands, particularly the 40/50 sand, were utilized. In these cases, the sand packing was often not as homogeneous, leading to a more wavy appearance of the capillary fringe across the full width of the chamber. Apparently, wall and edge effects played a greater role during packing of the finer sands, creating a less uniform pore size distribution, reflected by the appearance of a more disturbed, non-horizontal capillary fringe. The most acute cases of non-uniform packing associated with disturbed capillary fringes were discarded and the chamber was repacked.

During the experiments, the formation of NAPL lenses in the capillary fringe was visually observed. In all cases, the infiltrating NAPL completely penetrated the capillary fringe, i.e. the upper lens boundary always coincided with the initial location of the capillary fringe upper boundary. No zone above the capillary fringe remained at a NAPL saturation higher than the residual NAPL saturation (Fig. 3.6). In this study, we use the term "residual NAPL saturation" to identify NAPL retained in the zone above the

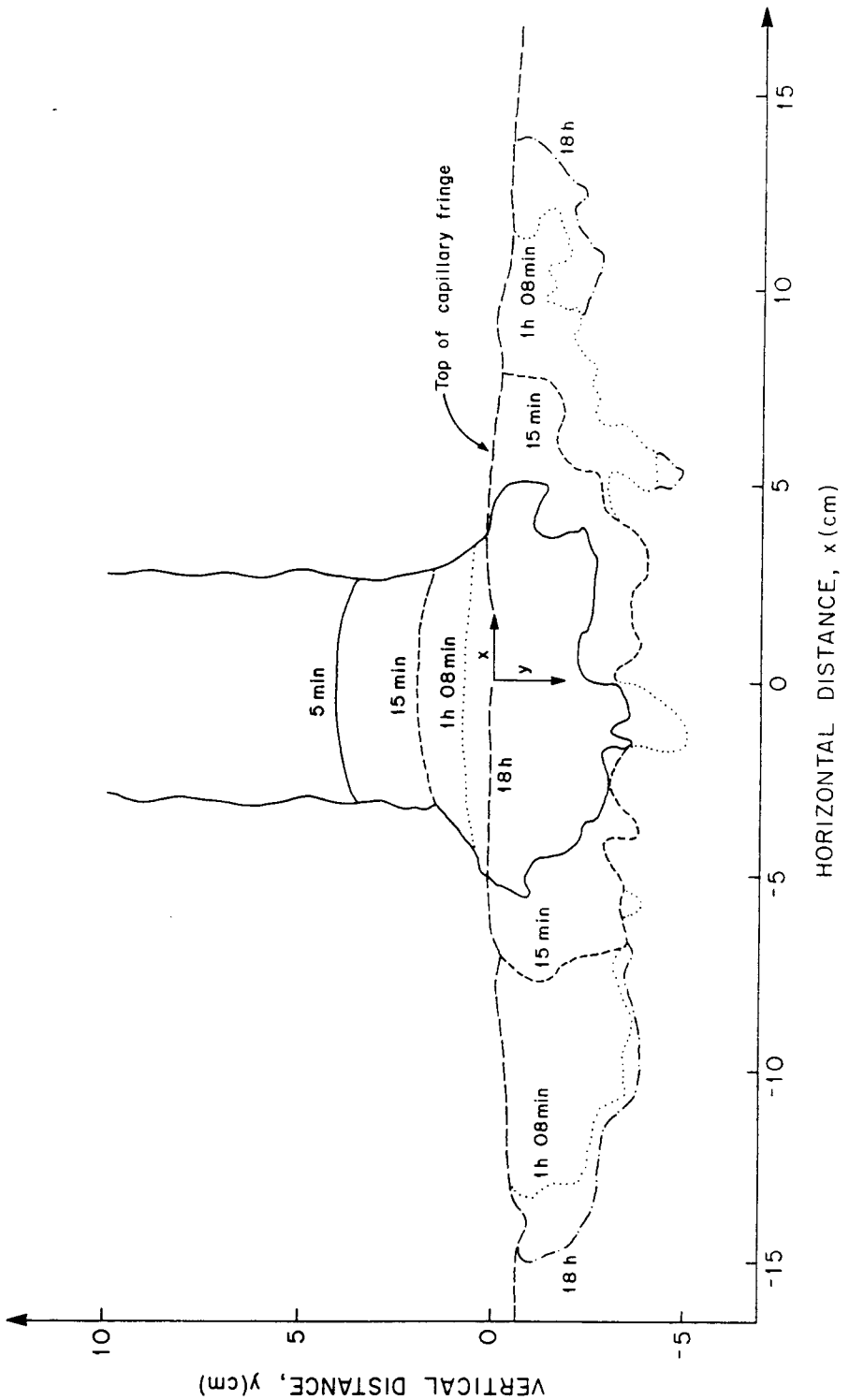

Figure 3.6 NAPL lens formation (Duoprime® 55 in Accusand® 12/20) as a function of time.

capillary fringe by any mechanism, e.g. NAPL retained by capillary retention, isolation of NAPL ganglia, or reduced NAPL mobility due to small NAPL relative permeability. No quantitative measurements of residual NAPL saturations were conducted.

Figures 3.7 (a) and (b) show the final equilibrium geometry and position of NAPL lenses formed during the emplacement experiments. The lines represent the average location of the lower lens boundary obtained by averaging coordinates of the digitized images for replicate experiments. The positions of the lenses are shown relative to the capillary fringe upper boundary of the respective experiments, correcting for non-horizontal, wavy capillary fringes. Digitizing the equilibrium lens images was found necessary since significant spatial variability of the lower (NAPL-water) lens boundary was observed within single experiments and between replicates.

Similar geometries and positions of NAPL lenses were obtained for Soltrol and Duoprime (Fig. 3.7), although their initial spreading coefficients were significantly different, i.e. +0.6 mN/meter for Soltrol and -3.9 mN/meter for Duoprime (Tab. 3.1). The observed similarity of lens shapes between the two NAPLs may therefore be attributed to the measured change of NAPL-water interfacial tensions as a function of time, rendering both NAPLs spreading within the time frame of the experiments. Intimate contact between water and NAPL was established once the NAPL encountered and penetrated the capillary fringe. A decrease in interfacial NAPL-water tension with time was therefore to be expected similar to the ones measured in pure liquid systems (Fig. 3.5), although a quantitative prediction of the change of interfacial tension is not attempted here due to the uncertainty in the appropriate model, as discussed earlier. The comparison of lens shapes is further complicated by the fact that NAPL saturations within the confines of the lenses are likely to be somewhat variable. This may cause the lens geometry not to be a simple function of interfacial tensions.

The cross-sectional area of the lenses were larger for Soltrol than for Duoprime (Tab. 3.3). Qualitative visual observation suggested similar NAPL saturation distributions within the lenses for both NAPLs. Thus, more Duoprime must have been left behind as residual NAPL saturation as it moved down from the point of release through the unsaturated zone until it encountered the capillary fringe. This effect may be

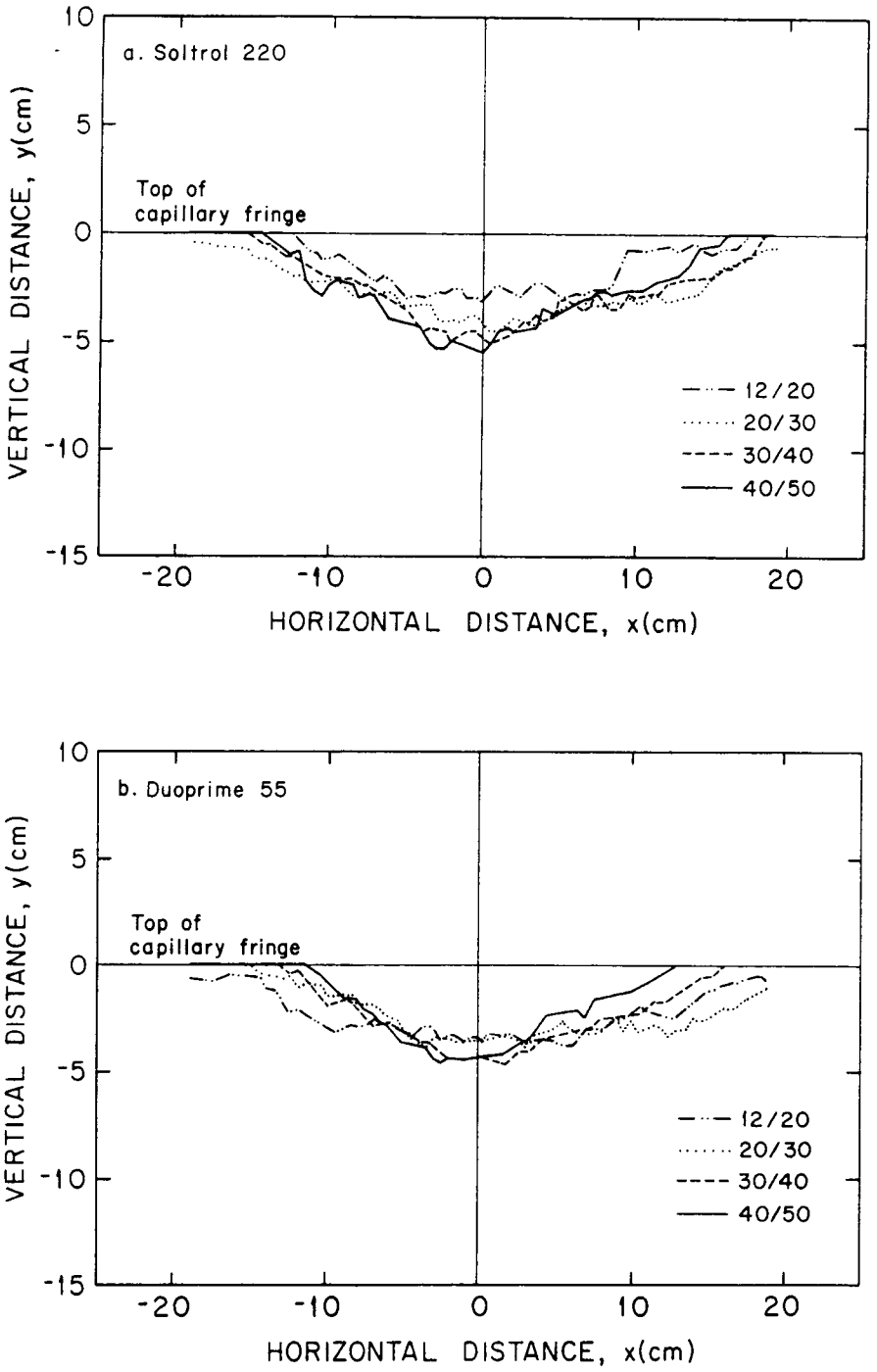

Figure 3.7 Average thickness of NAPL lenses for four sands: (a) Soltrol® 220, (b) Duoprime® 55.

Table 3.3 Measured cross-sectional areas (averages and standard deviations), computed NAPL saturations and measured averaged thicknesses (averages and standard deviations) of NAPL lenses formed during emplacement experiments in the capillary fringe.

	*Soltrol® 220			*Duoprime® 55		
Sand grade	Area (cm^2)	NAPL Saturation	Thickness (cm)	Area (cm^2)	NAPL Saturation	Thickness (cm)
12/20	**106.4 ± 6.4	0.58	2.75 ± 0.16	92.8 ± 5.5	0.68	3.60 ± 0.38
20/30	98.0 ± 12.1	0.63	4.08 ± 0.76	88.3 ± 5.6	0.70	3.68 ± 0.43
30/40	106.3 ± 21.5	0.58	4.65 ± 0.96	83.5 ± 11.4	0.74	4.62 ± 1.12
40/50	90.0 ± 15.8	0.69	4.92 ± 0.52	62.5 ± 12.1	0.99	4.46 ± 1.11

* with 0.01% by weight of Sudan® III dye, ** multiplied by 2, compensating for the smaller amount (10 ml) of Soltrol® 220 injected in these experiments.

caused by the initial difference in spreading coefficients of the two NAPLs. When the NAPLs were released into the sands, Soltrol was initially slightly spreading whereas Duoprime was non-spreading (Tab. 3.1). Non-spreading NAPLs ($c_{sp} < 0$) have less stable NAPL films within pores and can more easily be broken into isolated ganglia (Kalaydjian and Tixier, 1991). This would be expected to lead to higher residual NAPL saturations during NAPL movement. Our results seem to confirm this behavior for early times during NAPL infiltration and movement through the vadose zone.

To demonstrate that NAPL lenses in porous media can contain substantial amounts of water, we computed NAPL saturations within the NAPL lenses from measured cross-sectional areas, packing thickness, average porosity and volumes of NAPL injected (Tab. 3.3). For these computations, we assumed uniform NAPL saturations throughout the lenses, air saturations equal to zero, and, although not supported by visual observations, we assumed residual NAPL saturations above the capillary fringe equal to zero. Hence, saturations in Tab. 3.3 represent upper limits of NAPL saturations indicating the presence of substantial amounts of water within the confines of the NAPL lenses in most cases.

3.4.4 *Model Evaluation and Enhancement*

Pantazidou and Sitar (1993) presented a model to predict vertical dimensions of LNAPL lenses in the vadose zone. They assumed that LNAPL lenses form on top of the capillary fringe (point 2, Fig. 3.1). In addition, they assumed that the upper lens boundary (point 1, Fig. 3.1) is governed by an air-NAPL interface. Using similar simplifying assumptions, eq. 4 should also predict the total lens thickness T in our experiments.

Experimental lens thicknesses were obtained by averaging the thicknesses of the digitized lens images in the range of -2.5 cm $\leq x \leq$ +2.5 cm. Averaging was necessary due to the significant spatial variability of the lens thicknesses encountered. The above range was chosen from visual observation (Fig. 3.7), recognizing that the maximum lens thickness occurred near the center of the lens. Observed averaged lens thicknesses generally increased with decreasing porous media particle sizes, i.e. larger vertical thicknesses were obtained in finer porous media (Tab. 3.3).

To compute lens thicknesses using eq. 4, the respective pore neck diameter (d_n), interfacial tensions (σ_{ao} and σ_{ow}), as well as h_w, the height of point 2 above the water table (Fig. 3.1), must be known. In these experiments, h_w was directly measured for each experiment by using the light transmission method. The pore neck diameter d_n was calculated using Laplace's capillary rise equation :

$$d_n = (4\,\sigma_{aw}) / (\rho_w\, g\, h_{cap}) \qquad [11]$$

where h_{cap} is the capillary fringe height. The average capillary fringe height was measured for each experiment prior to adding NAPL. Using eq. 11 to calculate d_n implicitly accounts (through the term h_{cap}) for the pore geometry within each experiment. Thus, no estimating of d_n from literature values (Ng et al., 1978) or fitting of d_n (Pantazidou and Sitar, 1993), was required.

When NAPL-water interfacial tension values measured using a 1 min. contact time (ASTM, 1993, Tab. 3.1) were used, predicted lens thicknesses for both NAPLs were

in all cases larger than measured thicknesses (Fig. 3.8). When NAPL-water interfacial tension values were fitted using a non-linear least square routine (keeping air-water and air-NAPL interfacial tensions constant), best fits were obtained for NAPL-water interfacial tension values of 41.9 mN/meter for Soltrol and 38.8 mN/meter for Duoprime. This corresponds well with the observed behavior of decreasing NAPL-water interfacial tensions as a function of contact time (Fig. 3.5) when considering the time frame of the experiments (16 to 68 hours).

The good fit obtained in Fig. 3.8 for fitted NAPL-water interfacial tension values is somewhat misleading, however. Considering the fact that full penetration of the capillary fringe was observed in all experiments conducted, eq. 4, as developed by Pantazidou and Sitar (1993), is not in a fully explicit form in that the predicted quantity, T, is indirectly measured as an input parameter. This can be seen by noting that h_w, the height of point 2 above the water table (Fig. 3.1), can be expressed as:

$$h_w = h_{cap} - T \qquad [12]$$

When the above relationship is inserted in eq. 4, the expression for the total lens thickness becomes:

$$T = \frac{1}{\rho_o g}\left[\frac{4(\sigma_{ao}+\sigma_{ow})}{d_n} - \rho_w g h_{cap} + \rho_w g T\right] \qquad [13]$$

Solving eq. 11 for h_{cap}, substituting it into eq. 13 and solving for T gives a fully explicit equation for computing T:

$$T = \frac{4\ (\sigma_{ow}-\sigma_{ao}-\sigma_{ow})}{d_n g\,(\rho_w-\rho_o)} \qquad [14]$$

Using interfacial tension values measured after 1 min. of contact time (Tab. 3.1) in eq. 14 results in less accurate predictions of lens thicknesses for Soltrol (Fig. 3.9). Even worse, nonsensical negative thicknesses were predicted for Duoprime (not

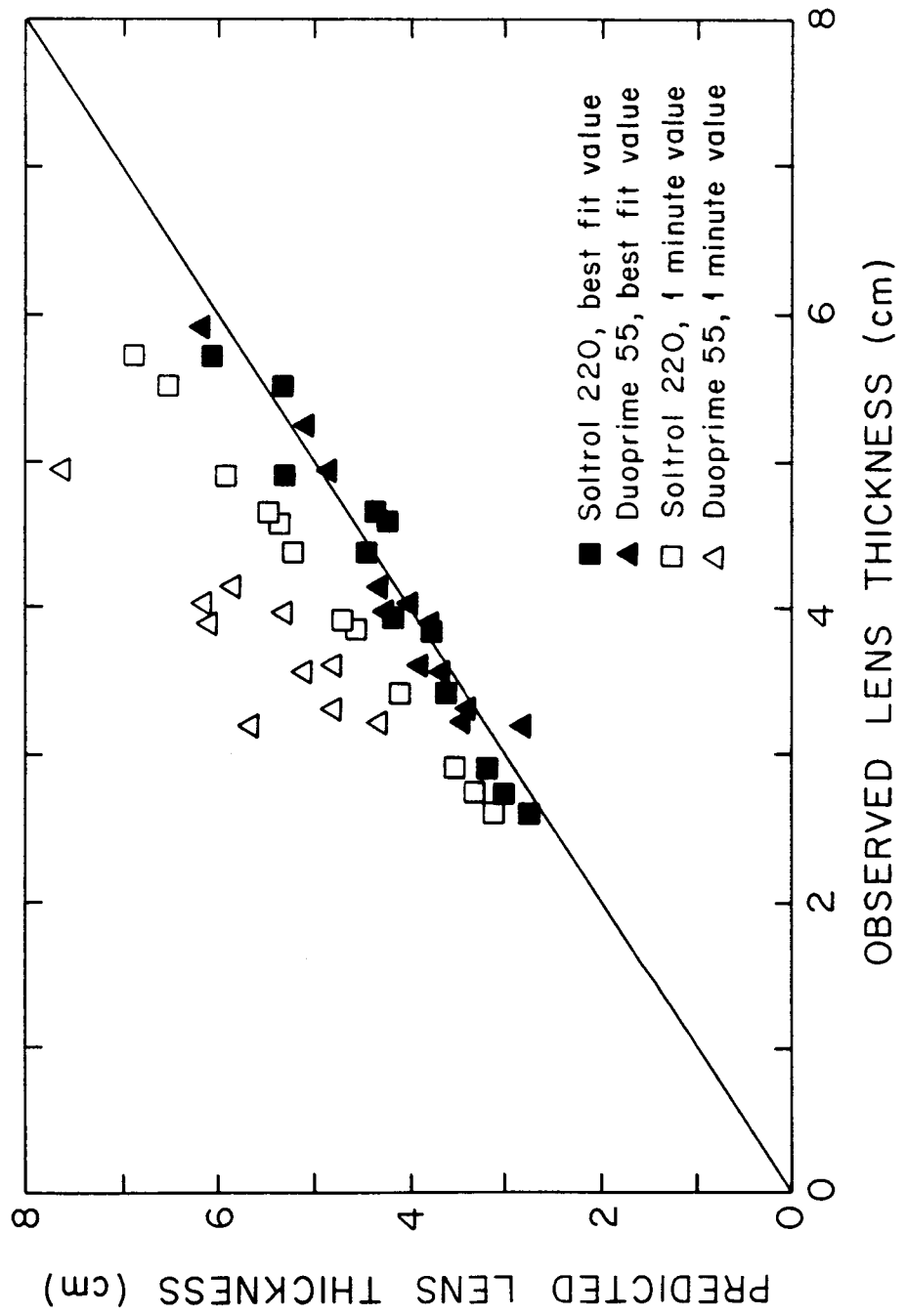

Figure 3.8 Observed versus predicted lens thickness using eq. 4. Closed symbols represent predictions using best fit interfacial tension values, open symbols show predictions using 1 min. interfacial tension values.

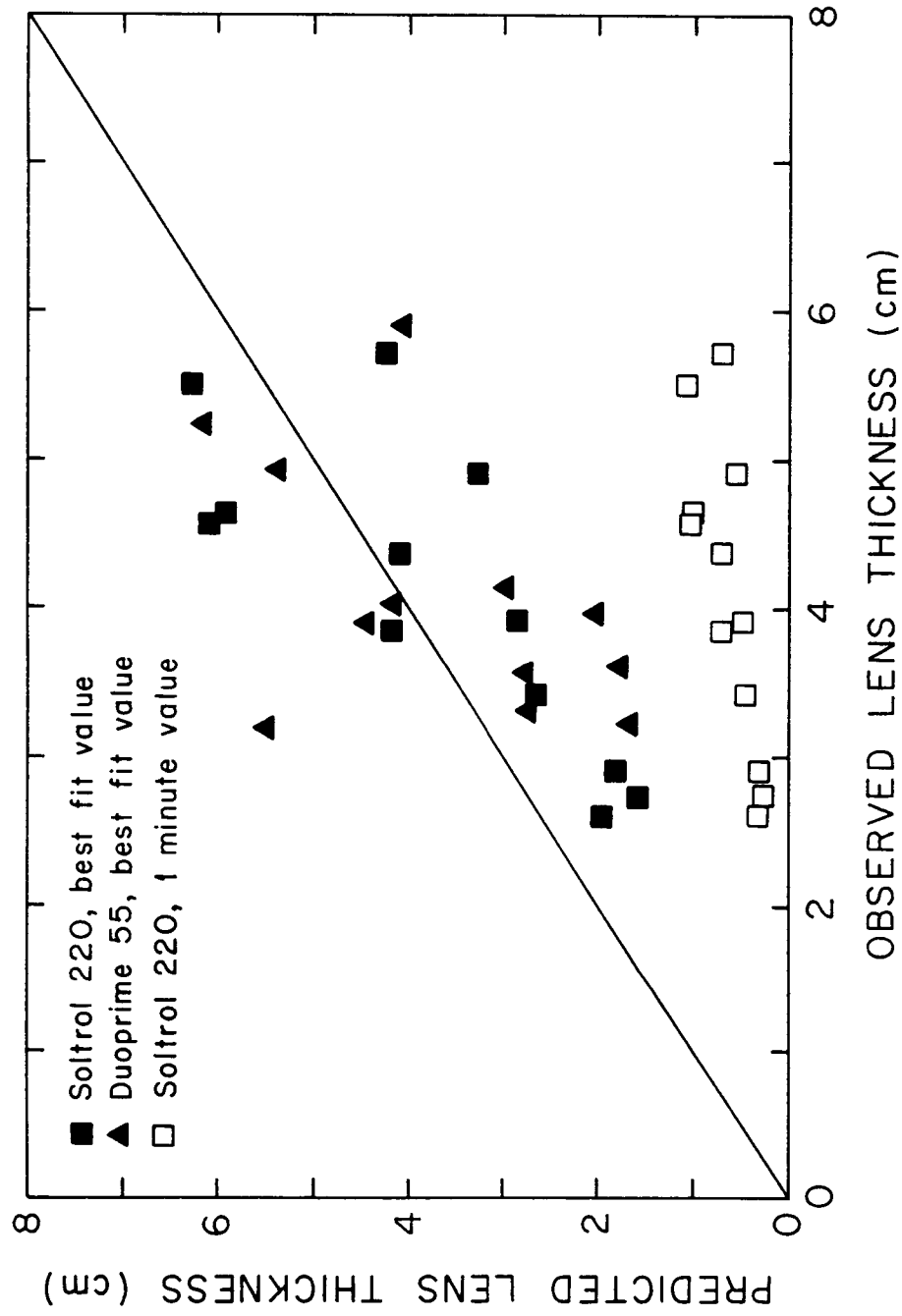

Figure 3.9 Observed versus predicted lens thickness using eq. 14. Closed symbols represent predictions using best fit interfacial tension values, open symbols show predictions using 1 min. interfacial tension values.

illustrated in Fig. 3.9) for this choice of interfacial tension values. Prediction of negative thicknesses is explainable by considering eq. 14 in detail. The term (σ_{aw} - σ_{ao} - σ_{ow}) represents the NAPL spreading coefficient (eq. 9), thus positive predictions for T will only be obtained for positive LNAPL spreading coefficients, since for LNAPLs $\rho_w > \rho_o$. When interfacial tensions were fitted, more scatter of the data around the line of coincidence occurred than when using eq. 4. Best fits for predicted versus observed lens thicknesses were obtained for interfacial tension values of 41.8 mN/meter for Soltrol and 38.9 mN/meter for Duoprime, which is within 0.3 % of the previous best fit results.

From the results presented here, it appears that eq. 14 is only of limited use for predicting NAPL lens thicknesses in the capillary fringe. Significant variability in the precision of the prediction was encountered for both NAPLs used, although experiment specific information (h_{cap}) was used to compute d_n.

To test the performance of eq. 14 for a case where no specific information about the pore geometry is available a priori, averages of observed lens thicknesses (Tab. 3.3) were compared to predicted values, where d_n for each sand was estimated from $d_n = 0.42\ d_{50}$, assuming a random packing of the sands (Ng et al., 1978). Results presented in Fig. 3.10 are similar to those in Fig. 3.9. Although observed thicknesses were averaged for NAPL-sand replicates, significant scatter of the best fit data limit the use of eq. 14 to predict lens thicknesses. It is important to recognize that the scatter observed in Figs. 3.9 and 3.10 was not due to geometric dissimilarities between the four sands, since their Miller similarity was demonstrated earlier (Fig. 3.4). Best fit interfacial tension values obtained were 41.1 mN/meter for Soltrol and 38.4 mN/meter for Duoprime, within 2 % of those obtained in the previous best fit computations.

A few comments regarding Pantazidou and Sitar's (1993) results given in eq. 5 are in order. In our experiments, the upper NAPL lens boundary always coincided with the former top of the capillary fringe. Curvature in the upper lens boundary was only observed in experiments where the capillary fringe was already curved prior to the NAPL infiltration. In this context, particular consideration needs to be given to the central portion of the upper lens boundary, through which the NAPL penetrated the capillary fringe (Fig. 3.6). Assuming a perfectly homogeneous packing, the pressure difference

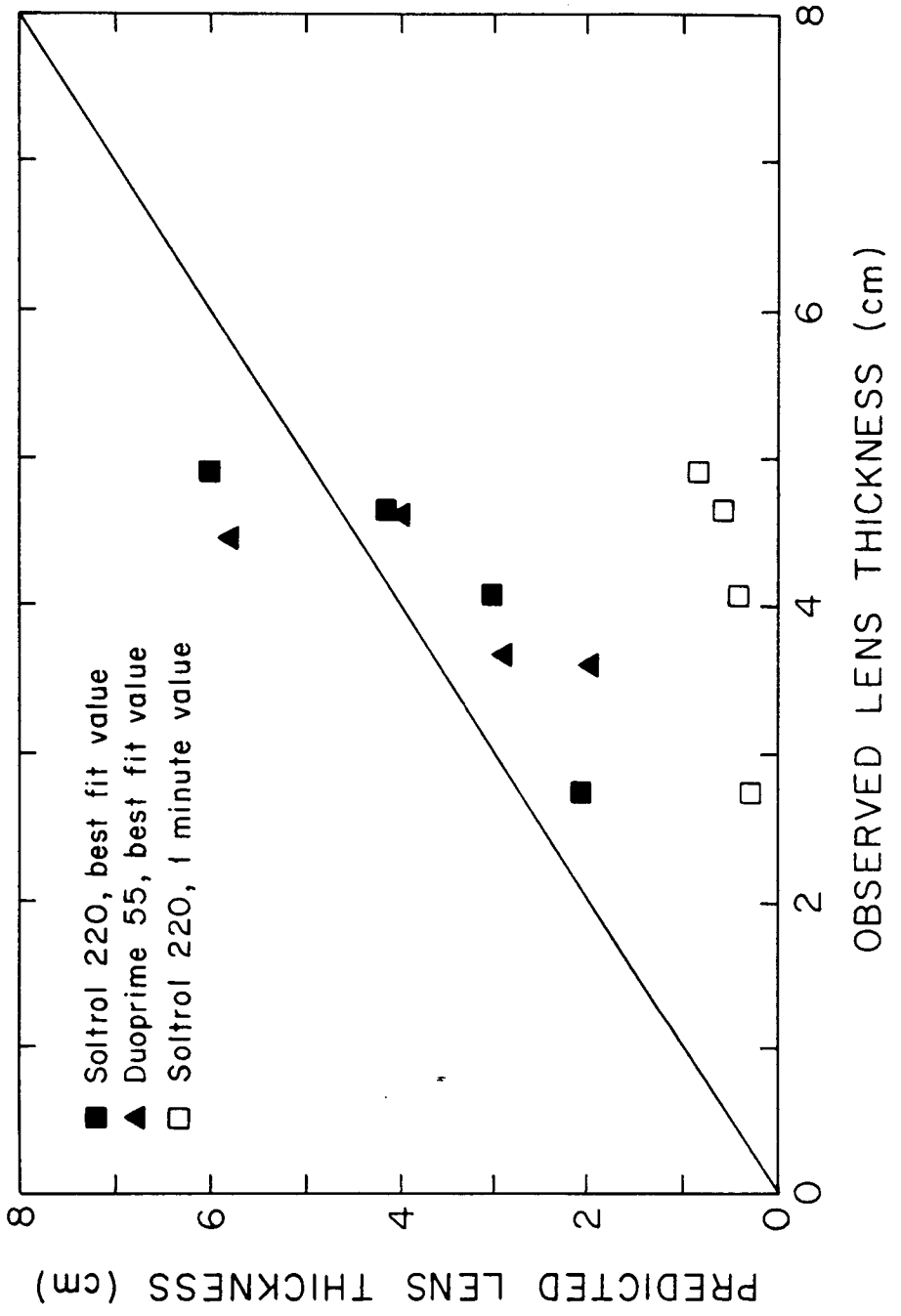

Figure 3.10 Average observed versus predicted lens thickness using eq. 14, assuming random packing of the porous media ($d_n = 0.42\ d_{50}$). Closed symbols represent predictions using best fit interfacial tension values, open symbols show predictions using 1 min. interfacial tension values.

across the air-NAPL interface along this portion is constant and so is the absolute NAPL capillary pressure at the interface. However, if the NAPL capillary pressure is constant along this portion of the upper lens boundary, any vertical distance between two points along that boundary would indicate non-equilibrium conditions, since the resulting NAPL pressure head ($\rho_o g h$) would not be compensated by capillary forces. In other words, in a perfectly homogeneous porous medium, the central portion of the upper lens boundary should be flat. The use of eq. 5 to compute the vertical distance L (Fig. 3.1) is not warranted from our experimental observations. In addition, its use is greatly hindered by having to fit or estimate d_b and thus it cannot be verified.

3.5 **Conclusions**

LNAPLs emplaced in the vadose zone formed lenses in the capillary fringe above a water table. Full penetration of the capillary fringe was observed in the sense that at equilibrium no area above the capillary fringe remained at NAPL saturations higher than residual saturations. In homogeneous sand packings, lens geometry consisted of flat upper and curved lower boundaries. Therefore, any observation of curvature of the upper lens boundary was attributed to either non-equilibrium conditions or was an artifact of pore size heterogeneity in the porous medium. Significant spatial variability of lens shape and vertical thickness within single experiments and between replicates created difficulties in predicting the exact lens geometry. Heterogeneities of natural systems will further increase the variabilities observed in laboratory experiments.

We demonstrated the importance of considering changes of NAPL-water interfacial tensions as a function of NAPL-water contact time for the prediction of equilibrium vertical lens thicknesses. Neglecting these changes can lead to erroneous predictions. Therefore, ASTM (1993) is not an adequate method for determining interfacial tensions in cases where the time frame of NAPL transport is similar to the time frame of interfacial tension change. For the fluids tested, a 10 % change in NAPL-water interfacial tension occurred in 1.5 to 6 hours. Changing interfacial tensions could also

lead to errors in computing constitutive relations (K-S-P) or hinder proper scaling of fluid parameters and thus limit the predictive use of these theories for these time frames. In our experiments, changing interfacial tensions as a function of NAPL-water contact time rendered both NAPLs spreading, although one was initially non-spreading, and this may be responsible for the formation of similar NAPL lenses in the capillary fringe.

Utilizing visual experimental observations of complete NAPL penetration into the capillary fringe, we showed that a previously derived equation to compute the maximum vertical lens thickness was implicit, thus rendering its promising predictive accuracy meaningless. When amended to a fully explicit form, less precision in the prediction of vertical lens thicknesses was observed. This effect was likely caused by the high sensitivity of the explicit equation to both fluid interfacial tension properties and the pore geometry. Changes of NAPL-water interfacial tensions due to aging interfaces and irregularities of pore sizes at the micro-scale made predictions of vertical lens thicknesses more difficult and less accurate. Nevertheless, the general trend observed in the experiments (larger vertical lens thicknesses with finer porous media) was captured reasonably well.

Finally, simplified underlying assumptions of simple pore geometry (represented by d_n) and the identification of respective governing air-NAPL and NAPL-water interfaces to compute capillary forces could be questioned and may be responsible for some of the predictive inaccuracy observed. Under these assumptions, the location of the air-NAPL and NAPL-water interfaces is in pores of the same diameter (d_n). Although sands with uniform particle size distributions were used in the experiments, a variety of pore sizes exist and the governing interfaces are likely not in identical size pores. To compute capillary forces correctly, however, it is important to know the location of the governing interfaces as well as to consider three-phase air-NAPL-water S-P relationships (Lenhard, 1992). This could introduce some error when predicting vertical lens thicknesses from capillary forces.

From the spatial variability observed in the experiments and the observed sensitivity of the explicit equation to pore geometry and fluid properties it appears likely

that predictions of vertical lens thicknesses in more natural settings will be significantly less accurate.

3.6 Acknowledgements

This work was funded by the U.S. Department of Energy (DOE) under DOE contract # DE-FG06-92ER61523 under the Subsurface Science Program.

3.7 References

Abdul, A.S., 1988. Migration of Petroleum Products Through Sandy Hydrogeologic Systems. Ground Water Monit. Rev., 8: 73-81.

Adamson, A.W., 1982. Physical Chemistry of Surfaces. Fourth Edition, John Wiley & Sons, Inc., New York.

ASTM, 1993. Designation: D 971-91, Standard Test Method for Interfacial Tension of Oil Against Water by the Ring Method. American National Standard, Annual Book of ASTM Standards, 05.01: 297-299.

Bear, J., 1972. Dynamics of Fluids in Porous Media. Dover Publications, Inc., New York.

Cary, J.W., C.S. Simmons and J.F. McBride, 1989b. Predicting Oil Infiltration and Redistribution in Unsaturated Soils. Soil Sci. Soc. Am. J., 53: 335-342.

Eckberg, D.K, and D.K. Sunada, 1984. Nonsteady Three-Phase Immiscible Fluid Distribution in Porous Media. Water Resour. Res., 20: 1891-1897.

Essaid, H.I., W.N. Herkelrath, and K.M. Hess, 1993. Simulation of Fluid Distributions Observed at a Crude Oil Spill Site Incorporating Hysteresis, Oil Entrapment, and Spatial Variability of Hydraulic Properties. Water Resour. Res., 29: 1753-1770.

Farr, A.M., R.J. Houghtalen, and D.B. McWhorter, 1990. Volume Estimation of Light Nonaqueous Phase Liquids in Porous Media. Ground Water, 28: 48-56.

Kalaydjian, F., and M. Tixier, 1991. Effect Of The Spreading Coefficient On Gas/Oil Capillary Pressure Curves In Presence Of Connate Water. SCA (Soc. Core Anal.) Conference Paper Number 9106, presented at the 5th SCA Annual Technical Conference, San Antonio, TX, Aug. 20-22, 1991.

Klute, A., 1986. Water Retention: laboratory methods. In: A. Klute (editor), Methods of soil analysis, Part 1: Physical and mineralogical methods. ASA monograph No. 9, second edition, American Society of Agronomy, Madison, WI, 635-662.

Lenhard, R.J., 1992. Measurement and modeling of three-phase saturation-pressure hysteresis. J. Contamin. Hydrol., 9: 243-269.

Lenhard, R.J., and J.C. Parker, 1987. A Model for Hysteretic Constitutive Relations Governing Multiphase Flow 2. Permeability-Saturation Relations. Water Resour. Res., 23: 2197-2206.

Lenhard, R.J., and J.C. Parker, 1990. Estimation of Free Hydrocarbon Volume from Fluid Levels in Monitoring Wells. Ground Water, 28: 57-67.

Miller, E.E., and R.D. Miller, 1956. Physical Theory for Capillary Flow Phenomena. J. Appl. Phys., 27: 324-332.

Ng, K.M., H.T. Davis, and L.E. Scriven, 1978. Visualization Of Blob Mechanics In Flow Through Porous Media. Chem. Eng. Sci., 33: 1009-1017.

Ostendorf, D.W., R.J. Richards, and F.P. Beck, 1993. LNAPL Retention in Sandy Soils. Ground Water, 31: 285-292.

Pantazidou, M., and N. Sitar, 1993. Emplacement of Nonaqueous Liquids in the Vadose Zone. Water Resour. Res., 29: 705-722.

Parker, J.C., and R.J. Lenhard, 1987. A Model for Hysteretic Constitutive Relations Governing Multiphase Flow 1. Saturation-Pressure Relations. Water Resour. Res., 23: 2187-2196.

U.S. Coast Guard, 1984. Chemical Hazard Response Information System, (CHRIS), Vol. 2, Hazardous Chemical Data, U.S. Department of Transportation, Washington, D.C.

4. THREE-PHASE IMMISCIBLE FLUID MOVEMENT IN THE VICINITY OF TEXTURAL INTERFACES

Martin H. Schroth, Jonathan D. Istok and John S. Selker

Departments of Civil and Bioresource Engineering
Oregon State University, Corvallis, OR 97331

submitted to
Water Resources Research
February, 1996

4.1 Abstract

The movement of light nonaqueous-phase liquids (LNAPLs) in heterogeneous vadose environments is poorly understood. We investigated LNAPL movement in the vicinity of a sloping textural interface of fine-grained sand overlying coarse-grained sand, forming a capillary barrier. Two-dimensional experiments were conducted in a glass chamber (50 cm x 60 cm x 1.0 cm) using two grades of silica sand (12/20 and 30/40 sieve sizes) to create fine-over-coarse interfaces. LNAPL (Soltrol® 220) was released at the sand surface under constant water irrigation to simulate a point-source discharge above the interface. Light transmission was used to visually observe water and LNAPL flow paths. LNAPL movement strongly depended on the water saturation in the fine-grained layer above the interface. At very low water saturation, LNAPL was fully diverted along the interface, whereas at moderately high water saturation partial penetration of the LNAPL into the coarse-grained layer was observed. At very high water saturation, LNAPL was fully diverted parallel to the interface, supported on the zone of very high water saturation. Hysteretic effects were noticed for LNAPL movement in case of very high water saturation in the fine-grained layer in the vicinity of the interface. These experiments demonstrated the critical role water saturation plays in determining LNAPL disposition in a heterogeneous vadose zone.

4.2 Introduction

Contamination of soil and aquifer systems by light nonaqueous-phase liquids (LNAPLs) has become a wide-spread problem. Fuel spills and leaks from commercial and domestic underground storage facilities are examples of LNAPL releases which typically occur near the soil surface in the vadose zone. Improved knowledge of LNAPL transport mechanisms in the subsurface is required for correct risk assessment and

remediation design. Unfortunately, the understanding of LNAPL movement, particularly in heterogeneous vadose environments, is still incomplete.

A basic element of vadose zone heterogeneity exists when a layer of fine-grained porous medium overlays a coarse-grained porous medium and the textural interface between the two layers is inclined (Fig. 4.1a). These fine-over-coarse sloping textural interfaces, frequently encountered in bedded sedimentary deposits, may form capillary barriers. At a capillary barrier, infiltrating water is held in the fine-grained layer by capillary forces and is diverted downdip, parallel to the textural interface. As streamlines of infiltrating water converge near the textural interface, the water saturation in the fine-grained layer above the interface increases until water breakthrough occurs into the underlying coarse layer (Fig. 4.1a).

An early experimental study of water flow in an unsaturated soil containing a capillary barrier was conducted by Miyazaki (1988), who observed lateral flow at inclined interfaces during steady water percolation. Analytical expressions describing the water flow characteristics of capillary barriers as a function of porous media hydraulic properties, water infiltration rate and angle of inclination (dip) of the textural interface were presented by Ross (1990). In particular, Ross (1990) derived expressions for the water diversion capacity (the maximum flux of water which can be diverted parallel to a textural interface), and the diversion length (the distance between the updip limit of a capillary barrier and the location where water first breaks into the underlying coarse-grained layer, Fig. 4.1a). Steenhuis et al. (1990) conducted laboratory experiments that demonstrated the importance of fingered flow instabilities for the hydraulic behavior of capillary barrier systems, and derived an alternate equation for the diversion length that included soil hydraulic properties of both layers. Field experiments were conducted by Kung (1990a, b), in which the author found strong evidence of preferential flow paths in the vadose zone due to the presence of capillary barriers. Oldenburg and Pruess (1993) conducted numerical simulations for a capillary barrier system and found reasonable agreement with Ross's (1990) analytical equation for the diversion length, but concluded that their results were more consistent with the suggestions of Steenhuis et al. (1990).

(a)

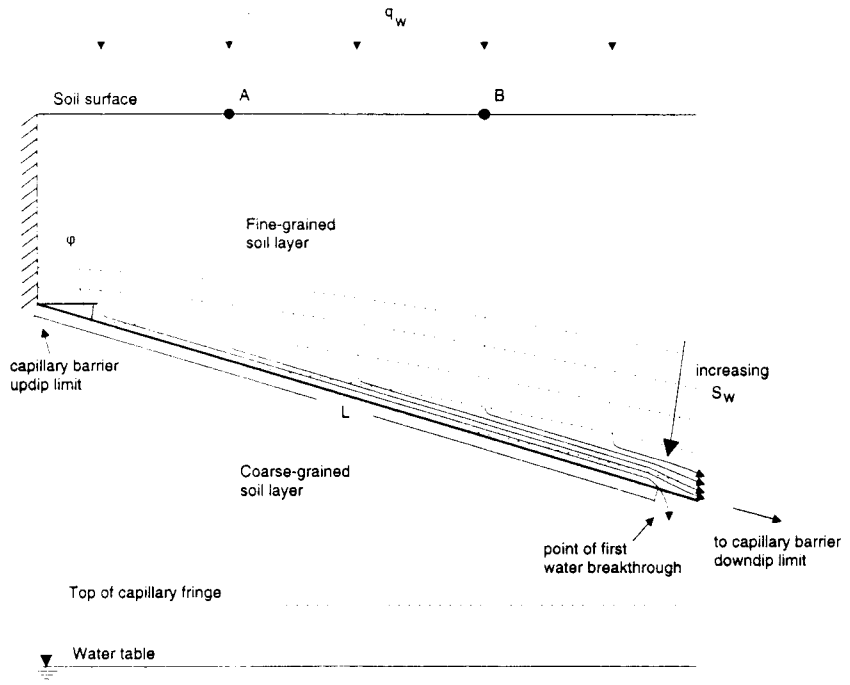

(b)

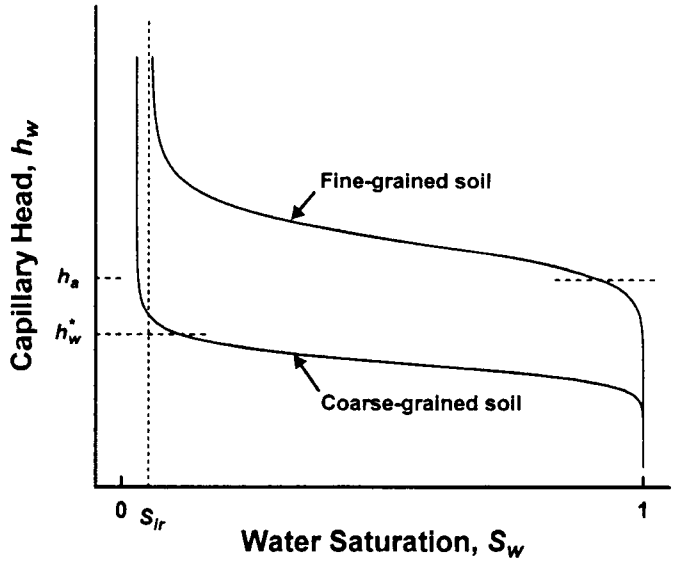

Figure 4.1 (a) Schematic of a textural interface forming a capillary barrier and its effect on water flow and water saturation in the fine-grained soil layer above the interface under steady-state water flow conditions, (b) Hypothetical water retention curves for a fine-grained and a coarse-grained soil used in the formation of a capillary barrier.

Based on Ross's (1990) analysis of the water diversion capacity of capillary barriers, Steenhuis et al. (1991) derived an improved equation for the diversion length, L:

$$L \leq \tan\varphi \left[\alpha^{-1}\left(\frac{K_s}{q_w} - 1\right) + \frac{K_s}{q_w}\left(h_a - h_w^*\right) \right] \qquad [1]$$

where φ is the slope of the textural interface, q_w is the unit flux of water entering the soil, h_a is the capillary head (defined on a water-height equivalent basis and taken to be positive) at which air effectively enters the fine-grained soil, h_w^* is the capillary head at which water effectively enters the coarse-grained soil, K_s is the saturated hydraulic conductivity of the fine-grained soil, and α is a parameter of the unsaturated conductivity function for the fine-grained layer (Rijtema, 1965):

$$K = K_s \qquad \text{for } |\psi| < h_a \qquad [2a]$$

$$K = K_s \exp\left[\alpha(\psi + h_a)\right] \qquad \text{for } |\psi| \geq h_a \qquad [2b]$$

where K is the hydraulic conductivity of the fine-grained layer, and ψ is the water pressure potential (taken to be negative). Assumptions made in the derivation of (1) are that both the soil surface and the water table are "far" from the textural interface, i.e. unit gradient flow conditions exist both in the fine-grained layer above the textural interface and in the coarse-grained layer below the interface (Ross, 1990). In addition, a no-flow boundary is assumed to exist at the updip limit of the capillary barrier, and the downdip limit of the capillary barrier is assumed "far" from the point of first water breakthrough so that it has no influence on water flow where the capillary barrier is effective, i.e. where water diversion occurs (Fig. 4.1a). Recently, Stormont (1995) extended the theory of water diversion by capillary barriers to incorporate anisotropy in the hydraulic conductivity of the fine-grained layer above the textural interface into the equations of Ross (1990) and Steenhuis et al. (1991).

The diversion length L (eq. [1]) depends on properties of both the fine-grained (K_s, α, h_a) and the coarse-grained layers (h_w^*). Of particular interest here are capillary

heads h_a and h_w^*. In order to obtain breakthrough of water into the coarse-grained layer, the capillary head of water, h_w, in the fine-grained layer has to decrease to h_w^* (Fig. 4.1b). In soils of uniform particle size distribution, the water saturation may have to increase to almost unity to achieve a sufficient decrease in h_w. As a consequence, a zone of increasing water saturation in the fine layer just above the textural interface will form between the updip limit of the capillary barrier and the point of first water breakthrough (Fig. 4.1a).

While water flow and aqueous-phase solute transport play important roles in the possible contamination of soil and aquifer systems, other contaminants, i.e. NAPLs, migrate through the subsurface as a separate liquid phase. Numerous researchers have investigated LNAPL movement in the vadose zone. Ostendorf et al. (1993) modeled field data from a gasoline spill site containing a uniform medium sand and found good agreement between observed and predicted LNAPL saturations. Previously, Osborne and Sykes (1986) simulated the migration of a LNAPL in groundwater at a field site and concluded that the extent of the LNAPL migration was greatly sensitive to heterogeneities and anisotropies of porous media hydraulic properties. Similar results were obtained numerically by Kueper and Frind (1992) and experimentally by Poulsen and Kueper (1992), who both found high sensitivity of LNAPL migration to spatial heterogeneities in porous media permeabilities and fluid retention properties. Essaid et al. (1993) investigated the fluid distribution at a crude oil spill site and found that the oil saturation distribution appeared at least in part to be influenced by heterogeneities in porous media hydraulic properties.

Controlled laboratory experiments of LNAPL infiltration in the vadose zone have been conducted by several researchers. One-dimensional vertical column experiments were conducted by Abdul (1988) in a homogeneous sandy porous medium using diesel fuel as LNAPL. He concluded that lateral spreading through the zone above a water table was a preferred mechanism for LNAPL redistribution in the vadose zone. Cary et al. (1989b) used hydrocarbon oils of different viscosities in columns homogeneously packed with silt loam and loamy sand soils to show that LNAPL infiltration was predictable using nonhysteretic soil-water retention and conductivity relationships and LNAPL

physical properties. Less agreement between observed and predicted LNAPL movement was obtained in columns packed with a uniform sand (Cary et al., 1989a), which the authors attributed in part to the effect of hysteresis (which was neglected) in their model. To investigate the geometry and position of LNAPL lenses that form in porous media near the water table, Schroth et al. (1995) conducted two-dimensional experiments using homogeneous sand packs. They observed that LNAPL lenses formed in the upper portion of the sand capillary fringe, accompanied by significant lateral spreading of LNAPL.

Cary et al. (1994) conducted LNAPL infiltration and redistribution experiments in one-dimensional vertical columns packed with horizontal layers of soils of different texture. The authors observed effects of layering on the distribution of water and LNAPL, and their experiments provided useful information for the verification of a predictive model for immiscible fluid flow. Unfortunately, the one-dimensional character of the experiments, i.e. the enforced fluid flow perpendicular to textural interfaces, severely limited a more general analysis of the influence of heterogeneity on immiscible fluid flow. Pantazidou and Sitar (1993) conducted two-dimensional LNAPL infiltration experiments in unsaturated homogeneous as well as heterogeneous (layered) sand packs. They found that LNAPL movement was strongly dependent on the number and horizontal continuity of layers and that in general more lateral spreading of LNAPL occurred in layered than in homogeneous sand packs. However, they did not analyze LNAPL flow behavior at fine-over-coarse textural interfaces in detail, and no comparison between LNAPL and water flow at these interfaces was provided. In addition, hysteretic effects on LNAPL and water flow in the vicinity of textural interfaces have not been addressed.

The main objective of this research was to study LNAPL movement in the vicinity of sloping textural interfaces that form capillary barriers. In particular, we wanted to determine the nature of interaction between LNAPL movement in the vicinity of capillary barriers and the degree of water saturation in the fine-grained layer above the interface. In addition, we wanted to determine if LNAPL and water exhibit parallel flow paths in the vicinity of capillary barriers and whether hysteresis plays an important role

for the LNAPL flow pattern. Finally, we wanted to compare our experimental findings to flow predictions based upon multiphase and capillary barrier flow theory.

4.3 Hypothesis for LNAPL Movement

Prediction of NAPL movement in porous media requires a model for constitutive conductivity-saturation-pressure (*K-S-P*) relationships for three-phase air-NAPL-water systems. A model which includes the effects of hysteresis and nonwetting fluid entrapment was developed by Lenhard and Parker (1987) and Parker and Lenhard (1987), and experimentally verified by Lenhard (1992) for a mixture of glass beads as well as a sand. In general, the total pore space in three-phase air-NAPL-water systems is shared by air, NAPL and water, such that $S_a + S_o + S_w = 1$, where S_a is the air saturation, S_o is the NAPL saturation ("o" stands for "oil" and is commonly used in formulae to refer to NAPL) and S_w is the water saturation. Here, the saturation of any fluid i (air, NAPL, water) is defined as $S_i = \theta_i / n$, where θ_i is the volumetric fluid content of fluid i, and n is the porous medium porosity. Assuming that the porous medium is water-wet, the wettability increases in the order of air < NAPL < water. Consequently, when three fluid phases are present, the smallest pores will be occupied by water, intermediate size pores will be occupied by NAPL, and the largest pores will be air-filled. When nonwetting fluid entrapment is negligible, S_w and the total liquid saturation, S_t, with $S_t = S_w + S_o$, determine the pore sizes in which air-NAPL and NAPL-water interfaces reside. Fluid pressures and relative permeabilities are directly controlled by the location of these interfaces. Hence, the knowledge of pore sizes where air-NAPL and NAPL-water interfaces are located is critical for the prediction of NAPL movement in three-phase air-NAPL water systems through constitutive *K-S-P* relationships (Lenhard, 1992).

Our hypothesis is that LNAPL movement in the vicinity of capillary barriers is dependent on the degree of water saturation in the fine-grained layer above the sloping textural interface. To explain our hypothesis, we will consider LNAPL movement under three distinctly different conditions of water saturation in that layer.

4.3.1 *LNAPL Flow at Very Low Water Saturation*

We first consider LNAPL movement in the vicinity of a capillary barrier at a location where the water saturation in the fine-grained layer above the interface is very low. For example, under hydrostatic conditions ($q_w = 0$ in eq. [1]), and if the water table is located "far" below the textural interface (Fig. 4.1a), the water saturation in the fine-grained layer at any point along the interface will be near the irreducible water saturation, S_{ir} (Fig. 4.1b). LNAPL released at location A or B (Fig. 4.1a) will essentially have pores of all sizes available for movement. Hence, this three-phase air-LNAPL-water system may be regarded as a two-phase air-LNAPL system ($S_t \approx S_o$). Since LNAPL is the wetting fluid in an air-LNAPL system, it should reside in smaller pores, whereas larger pores should be air-filled. Therefore, similar to the diversion of water along a sloping textural interface, LNAPL should be retained in the fine-grained layer by capillary forces and diverted parallel to the interface. If we consider the LNAPL to be released as a point-source (point A or B, Fig. 4.1a), once diverted, no breakthrough like in the case of water diversion is expected.

4.3.2 *LNAPL Flow at Moderately High Water Saturation*

Next, let us consider LNAPL movement in the vicinity of a capillary barrier where the water saturation in the fine-grained layer above the interface is moderately high, e.g. under steady-state water flow ($0 < q_w << K_s$ in eq. [1]), and in the vicinity of the capillary barrier updip limit (Fig. 4.1a). In this case, a significant amount of large pores are still air-filled. LNAPL released at location A will migrate vertically downward in pores sizes larger than those occupied by water (Fig. 4.1a). As the LNAPL encounters the zone of moderately high water saturation above the textural interface, it will be forced to move into larger pores than those occupied by water. Hence, the LNAPL capillary head must decrease. This decrease in capillary head may be sufficient to allow LNAPL entry into the coarse-grained soil layer.

4.3.3 *LNAPL Flow at Very High Water Saturation*

Finally, we consider LNAPL movement in the vicinity of a capillary barrier where the water saturation in the fine-grained layer above the interface is very high. This will be the case e.g. under steady-state water flow ($0 < q_w < Ks$ in eq. [1]), and in the upgradient vicinity of the point of first water breakthrough (Fig. 4.1a). LNAPL released at location B will migrate vertically downward toward the textural interface in similar pore sizes as in the previous case (infiltration at location A, Fig. 4.1a). However, in this case it encounters a zone above the textural interface where almost all of the pores are water-filled. Under these conditions, the LNAPL may not be able to reach the textural interface at all, but may emplace itself in this zone of very high water saturation, much like LNAPL lenses form in the capillary fringe of a porous medium (Abdul, 1988; Schroth et al., 1995). Due to the hydraulic gradient in this zone of very high water saturation, the LNAPL would be expected to move downgradient, parallel to the textural interface, supported in the upper portion of the zone of very high water saturation.

4.3.4 *Effects of Hysteresis on LNAPL Flow*

So far, we discussed some aspects of *S-P* relationships which may be important to LNAPL movement in the vicinity of capillary barriers. However, *S-P* relationships for three-phase air-NAPL-water systems are also known to be hysteretic, depending on both S_w and S_t path histories (Parker and Lenhard, 1987). Thus, for any given pair of S_w and S_t, the corresponding capillary heads will depend on the respective S_w and S_t path histories, which could lead to alterations in the observed LNAPL flow pattern in the vicinity of a capillary barrier. In addition, *K-S* relationships may also be effected by hysteresis (Lenhard and Parker, 1987). When a wetting fluid imbibes into pores filled with nonwetting fluid, entrapment of nonwetting fluid within the body of wetting fluid may occur. As a consequence, the interface between the bulk nonwetting and the bulk wetting fluid will reside in larger pore sizes than without entrapment of nonwetting fluid. This

may increase the relative conductivity of the wetting fluid, particularly for high wetting fluid saturations (Lenhard and Parker, 1987), and could play a role in the simultaneous movement of water and LNAPL in the vicinity of a capillary barrier by restricting LNAPL flow to larger pore sizes.

4.4 **Materials and Methods**

Transient two-dimensional LNAPL flow experiments were performed in a chamber designed to simulate three-phase immiscible fluid movement in the vicinity of a capillary barrier, generated by a sloping layer of fine-grained sand overlying a layer of coarse-grained sand. The chamber consisted of two 1.27 cm thick glass panels (50 cm wide x 60 cm high), separated by 1.0 cm thick aluminum spacers with inset rubber seals (Fig. 4.2). Experiments 1 to 5 were conducted using hydrostatic conditions and steady-state water flow to generate different water saturation conditions in the fine-grained layer above the interface (Tab. 4.1). Three additional steady-state water flow experiments (no. 6 to 8) were conducted to include hysteretic effects in the initial water flow conditions (Tab. 4.1). A model LNAPL was released at two locations at the sand surface and light transmission was used to qualitatively observe LNAPL and water movement in the vicinity of the capillary barrier.

4.4.1 *Porous Media and Fluid Properties*

Experiments were conducted using two different grades of silica sand (Accusand® 12/20 and 30/40 sieve sizes), manufactured by Unimin Corp., Le Sueur, MN. The sands were obtained prewashed (with water) and presieved by the manufacturer. Both sands feature high uniformity (d_{60}/d_{10} is 1.23 for 12/20 sand, 1.21 for 30/40 sand), high sphericity (0.9 for both sands), high chemical purity and very low organic matter content (< 0.04%) (Schroth et al., 1996). Hysteretic water retention functions, determined by

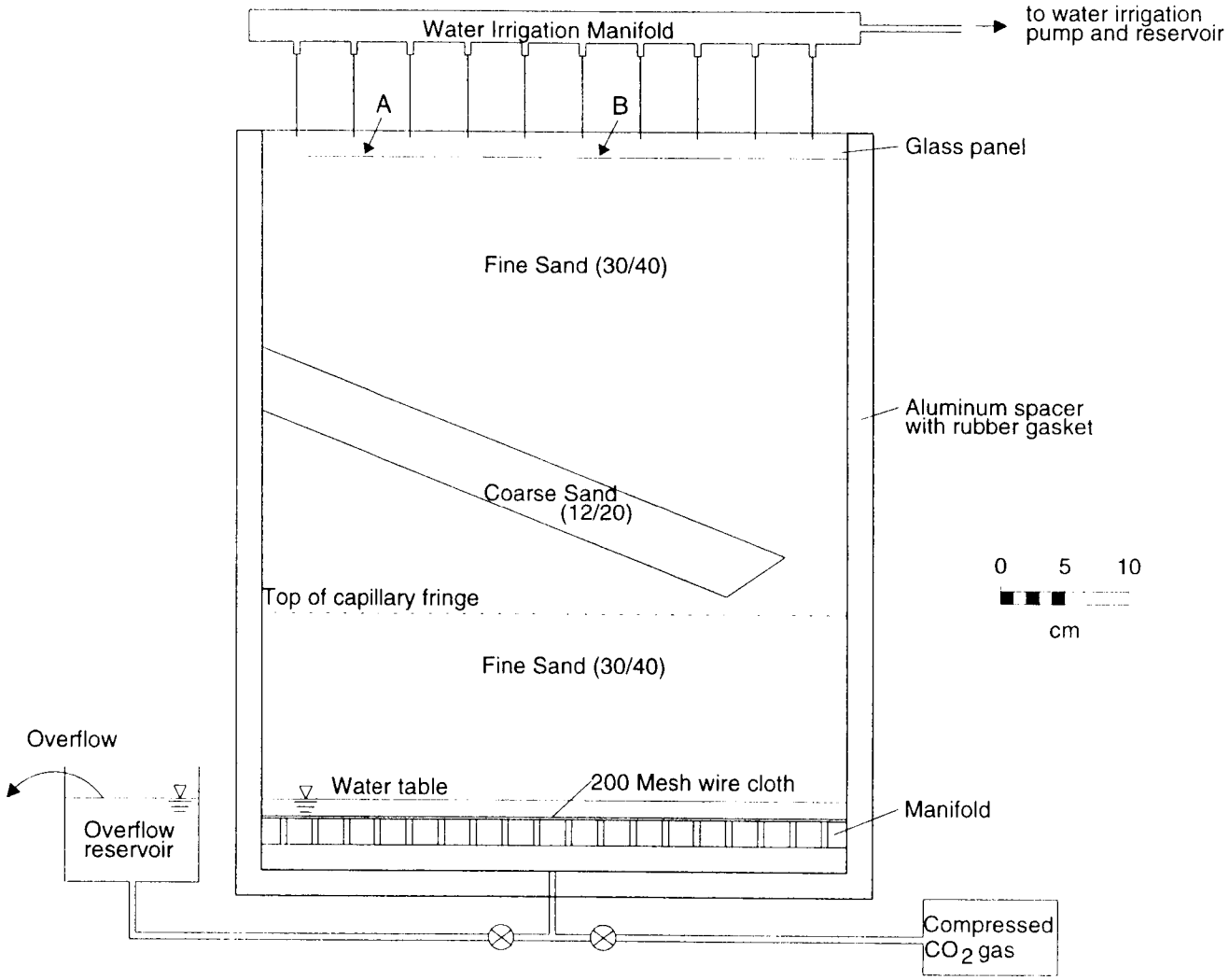

Figure 4.2 Schematic of the two-dimensional experimental chamber.

Table 4.1 Summary of two-dimensional LNAPL release experiments.

Experiment No.*	Water saturation, S_w†	Water S-P path prior to LNAPL release	Duration of LNAPL release [min]	LNAPL Volume released [cm^3]	LNAPL penetration‡ observed
			LNAPL release - Location A		
1	very low	main drainage	77	20.8	no
2	very low	main drainage	116§	30.2	no
3	moderately high	main drainage	45	12.0	yes
4	moderately high	main drainage	43	12.0	yes
5	moderately high	main drainage	67	16.1	yes
6	moderately high	primary imbibition	47	12.0	yes
7	moderately high	primary imbibition	41	12.0	yes
8	moderately high	primary imbibition	45	12.0	yes
			LNAPL release - Location B		
3	very high	main drainage	45	12.0	no
4	very high	main drainage	46	12.0	no
5	very high	main drainage	39	12.0	no
6	very high	primary imbibition	39	12.0	no
7	very high	primary imbibition	41	12.7	no
8	very high	primary imbibition	45	12.0	no

* Experiments 1 and 2 conducted under hydrostatic conditions, experiments 3 to 8 at steady-state water flow (q_w = 0.23 cm/min).

† saturation in fine-grained (30/40) sand just above the textural interface at horizontal position where LNAPL plume encounters the interface.

‡ penetration of LNAPL into coarse-grained (12/20) sand.

§ continuous LNAPL release for the duration of the experiment.

Schroth et al. (1996) from water retention measurements obtained using the method of Lenhard (1992), feature well-defined air and water entry pressures (Fig. 4.3). Prior to conducting experiments, the sands were rinsed with distilled water to remove fine dusts generated during transport. The sands were then oven dried at 50° C. No further treatment was employed.

LNAPL movement in the vicinity of capillary barriers was investigated using Soltrol® 220 (Phillips Petroleum Co., Bartlesville, OK), hereafter referred to as Soltrol, which has been widely used to study LNAPL behavior in the subsurface environment (e.g. Lenhard (1992); Cary et al. (1989a, b); Cary et al. (1994)). Soltrol is a mixture of branched C_{13} to C_{17} alkanes that occur in a variety of petrochemical products, e.g. gasoline. Soltrol has a specific gravity of 0.81, a negligible solubility in water, a very low volatility at room temperature as well as a low health hazard. To improve the delineation between water and Soltrol by light transmission, Soltrol was dyed with 0.01% by weight of Sudan® III (Matheson, Coleman and Bell, Manufacturing Chemists, Norwood, OH), a hydrophobic stain of bright red color which is virtually insoluble in water. Distilled water was used as the aqueous phase in our experiments.

4.4.2 *Chamber Packing and Water Saturation*

Capillary barriers were built by packing the chamber in three consecutive steps with 30/40 sand, 12/20 sand, and again with 30/40 sand. Before packing the chamber with sand, the desired contour of the capillary barrier was drawn onto the front glass panel. In all experiments, the capillary barrier had a slope of 21.8 degrees (4:10), a vertical thickness of 5.0 cm, was located 17 cm below the sand surface at the left edge of the sand pack, and had its downdip limit 5.0 cm (horizontally) from the right edge of the sand pack (Fig. 4.2). Slope and position of the capillary barrier were predetermined to assure that the slope was smaller than the angle of repose for either sand grade and that sufficient cross-sectional area existed between the downdip limit and the right edge of the sand pack (within the 30/40 sand) to allow unrestricted water movement in the case of

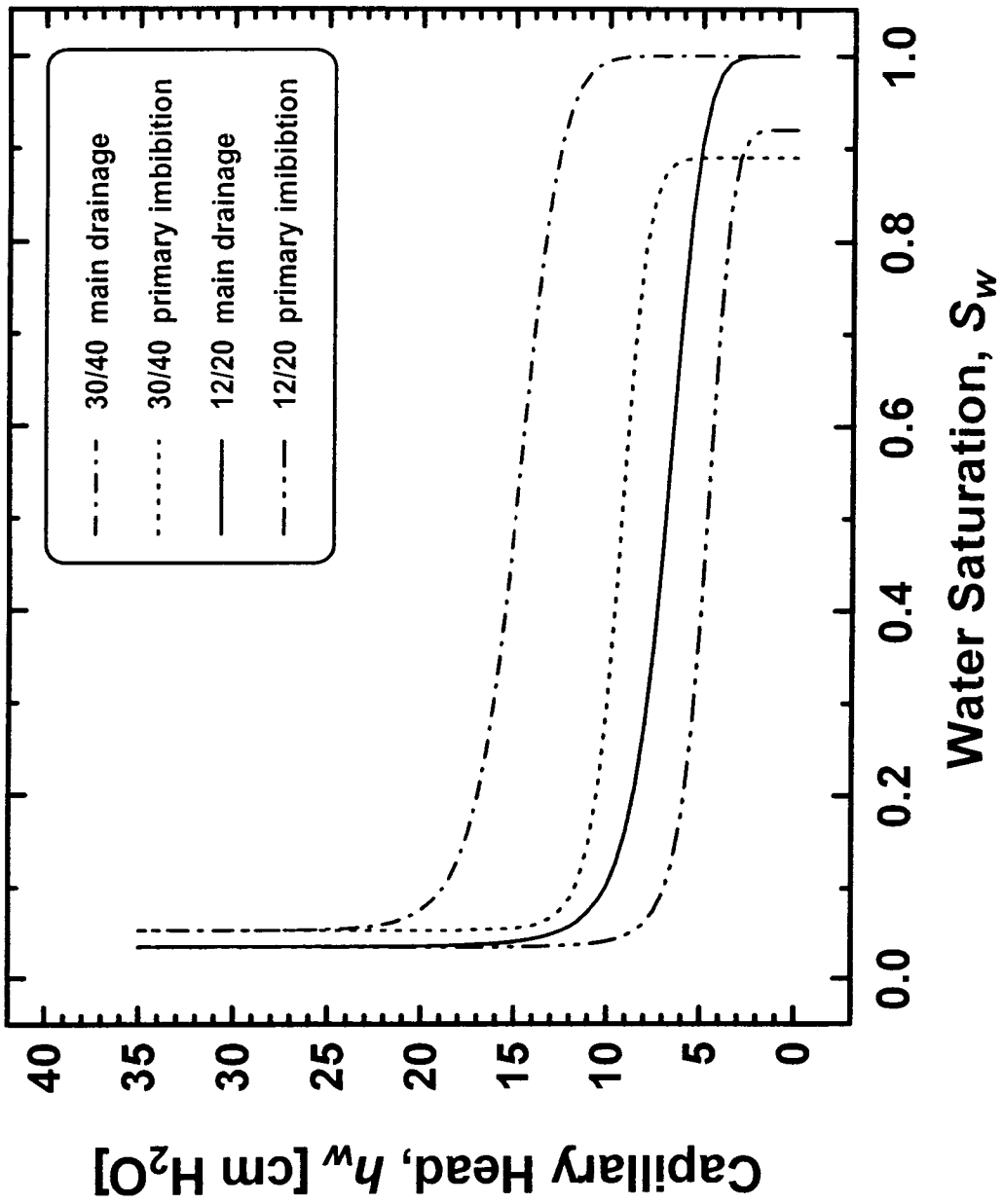

Figure 4.3 Water retention functions (main drainage and primary imbibition) obtained by fitting van Genuchten's (1980) equation to hysteretic air-water saturation-pressure (S-P) measurements conducted using the method of Lenhard (1992).

full water diversion by the barrier. To pack each sand grade, air-dry sand was continuously poured through a prismatic funnel that fit the full width of the chamber. This funnel contained a series of coarse sieves which randomized particle motion as the sand fell into the chamber to generate a homogeneous packing. Continuous pouring was used to prevent local gradations in particle size, which were observed to form when particle flow was interrupted during packing. To minimize the effect of packing interruption at interfaces between different sand grades when building the capillary barrier, more sand of each grade than required to build the barrier was packed into the chamber. Excess sand was then removed from the top of the pack using a narrow tube connected to a vacuum until the pack boundary matched the desired contour of the capillary barrier. The total mass of the sand pack and the packing height were recorded for each experiment and used to calculate the average porosity.

In all experiments, the sand packed chamber was first purged of air with CO_2 gas injected through the manifold which formed the lower porous medium boundary (Fig. 4.2). The sand pack was then water-saturated from below by connecting the manifold to a water reservoir. Flushing with CO_2, which has a higher solubility in water than air, and water-saturating the sand pack from below were employed to minimize the amount of air entrapment during water imbibition. Any small quantity of initially trapped CO_2 was assumed to dissolve in the water. Visual observation showed no visible gas bubbles in the sand pack following water saturation.

The computed average porosity of the sand packs (combined 12/20 and 30/40 sand) was 0.35 ± 0.01, indicating that consistent packing of the experimental chamber was achieved. This porosity is identical to sand porosities that existed during water retention measurements for these sands (Schroth et al., 1996). Hence, the water retention functions presented in Fig. 4.3 should be representative of the S-P relationships of the two sand grades packed in our experimental chamber. Local packing variability was visible in the slightly wavy appearance of the capillary fringe. This phenomenon has been observed previously (Schroth et al., 1995). However, its effect on the LNAPL flow experiments was negligible, as verified by the consistent results found in replicate runs (each freshly packed) for each set of boundary conditions.

4.4.3 *LNAPL Flow Experiments*

To generate conditions of very low water saturation in the fine-grained sand layer above the textural interface, two LNAPL flow experiments (no. 1 and 2) were conducted under hydrostatic conditions (Tab. 4.1). The sand pack was first water saturated as described in the previous section. Then the water reservoir was lowered and water was allowed to monotonically drain, creating a capillary fringe approximately 5 cm below the lowest point of the capillary barrier (Fig. 4.2). The top of the chamber was covered with plastic wrap to minimize water evaporation. Small holes were punched in the plastic wrap to insure that the air inside the chamber remained at atmospheric pressure. At least 12 hours were allowed for drainage of water prior to the release of LNAPL. Using a syringe needle connected to a peristaltic pump and LNAPL reservoir, Soltrol was then released at the sand surface at location A (Fig. 4.2) at a flow rate of 0.28 ± 0.02 cm^3/min. In experiment 1, the LNAPL release was terminated when the developing plume reached the textural interface. In experiment 2, LNAPL release was continuous until the end of the experiment. The mass of LNAPL released (measured gravimetrically) and the duration of the LNAPL release were recorded for all experiments (Tab. 4.1).

To generate conditions of moderately high and very high water saturation in the fine-grained sand layer above the textural interface, three LNAPL flow experiments (no. 3 to 5) were conducted under steady-state water flow conditions. The sand pack was first water saturated as described in the previous section. Then a water irrigation manifold containing ten equally-spaced syringe needles, was placed on top of the chamber (Fig. 4.2), and water was applied to the soil surface at a rate of 0.23 cm/min, supplied by a piston pump. During irrigation, the water reservoir was lowered to establish a water table at the bottom of the chamber above the manifold (Fig. 4.2), thus creating a main drainage water saturation path within both sands (Fig. 4.3). At least 12 hours under continuous irrigation were allowed for drainage of water prior to the release of LNAPL. Using a syringe needle connected to a peristaltic pump and LNAPL reservoir, a pulse of Soltrol was then released at location B at the sand surface (Fig. 4.2) at a flow rate of 0.28 ± 0.02 cm^3/min for between 43 and 67 minutes. A similar Soltrol pulse was released at location

A (Fig. 4.2) approximately 2.5 h after the release of Soltrol at location B (Tab. 4.1), when the plume released at location B had reached the vicinity of the textural interface. The experiments were terminated once the developing plume of LNAPL released at location A reached the plume of LNAPL released at location B.

To include hysteresis in the initial water flow for conditions of moderately high and very high water saturation in the fine-grained sand layer above the interface, we conducted three additional LNAPL flow experiments (no. 6 to 8, Tab. 4.1). The sand pack was first water saturated as described in the previous section. Then the water reservoir was lowered and water was allowed to monotonically drain, creating a capillary fringe approximately 5 cm below the lowest point of the capillary barrier (Fig. 4.2). After at least 12 hours of drainage, a water irrigation manifold was placed on top of the chamber and water was applied to the sand surface at a rate of 0.23 cm/min, thus creating a primary imbibition water saturation path in the fine-grained layer above the interface (Fig. 4.3). Once steady-state water flow was reached, LNAPL releases were performed using procedures described in the previous paragraph.

4.4.4 *Water and NAPL Flow Visualization*

Light transmission was used to delineate water and LNAPL flow paths and areas of varying water saturation within the sand pack. A light source was positioned behind the experimental chamber and plastic film was taped to the front glass panel. To identify water flow paths during steady-state water flow experiments, we visually traced the movement of a blue dye (FD&C Blue #1, Crompton & Knowles, Reading, PA) by releasing approximately 1 ml at the left corner of the chamber at the sand surface prior to and after the release of LNAPL. The dye was flushed out of the sand pack prior to the release of LNAPL. LNAPL flow paths were recorded manually by tracing the outline of the dyed Soltrol plume on the plastic film. Areas of high water saturation within the sand pack were delineated by the brightness of light transmitted through the chamber and recorded manually on the plastic film. The ambient room temperature was kept constant

throughout the experiments at 23°C. No increase in fluid temperatures due to heat generated by the light source was observed.

4.5 **Results and Discussion**

4.5.1 *LNAPL Flow at Very Low Water Saturation*

Full diversion of the migrating LNAPL plume along the sloping textural interface was observed in experiments 1 and 2, in which the water saturation in the fine-grained sand layer above the textural interface was very low (Tab. 4.1). In other words, no portion of the LNAPL penetrated the underlying coarse-grained sand layer throughout the duration of the experiments. In experiment 1, the diversion of LNAPL along the textural interface occurred during LNAPL redistribution, since the LNAPL release at location A was terminated once the developing plume had reached the interface (Fig. 4.4). The experiment was terminated when LNAPL started to spill over the capillary barrier downdip limit. In experiment 2, LNAPL was released continuously until the experiment was terminated, eliminating redistribution (Fig. 4.5). While the LNAPL plumes in experiments 1 and 2 were similar in appearance, two differences were observed. First, the LNAPL plume in experiment 2 (Fig. 4.5) required less time to reach the capillary barrier downdip limit than the plume in experiment 1. Second, more lateral spreading of LNAPL in the fine-grained layer above the textural interface was noticed in experiment 1 (Fig. 4.4). Both observations may be attributed to the difference in LNAPL release. During LNAPL redistribution in experiment 1 (after the LNAPL release was terminated), S_o began to decrease in the zone where LNAPL migrated vertically downward, i.e. LNAPL drained from the pore space below the point of release. This caused an increase in the LNAPL capillary head, h_o, which, if S_o and S_w were measured quantitatively, could be predicted from water retention functions (Fig. 4.3) by applying appropriate scaling factors (Parker and Lenhard, 1987; Lenhard, 1994). As a result, capillary forces became

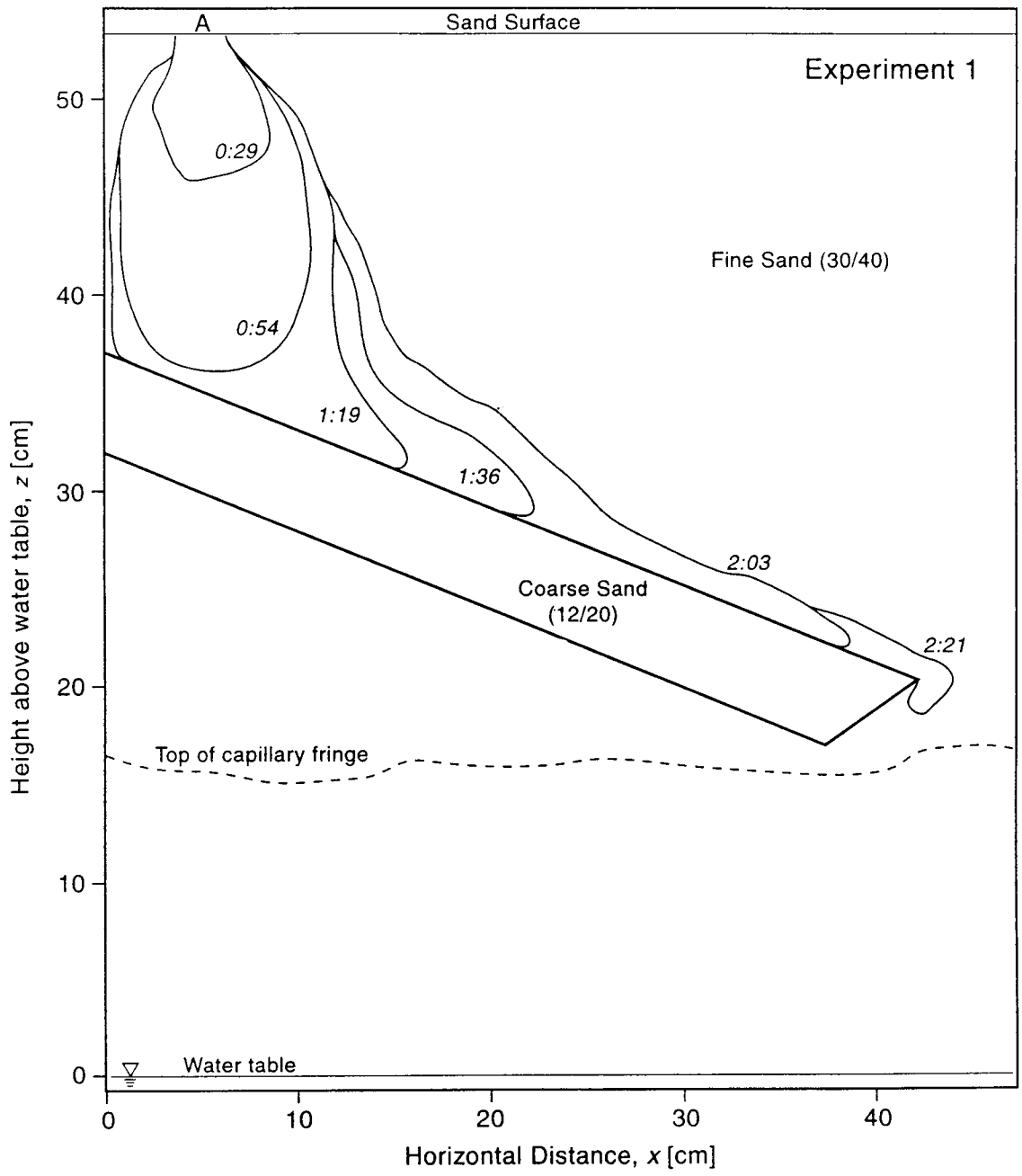

Figure 4.4 Full LNAPL diversion for very low water saturation in fine-grained sand layer above the textural interface under hydrostatic conditions. Plume boundaries are shown for elapsed times (hours:minutes) since start of LNAPL release. LNAPL release was terminated after 1h 17min

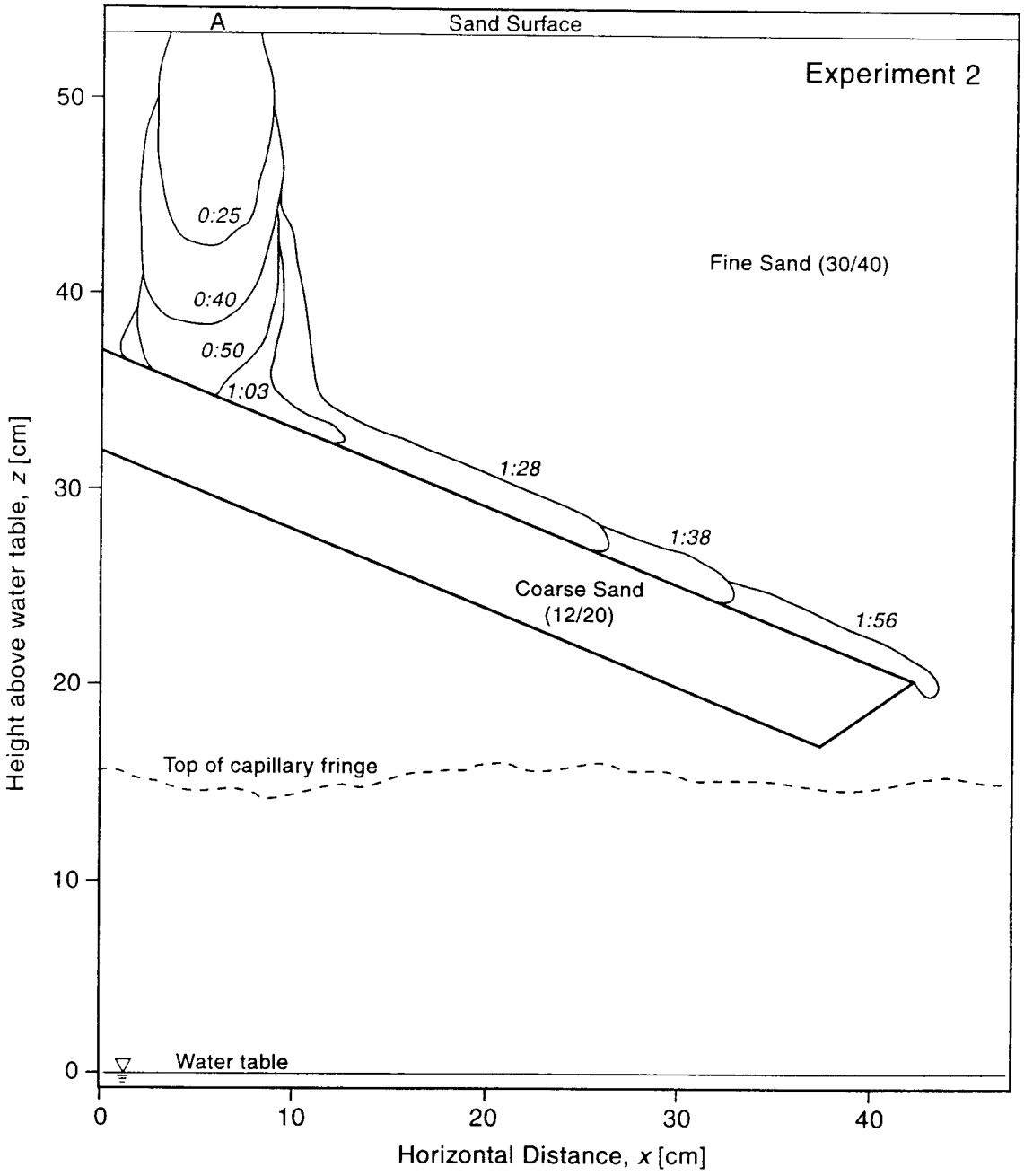

Figure 4.5 Full LNAPL diversion for very low water saturation in fine-grained sand layer above the textural interface under hydrostatic conditions. Plume boundaries are shown for elapsed times (hours:minutes) since start of LNAPL release. LNAPL release was continuous throughout the experiment.

dominant compared to the gravitational force, allowing for more lateral spreading of the LNAPL (Fig. 4.4). In addition, the increase in h_o caused a decrease in the total LNAPL potential, thus slowing down the movement of the LNAPL plume in experiment 1 compared to experiment 2 (Fig. 4.5).

While Figs. 4.4 and 4.5 show boundaries of migrating LNAPL plumes, they do not provide information on S_o within the confines of the plumes. In both experiments, a significant increase in S_o was visually observed just above the textural interface where the LNAPL plume reached the interface, compared to the zone where the LNAPL migrated vertically downward through the fine-grained layer. Once increased, S_o along the interface appeared fairly uniform, particularly in experiment 2. This phenomenon may be explained by analyzing experiment 2 in more detail (Fig. 4.5). At steady-state flow in the region well above the interface, the LNAPL is at approximately constant pressure in a unit gradient flow condition. At the interface, the cross-sectional area of flow is substantially reduced, and the potential gradient is reduced to $sin\ \varphi = 0.37$. The combined reduction of area and potential gradient implies an increase in LNAPL relative conductivity, K_{ro}, to maintain steady-state flow. This is obtained by way of increased S_o, as observed. At a sufficiently high LNAPL flux q_o, however, the increased saturation and decreased LNAPL capillary head at the interface may allow penetration of LNAPL into the underlying coarse media.

The observed behavior of full LNAPL diversion along the textural interface (Figs. 4.4 and 4.5) may have important implications with regard to the general disposition of LNAPL in a heterogeneous vadose environment. First, LNAPL spread extensively in the lateral direction away from the point of release. This is in agreement with findings of Pantazidou and Sitar (1993), who observed increased lateral LNAPL spreading in their heterogeneous (layered) sand pack experiments. Second, as observed for water flow (Kung, 1990a,b), flow of LNAPL is funneled near the textural interface, i.e. LNAPL migrates through a smaller cross-sectional area with increased K_{ro}. This may lead to less LNAPL left behind as residual, defined in this context as LNAPL retained in the vadose zone by capillary forces, as isolated LNAPL ganglia, or retained due to decreased LNAPL mobility caused by a small K_{ro} during drainage. Hence, more LNAPL may reach

and contaminate an underlying aquifer. Finally, due to the increase in K_{rn} by the mechanism of funneling, LNAPL migration is faster, and although diverted laterally, LNAPL may reach an aquifer sooner than by strict vertical migration. Note that since buoyancy effects did not enter our line of reasoning, this behavior would also be expected for dense NAPLs (DNAPLs) under these conditions.

4.5.2 *LNAPL Flow at Moderately High Water Saturation*

To generate conditions of variable S_w in the fine-grained sand layer above the textural interface, experiments 3 to 8 were conducted under steady-state water flow conditions. In experiments 3 to 5, water within both sands was on the main drainage *S-P* path prior to the release of LNAPL, whereas in experiments 6 to 8 water was on a primary imbibition *S-P* path in the fine-grained layer above the interface (Tab. 4.1). In all experiments, full water diversion along the textural interface was observed prior to the release of LNAPL, by tracing the movement of the blue dye (Fig. 4.6). In rare cases, some water breakthrough into the coarse-grained layer was observed near the downdip limit of the capillary barrier. This was attributed to local variability in packing causing a disruption of the pore size distribution in the coarse- or fine-grained sand layer at the textural interface, or may be due to the existence of instable wetting fronts (Steenhuis et al., 1991). These experiments were discarded and the chamber was repacked.

We computed the expected water diversion length L in our experiments using eq. [1]. For experiments 3 to 5, h_a and h_w^* were estimated from the main drainage water retention functions of the two sand grades, to equal 12.0 cm and 9.0 cm, respectively (Fig. 4.3). K_S of the fine-grained sand was 8.9 cm/min (Schroth et al., 1996). The value of $\alpha = 0.61$ cm^{-1} was determined from fitting eq. [2] to measured unsaturated hydraulic conductivity data of the fine-grained sand (Schroth et al., 1996). Using these values, we predicted $L \leq 71.2$ cm. To compute L for experiments 6 to 8, h_a and h_w^* were estimated from the primary imbibition water retention functions of the two sand grades, to equal 7.5 cm and 6.0 cm, respectively (Fig. 4.3). In this case, we predicted $L \leq 47.9$ cm.

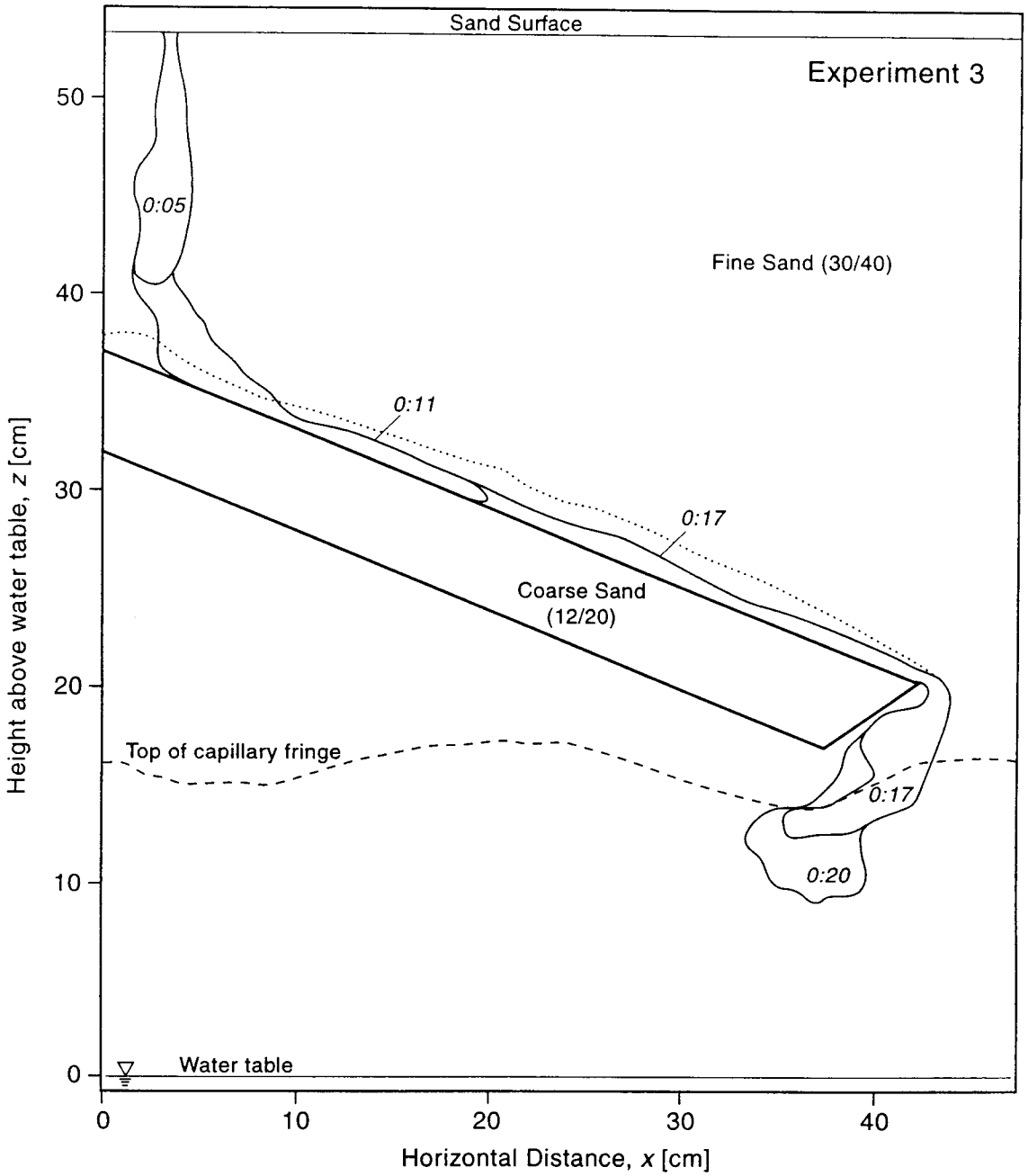

Figure 4.6 Water diversion in the vicinity of a sloping textural interface under steady-state water flow conditions prior to the release of LNAPL. Dye plume boundaries are shown for elapsed times since release (hours:minutes). The dotted line represents the contour of the zone of higher water saturation above the interface.

The actual length of the textural interface in our experiments was approximately 44.2 cm. Considering that the predicted value of L was > 44.2 cm in all cases, full water diversion along the textural interface should be expected. Uncertainty in the expected diversion length exists due to the inequality in eq. [1]. This inequality is due to an assumption in the initial derivation of the expression for the water diversion capacity of a capillary barrier (Ross, 1990). He mathematically solved a capillary barrier system at the "asymptotic downdip limit", which he defined as the location where the vertical unit flux of water into the coarse-grained sand equals the infiltration rate q_w, i.e. where the capillary barrier becomes totally ineffective in diverting water. Therefore, the water diversion length between the updip limit of the capillary barrier and the point of first water breakthrough may be smaller than predicted from the right side of (1). Ross (1990) pointed out, however, that the distance between the point of first water breakthrough and the asymptotic downdip limit may be fairly small, particularly in media with sharply contrasting hydraulic properties. Another factor to consider in our analysis is that we experimentally violated the assumption that the downdip limit of the capillary barrier was "far" downgradient from the point of first water breakthrough (Ross, 1990). As diverted water began to spill over the downdip limit of the capillary barrier, the hydraulic gradient increased because water could resume its flow in direction of the gravitational vector (Fig. 4.6). Due to the higher hydraulic gradient in this zone, the first point of water breakthrough may have shifted downgradient, allowing more water to be diverted along the textural interface. This should lead to an increase in L and contribute to our prediction of full water diversion in a positive manner. It may at least in part be the reason for our general observation of full water diversion along the textural interface in most cases.

Due to water diversion along the textural interface, a zone of higher S_w in the fine-grained sand layer above the textural interface was visually observed in all experiments under steady-state water flow conditions (Fig. 4.6). While no quantitative measurements of S_w were conducted, the thickness of the zone of higher S_w appeared to increase in the downgradient direction of the textural interface, which agrees with our theoretical analysis of a capillary barrier (Fig. 4.1a). However, the thickness of this zone decreased

near the end of the capillary barrier due to the increase in the hydraulic gradient, as discussed. In all experiments, a small increase in S_w was visible at the updip limit of the capillary barrier and was attributed to wall effects during packing (Fig. 4.6). However, its effect on the LNAPL release experiments was negligible.

LNAPL released at location A in experiments 3 to 5 encountered the textural interface in a zone where S_w in the fine-grained sand layer above the interface was moderately high (Tab. 4.1). In all cases, partial penetration of the LNAPL into the coarse-grained sand layer occurred, with a larger portion of the LNAPL being diverted, supported in the upper portion of the zone of moderately high S_w above the interface (Fig. 4.7). As LNAPL migrated vertically downward through the fine-grained layer, it moved through pores sizes larger than those occupied by percolating water. In the vicinity of the interface, the LNAPL plume encountered a zone of moderately high S_w, where pores occupied by water were unavailable to LNAPL flow, thus acting as a flow barrier. This caused S_o to increase, accompanied by an increase in K_{ro} and a decrease in h_o, allowing LNAPL to enter larger pore sizes. In addition, LNAPL may have displaced some water from the largest pores that were previously water-filled in this zone by lowering h_w locally. This could occur when LNAPL moved into air-filled pores, and air-water interfaces were replaced by air-NAPL and NAPL-water interfaces. In this case, h_w becomes a function of the NAPL-water interfacial tension and h_o, and may have decreased, causing water to drain from the largest pores it previously occupied. As a consequence of both processes, LNAPL was now able to penetrate the zone of moderately high S_w in larger pores. This allowed a portion of the LNAPL to reach the textural interface and penetrate the coarse-grained sand layer.

The observed LNAPL flow pattern of partial penetration into the coarse-grained layer (Fig. 4.7) may have important implications on general LNAPL disposition in heterogeneous vadose environments. When moving across the textural interface, a portion of LNAPL became isolated from the remainder of the plume which spread laterally. In addition, this portion was also isolated from the region of water movement, i.e. water did not flow across the interface at that location. This may lead to higher LNAPL residual in the vadose zone, which could become a long-term source of

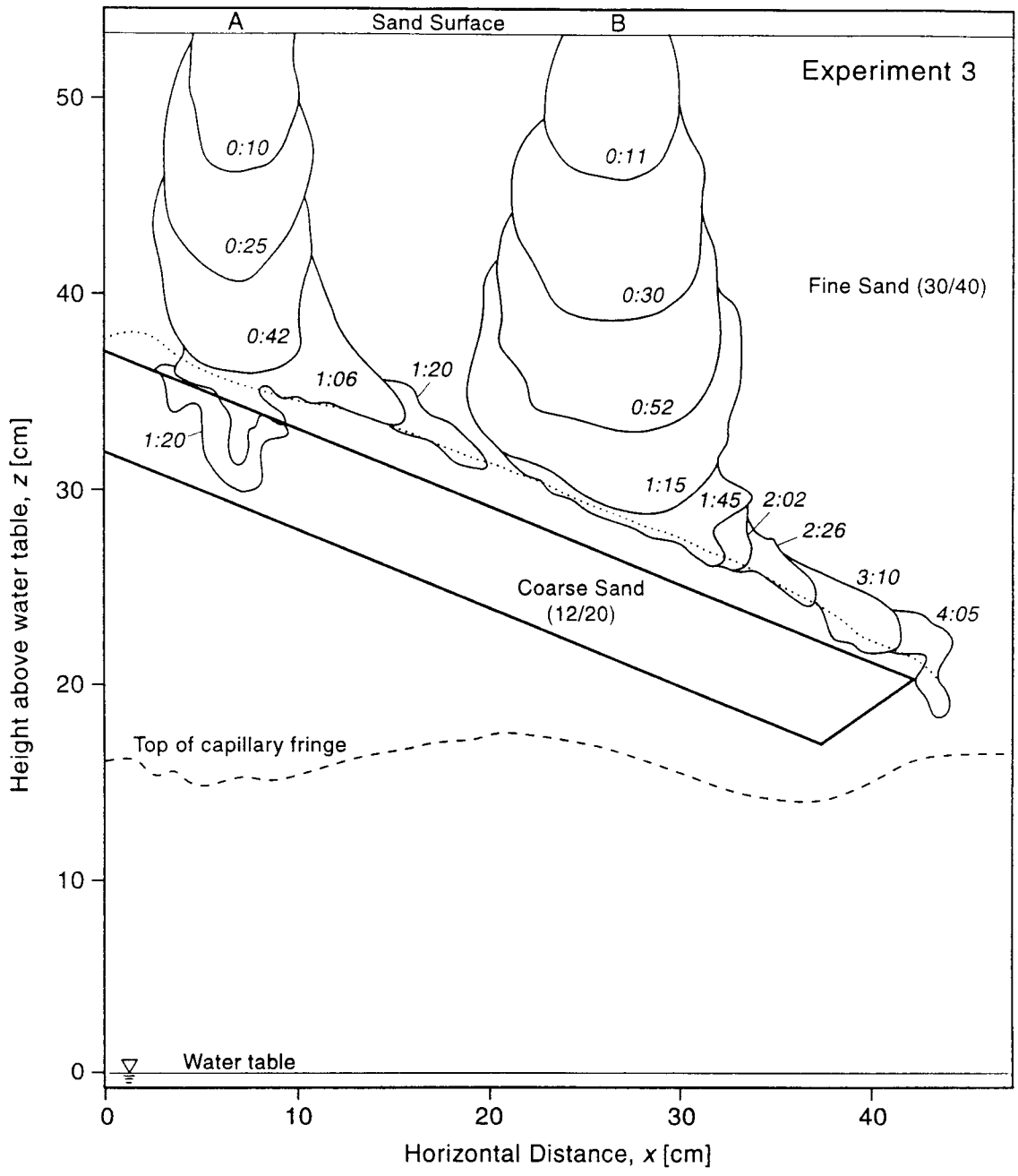

Figure 4.7 Partial LNAPL penetration for moderately high water saturation in fine-grained layer above the textural interface (LNAPL released at location A), and full LNAPL diversion for very high water saturation in fine-grained layer above the textural interface (LNAPL released at location B), under steady-state water flow conditions. Plume boundaries are shown for elapsed times (hours:minutes) since start of LNAPL release. Water was on the main drainage *S-P* path prior to the release of LNAPL. The dotted line represents the contour of the zone of higher water saturation above the interface.

contamination, particularly if the LNAPL were volatile. As a result, remediation of this portion of the LNAPL plume may be more complicated due to diverging LNAPL and water flow paths. Similar results would be expected in the case of DNAPLs, but with more DNAPL breakthrough into the coarse layer due to the lack of buoyancy effects.

A similar result was also obtained in experiment 5 when approximately 50% more LNAPL was released at location A under otherwise identical conditions (Fig. 4.8, Tab. 4.1). The total volume of LNAPL appeared to have no influence on the LNAPL flow path. As discussed earlier, q_o rather than the volume of LNAPL is expected to dictate which pore sizes are occupied by LNAPL, thus controlling *K-S-P* relationships and LNAPL flow behavior in the vicinity of a textural interface. No picture is provided for experiment 4, which was a replication of experiment 3.

4.5.3 *LNAPL Flow at Very High Water Saturation*

LNAPL released at location B in experiments 3 to 5 encountered the textural interface in a zone where S_w in the fine-grained sand layer above the interface was very high (Tab. 4.1). In all cases, full diversion of the LNAPL plume was observed, with LNAPL moving downgradient, supported in the upper portion of the zone of very high S_w above the interface (Figs. 4.7 and 4.8). This may be explained by considering the water retention functions of our media (Fig. 4.3). Due to the narrow particle size distributions of the media, conditions of almost complete water saturation ($S_w \approx 1$) must exist in the fine-grained sand prior to water entering the coarse-grained sand. Therefore, most pores in the fine-grained sand may be water-filled in the upgradient vicinity of the point of first water breakthrough (Fig. 4.1a). With the pore space effectively blocked by water, LNAPL diverted parallel to the interface, supported in the upper portion of the zone of very high S_w (Figs. 4.7 and 4.8). The latter agrees with findings of Schroth et al. (1995), who observed LNAPL emplacement in the upper portion of the capillary fringe in homogeneous sand packs. However, in our experiments the depth of LNAPL penetration into the zone of very high S_w was less than the depth of LNAPL penetration into the

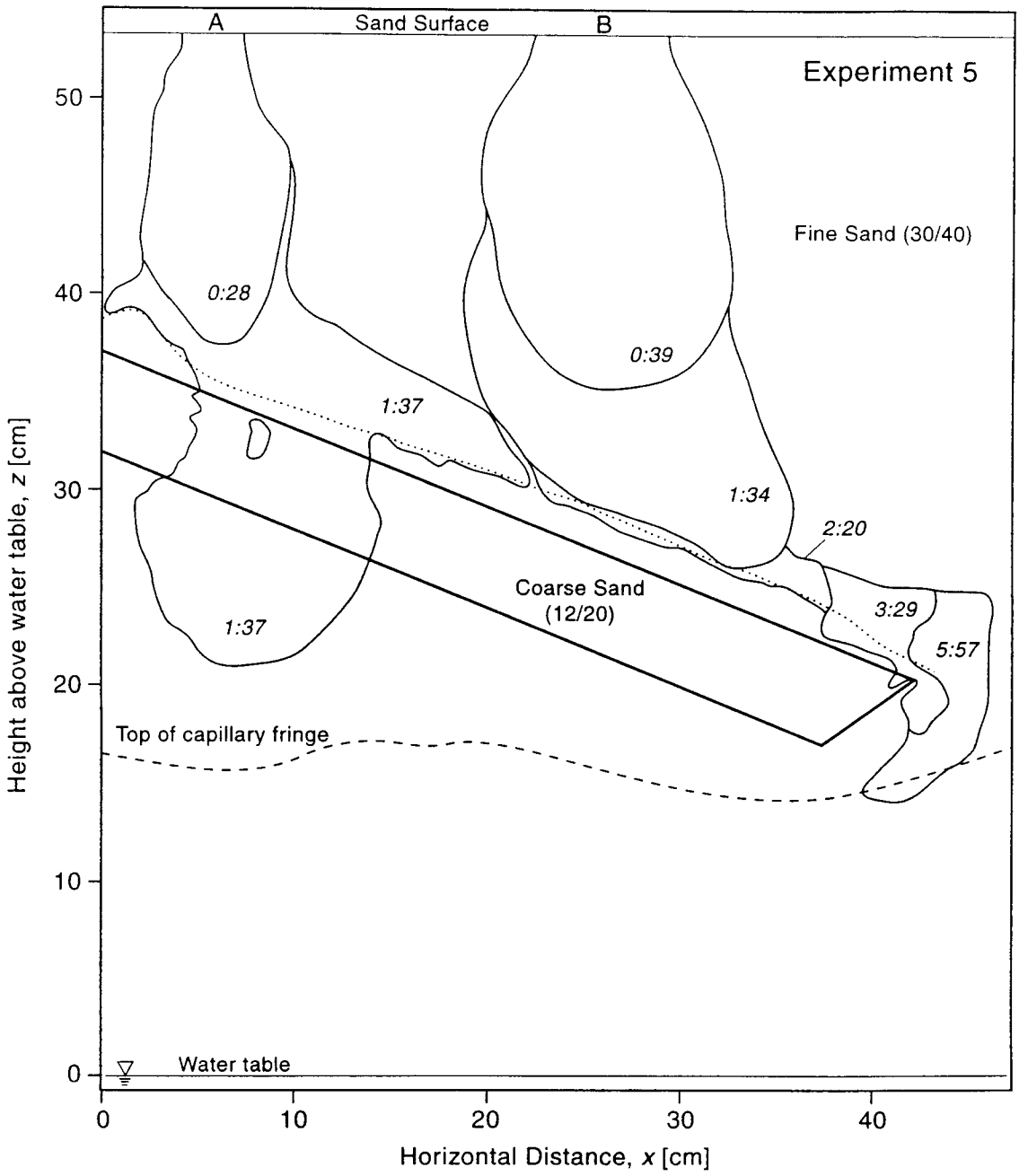

Figure 4.8 Partial LNAPL penetration for moderately high water saturation in fine-grained layer above the textural interface (larger LNAPL volume released at location A), and full LNAPL diversion for very high water saturation in fine-grained layer above the textural interface (LNAPL released at location B), under steady-state water flow conditions. Plume boundaries are shown for elapsed times (hours: minutes) since start of LNAPL release. Water was on the main drainage *S-P* path prior to the release of LNAPL. The dotted line represents the contour of the zone of higher water saturation above the interface.

capillary fringe (approximately 4.7 cm) observed by Schroth et al. (1995) for the identical LNAPL / sand combination . This is due to the downdip potential gradient in our experiments, which caused LNAPL to divert downgradient and thus increased h_o at the location where LNAPL first encountered the zone of very high S_w. Due to the proximity of the capillary barrier downdip limit and its influence on water flow, a small amount of LNAPL reached the interface at the downdip limit in experiment 5, and, while spilling over the downdip limit, penetrated the coarse-grained layer (Fig. 4.8).

While water was fully diverted along the capillary barrier prior to the release of LNAPL in experiments 3 to 5, the LNAPL addition at location B caused water breakthrough into the coarse-grained layer (data not shown). The breakthrough occurred approximately at the horizontal midpoint of the textural interface and continued downgradient along the interface. During LNAPL emplacement in the upper portion of the zone of very high S_w, water drained from this zone due to a decrease in h_w, as discussed earlier. Having less pore space available for water flow near the interface increased S_w in the fine-grained layer upstream of the LNAPL plume, accompanied by a decrease in h_w. This decrease of h_w may have caused water to enter the coarse-grained layer.

Water and LNAPL flow paths, as a consequence, were partially diverging under conditions of very high S_w in the fine-grained layer above the interface. Lateral movement of LNAPL away from the point of release occurred due to full LNAPL diversion, while water breakthrough into the coarse-grained layer was observed. Due to the lack of buoyancy, different results would be expected for DNAPL flow patterns in this case.

4.5.4 *Effects of Hysteresis on LNAPL Flow*

In experiments 6 to 8, we introduced additional hysteresis into the system prior to the release of LNAPL by allowing water to be on a primary imbibition path in the fine-grained layer above the interface (Tab. 4.1). In comparison, water was on the main

drainage path in experiments 3 to 5 prior to the LNAPL release (see methods section for LNAPL flow experiments, Fig. 4.3). Note that hysteretic conditions were present in all experiments due to the imbibition of LNAPL upon release at the sand surface, i.e. S_t was on an imbibition path during LNAPL release, followed by a draining path during LNAPL redistribution.

In general, effects of hysteresis on LNAPL flow patterns appeared to be small. This may be due to specific conditions (S_w, S_t) during our experiments, or due to the fact that some hysteretic effects were present in all experiments. When LNAPL was released at location A in experiments 6 to 8, similar LNAPL flow patterns were observed as in experiments 3 to 5 (Fig. 4.9, Tab. 4.1). While it appeared that a slightly larger portion of the released LNAPL penetrated the coarse-grained layer in experiments 3 to 5, this observation remained uncertain due to the qualitative character of the methods employed. More differences between experiments 3 to 5 and experiments 6 to 8 existed when LNAPL was released at location B. Although the same basic flow pattern of full diversion of LNAPL was observed, faster migration of the LNAPL plume during diversion occurred in experiments 6 to 8 (Fig. 4.9). In addition, the diverted LNAPL plume remained further above the interface in experiments 6 to 8 near the downdip limit of the capillary barrier (Fig. 4.9). Both observations may be due to hysteretic effects, in that an increase in K_{ro} may have occurred due to the entrapment of nonwetting fluid (air in water and air in LNAPL) in these experiments. In agreement with Lenhard and Parker (1987), we would expect such an effect to be most pronounced at very high wetting fluid saturations (S_w, S_t). Due to the entrapment of air in water, water provided a barrier to LNAPL flow in even larger pore sizes, forcing the LNAPL to divert further above the textural interface. No figures are provided for experiments 7 and 8, which were replicates of experiment 6 with similar results (Tab. 4.1).

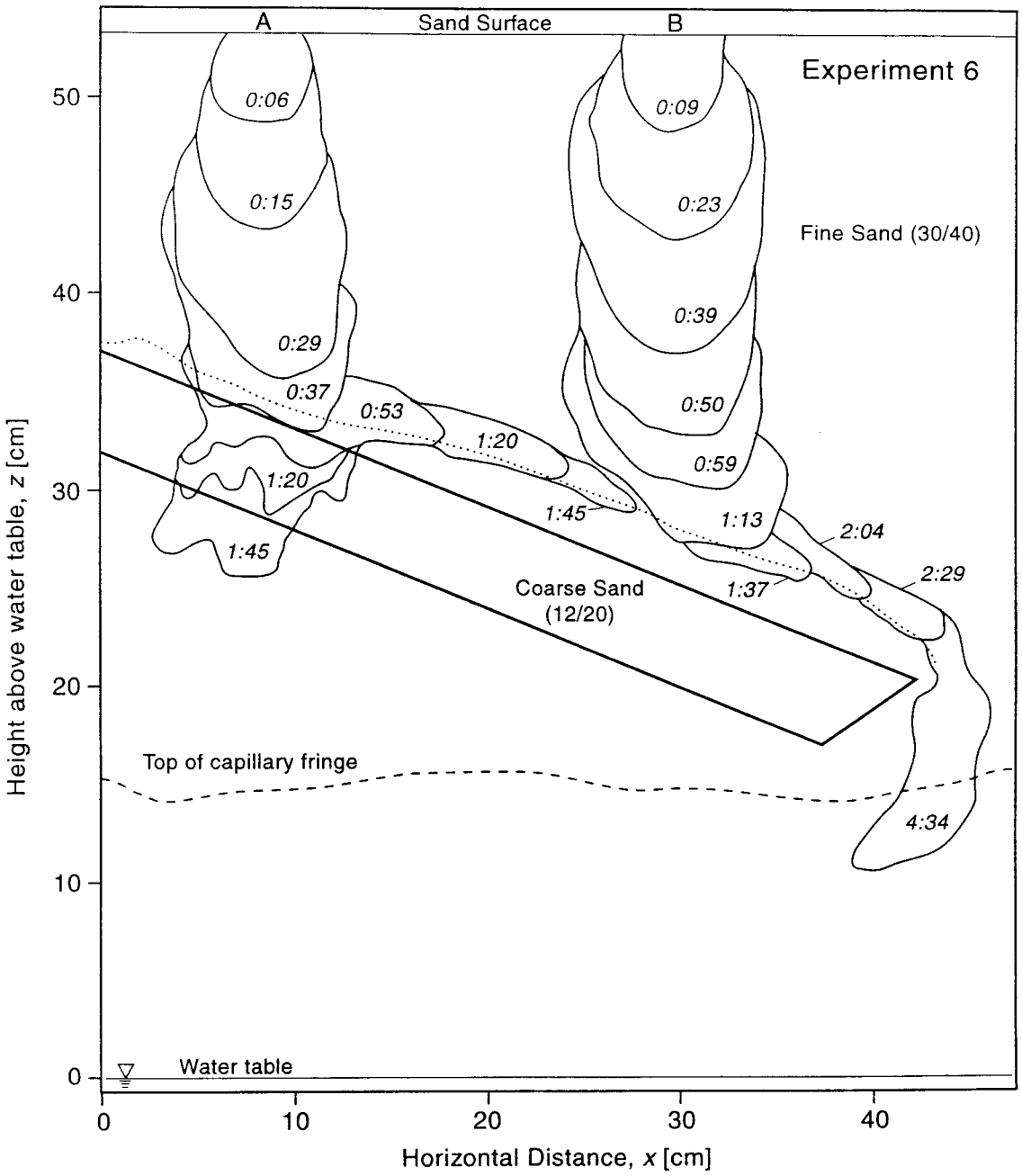

Figure 4.9 Partial LNAPL penetration for moderately high water saturation in fine-grained layer above the textural interface (LNAPL released at location A), and full LNAPL diversion for very high water saturation in fine-grained layer above the textural interface (LNAPL released at location B), under steady-state water flow conditions. Plume boundaries are shown for elapsed times (hours:minutes) since start of LNAPL release. Water was on the primary imbibition *S-P* path prior to the release of LNAPL. The dotted line represents the contour of the zone of higher water saturation above the interface.

4.6 Summary and Conclusions

We investigated the nature of LNAPL movement in the vicinity of a sloping textural interface, a basic form of vadose zone heterogeneity. The interface was generated by a fine-grained sand layer overlying a coarse-grained sand layer. Hydrostatic as well as steady-state water flow conditions were used to generate instances of very low, moderately high and very high water saturation at distinct locations in the fine-grained layer just above the interface.

LNAPL movement strongly depended on the water saturation at these locations. Partial penetration of LNAPL into the coarse-grained layer was observed when the LNAPL plume encountered the textural interface at a moderately high water saturation in the fine-grained layer. For both very low and very high water saturation in the fine-grained layer, LNAPL was fully diverted parallel to the interface. In case of a very low water saturation, the diversion occurred along the interface, whereas in case of a very high water saturation, the diversion occurred in the upper portion of the zone of very high water saturation, which supported the LNAPL.

Flow paths of LNAPL and water were most often divergent in the vicinity of the textural interface. At moderately high water saturation in the fine-grained layer above the interface, a portion of LNAPL penetrated the coarse-grained layer, leading to LNAPL isolation in a zone where no water flow occurred. In contrast, when LNAPL was fully diverted parallel to the interface, supported in the upper portion of a zone of very high water saturation, water breakthrough into the underlying coarse-grained layer occurred. Extensive lateral spreading of LNAPL, away from the point of release, was observed for both very low and very high water saturation in the fine-grained layer above the interface, and is also expected for the portion of LNAPL diverted at moderately high water saturation. The LNAPL flow patterns observed in our experiments should greatly affect LNAPL disposition in a heterogeneous vadose environment, and may explain some of the heterogeneity in LNAPL distribution observed by others (e.g. Osborne and Sykes (1986), Poulsen and Kueper (1992) and Essaid et al. (1993)) at LNAPL contaminated field sites. The observed LNAPL flow patterns may also complicate LNAPL remediation efforts as

well as be important to the design of engineered capillary barrier systems for waste disposal purposes, and should therefore be further investigated.

In our experiments, effects of hysteresis appeared to play a minor role on LNAPL flow patterns in the vicinity of textural interfaces, obvious only for LNAPL flow at very high water saturation in the fine-grained layer above the textural. However, conditions specific to our experiments may have contributed to this effect. There is evidence that including hysteretic effects may greatly improve the agreement between observed and predicted LNAPL saturations at contaminated field sites (Ostendorf et al., 1993), and that neglecting effects of hysteresis and nonwetting fluid entrapment in general may lead to erroneous predictions of subsurface multiphase fluid flow (Lenhard, 1992).

Finally, good agreement was found between experimental observations and predictions of LNAPL movement in the vicinity of textural interfaces, the latter based upon multiphase and capillary barrier flow theory. Constitutive three-phase *K-S-P* relationships appeared to be a critical component in the correct assessment of multiphase flow under the given conditions. We hypothesize that the prediction of LNAPL movement in the vicinity of capillary barriers using numerical simulations may be successful if constitutive *K-S-P* theory is included in the numerical code and applicable boundary conditions are well defined. On the other hand, deterministic prediction of LNAPL disposition in a natural environment with textural interfaces should not be expected. Our results suggest that both the character of bedding of geologic media as well as water and LNAPL flux conditions (which both may be highly variable in space and time) are control to the likely pattern of LNAPL disposition.

4.7 **Acknowledgements**

This work was funded by the U.S. Department of Energy (DOE), under the Subsurface Science Program, under DOE contract # DE-FG06-92ER61523. The authors would like to thank Rose Francis and Aaron Burkhardt for their help in conducting the experiments.

4.8 References

Abdul, A.S., 1988. Migration of petroleum products through sandy hydrogeologic systems, Ground Water Monit. Rev., 8, 73-81.

Cary, J.W., J.F. McBride, and C.S. Simmons, 1989a. Observation of water and oil infiltration into soil: Some simulation challenges, Water Resour. Res., 25, 73-80.

Cary, J.W., C.S. Simmons, and J.F. McBride, 1989b. Predicting oil infiltration and redistribution in unsaturated soils, Soil Sci. Soc. Am. J., 53, 335-342.

Cary, J.W., C.S. Simmons, and J.F. McBride, 1994. Infiltration and redistribution of organic liquids in layered porous media, Soil Sci. Soc. Am. J., 58, 704-711.

Essaid, H.I., W.N. Herkelrath, and K.M. Hess, 1993. Simulation of fluid distributions observed at a crude oil spill site incorporating hysteresis, oil entrapment, and spatial variability of hydraulic properties, Water Resour. Res., 29, 1753-1770.

Kueper, B.H., and E.O. Frind, 1991. Two-phase flow in heterogeneous porous media, 2, Model application, Water Resour. Res., 27, 1059-1070.

Kung, K-J. S., 1990a. Preferential flow in a sandy vadose zone:, 1, Field observation, Geoderma, 46, 51-58.

Kung, K-J. S., 1990b. Preferential flow in a sandy vadose zone:, 2, Mechanism and implications, Geoderma, 46, 59-71.

Lenhard, R.J., 1992. Measurement and modeling of three-phase saturation-pressure hysteresis, J. Contamin. Hydrol., 9, 243-269.

Lenhard, R.J., 1994. Scaling fluid content - pressure relations of different fluid systems in porous media, in Proc. 14th Annual AGU Hydrology Days, ed. H.J. Morel-Seytoux, Hydrology Days Publ., Atherton, CA.

Lenhard, R.J., and J.C. Parker, 1987. A model for hysteretic constitutive relations governing multiphase flow, 2, Permeability-saturation relations, Water Resour. Res., 23, 2197-2206.

Miyazaki, T., 1988. Water flow in unsaturated soil in layered slopes, J. Hydrol., 102, 201-214.

Oldenburg, C.M., and K. Pruess, 1993. On Numerical Modeling of Capillary Barriers, Water Resour. Res., 29, 1045-1056.

Osborne, M., and J. Sykes, 1986. Numerical modeling of immiscible organic transport at the Hyde Park landfill, Water Resour. Res., 22, 25-33.

Ostendorf, D.W., R.J. Richards, and F.P. Beck, 1993. LNAPL retention in sandy soil, Ground Water, 31, 285-292.

Pantazidou, M., and N. Sitar, 1993. Emplacement of nonaqueous liquids in the vadose zone, Water Resour. Res., 29, 705-722.

Parker, J.C., and R.J. Lenhard, 1987. A model for hysteretic constitutive relations governing multiphase flow, 1, Saturation-pressure relations, Water Resour. Res., 23, 2187-2196.

Parker, J.C., R.J. Lenhard, and T. Kuppusamy, 1987. A parametric model for constitutive properties governing multiphase flow in porous media, Water Resour. Res., 23, 618-624.

Poulsen, M.M., and B.H. Kueper, 1992. A field experiment to study the behavior of tetrachloroethylene in unsaturated porous media, Environ. Sci. Technol., 26, 889-895.

Ross, B., 1990. The diversion capacity of capillary barriers, Water Resour. Res., 26, 2625-2629.

Schroth, M.H., J.D. Istok, S.J. Ahearn, and J.S. Selker, 1995. Geometry and position of light nonaqueous-phase liquid lenses in water-wetted porous media, J. Contain. Hydrol., 19, 269-287.

Schroth, M.H., S.J. Ahearn, J.S. Selker, and J.D. Istok, 1996. Characterization of Miller-similar silica sands for laboratory subsurface hydrologic studies, in press, Soil Sci. Soc. Am. J., February 1996.

Steenhuis, T.S., K-J. S. Kung, J.-Y. Parlange, J. S. Selker, and X-X. Chen, 1990. Flow regimes in sandy soils with inclined layers, presented at the Tenth Annual Hydrology Days, AGU, Fort Collins, CO, April 10-12.

Steenhuis, T.S., J.-Y. Parlange, and K.-J. S. Kung, 1991. Comment on "The diversion capacity of capillary barriers" by Benjamin Ross, Water Resour. Res., 27, 2155-2156.

Stormont, J.C., 1995. The effect of constant anisotropy on capillary barrier performance, Water Resour. Res., 31, 783-785.

van Genuchten, M.Th., 1980. A closed-form equation for predicting the hydraulic conductivity of unsaturated soils, Soil Sci. Soc. Am. J., 44, 892-898.

5. SUMMARY

In chapter 2, we presented a comprehensive set of hydrologically relevant parameters for four commercially-available silica sands. The sands featured narrow particle size distributions and were found very amenable to Miller-scaling for both hydrostatic (water retention) and hydrodynamic (saturated hydraulic conductivity) parameters.

Parameterization of water retention data for four Accusand grades was obtained by fitting a general equation (van Genuchten, 1980) to the experimental data. A numerical correction procedure was developed to be used during the fitting of the general equation to compensate for an error in the analysis of experimental water retention data due to a commonly made assumption. Three-phase S-P model parameters (Lenhard, 1992) were obtained for a widely used model NAPL.

Reasonable agreement was found between measured and predicted values of relative hydraulic conductivity using corrected water retention fitting parameters in the van Genuchten-Mualem model (van Genuchten, 1980). Poor agreement between measured and predicted values of relative hydraulic conductivity was observed using uncorrected water retention fitting parameters, demonstrating the importance of the numerical correction procedure when using predictive models to determine relative hydraulic conductivities for the porous media used in this study.

The four Accusand grades appear to be a suitable set of media for a broad range of subsurface flow and transport studies due to their availability in large quantities, high batch to batch consistency, chemical purity, well-defined hydrologic properties as well as their Miller-similarity.

In chapter 3, we investigated the geometry and position of LNAPL lenses emplaced in the capillary fringe above a water table. Full penetration of the capillary fringe was observed in the sense that at equilibrium no area above the capillary fringe remained at NAPL saturations higher than residual saturations. Significant spatial variability of lens shape and vertical thickness within single experiments and between

replicates created difficulties in predicting the exact lens geometry. Heterogeneities of natural systems will further increase the variabilities observed in laboratory experiments.

We demonstrated the importance of considering changes of NAPL-water interfacial tensions as a function of NAPL-water contact time for the prediction of equilibrium vertical lens thicknesses. Neglecting these changes can lead to erroneous predictions.

Utilizing visual experimental observations of complete NAPL penetration into the capillary fringe, we showed that a previously derived equation to compute the maximum vertical lens thickness was implicit, thus rendering its promising predictive accuracy meaningless. When amended to a fully explicit form, less precision in the prediction of vertical lens thicknesses was observed. Nevertheless, the general trend observed in the experiments (larger vertical lens thicknesses with finer porous media) was captured reasonably well.

Finally, simplified underlying assumptions of simple pore geometry (represented by d_n) and the identification of respective governing air-NAPL and NAPL-water interfaces to compute capillary forces could be questioned and may be responsible for some of the predictive inaccuracy observed. From the spatial variability observed in the experiments and the observed sensitivity of the explicit equation to pore geometry and fluid properties it appears likely that predictions of vertical lens thicknesses in more natural settings will be significantly less accurate.

In chapter 4, we investigated the nature of LNAPL movement in the vicinity of a sloping textural interface, a basic form of vadose zone heterogeneity. The interface was generated by a fine-grained sand layer overlying a coarse-grained sand layer. Hydrostatic as well as steady-state water flow conditions were used to generate instances of very low, moderately high and very high water saturation at distinct locations in the fine-grained layer just above the interface.

LNAPL movement strongly depended on the water saturation at these locations. Partial penetration of LNAPL into the coarse-grained layer was observed when the LNAPL plume encountered the textural interface at a moderately high water saturation in the fine-grained layer. For both very low and very high water saturation in the fine-

grained layer, LNAPL was fully diverted parallel to the interface. In case of a very low water saturation, the diversion occurred along the interface, whereas in case of a very high water saturation, the diversion occurred in the upper portion of the zone of very high water saturation, which supported the LNAPL.

Flow paths of LNAPL and water were most often divergent in the vicinity of the textural interface. At moderately high water saturation in the fine-grained layer above the interface, a portion of LNAPL penetrated the coarse-grained layer, leading to LNAPL isolation in a zone where no water flow occurred. In contrast, when LNAPL was fully diverted parallel to the interface, supported in the upper portion of a zone of very high water saturation, water breakthrough into the underlying coarse-grained layer occurred. Extensive lateral spreading of LNAPL, away from the point of release, was observed for both very low and very high water saturation in the fine-grained layer above the interface, and is also expected for the portion of LNAPL diverted at moderately high water saturation. The LNAPL flow patterns observed in our experiments should greatly affect LNAPL disposition in a heterogeneous vadose environment, and may explain some of the heterogeneity in LNAPL distribution observed by others (e.g. Osborne and Sykes [1986], Poulsen and Kueper [1992] and Essaid et al. [1993]) at LNAPL contaminated field sites. They may also complicate LNAPL remediation efforts as well as be important to the design of engineered capillary barrier systems for waste disposal purposes, and should therefore be further investigated.

In our experiments, effects of hysteresis appeared to play a minor role on LNAPL flow patterns in the vicinity of textural interfaces, obvious only for LNAPL flow at very high water saturation in the fine-grained layer above the textural. However, conditions specific to our experiments may have contributed to this effect, and there is evidence [Ostendorf et al., 1993] that including hysteretic effects may greatly improve the agreement between observed and predicted NAPL saturations at contaminated field sites.

Finally, good agreement was found between experimental observations and predictions of LNAPL movement in the vicinity of textural interfaces, the latter based upon multiphase and capillary barrier flow theory. Constitutive three-phase *K-S-P* relationships appeared to be a critical component in the correct assessment of multiphase

flow under the given conditions. We hypothesize that the prediction of LNAPL movement in the vicinity of capillary barriers using numerical simulations may be successful if constitutive *K-S-P* theory is included in the numerical code. On the other hand, deterministic prediction of LNAPL disposition in a natural environment with textural interfaces should not be expected. Our results suggest that both the character of bedding of geologic media as well as water flux conditions (which may be highly variable in space and time) are control to the likely pattern of LNAPL disposition.

BIBLIOGRAPHY

Abdul, A.S., 1988. Migration of Petroleum Products Through Sandy Hydrogeologic Systems. Ground Water Monit. Rev., 8: 73-81.

Adamson, A.W., 1982. Physical Chemistry of Surfaces. Fourth Edition, John Wiley & Sons, Inc., New York.

API, 1986. Recommended practices for testing sand used in gravel packing operations (API RP - 58). 1st ed. American Petroleum Institute, Washington, D.C.

Artiola, J.F. 1990. Determination of carbon, nitrogen, and sulfur in soils, sediments, and wastes: a comparative study. Intern. J. Environ. Anal. Chem., 41: 159-171.

ASTM, 1987. Standard Specification for Wire-Cloth Sieves for Testing Purposes (ASTM E11 - 87). In 1993 Annual book of ASTM standards, Vol. 14.02, American Society of Testing Materials, Philadelphia, PA., 13-16.

ASTM, 1990. Standard Test Method for Particle-Size Analysis of Soils (ASTM D 422 - 63 (Reapproved 1990)). In 1993 Annual book of ASTM standards, Vol. 04.08, American Society of Testing Materials, Philadelphia, PA., 93-99.

ASTM, 1993. Designation: D 971-91, Standard Test Method for Interfacial Tension of Oil Against Water by the Ring Method. American National Standard, Annual Book of ASTM Standards, 05.01: 297-299.

Ayral, A., J. Phalippou, and T. Woignier. 1992. Skeletal density of silica aerogels determined by helium pycnometry. J. Materials Sci., 27: 1166-1170.

Bear, J., 1972. Dynamics of Fluids in Porous Media. Dover, New York, NY.

Brooks, R.H., and A.T. Corey, 1964. Hydraulic properties of porous media. Hydrology paper No. 3, Colorado State University, Fort Collins, CO. 27 pp.

Cary, J.W., J.F. McBride, and C.S. Simmons, 1989a. Observation of water and oil infiltration into soil: Some simulation challenges, Water Resour. Res., 25, 73-80.

Cary, J.W., C.S. Simmons and J.F. McBride, 1989b. Predicting Oil Infiltration and Redistribution in Unsaturated Soils. Soil Sci. Soc. Am. J., 53: 335-342.

Cary , J.W., C.S. Simmons, and J.F. McBride, 1994. Infiltration and redistribution of organic liquids in layered porous media. Soil Sci. Soc. Am. J., 58: 704-711.

Eckberg, D.K, and D.K. Sunada, 1984. Nonsteady Three-Phase Immiscible Fluid Distribution in Porous Media. Water Resour. Res., 20: 1891-1897.

Essaid, H.I., W.N. Herkelrath, and K.M. Hess, 1993. Simulation of Fluid Distributions Observed at a Crude Oil Spill Site Incorporating Hysteresis, Oil Entrapment, and Spatial Variability of Hydraulic Properties. Water Resour. Res., 29: 1753-1770.

Farr, A.M., R.J. Houghtalen, and D.B. McWhorter, 1990. Volume Estimation of Light Nonaqueous Phase Liquids in Porous Media. Ground Water, 28: 48-56.

Gardner, W.R., 1958. Some steady-state solutions of the unsaturated moisture flow equation with application to evaporation from a water table. Soil Sci., 85: 244-249.

Kalaydjian, F., and M. Tixier, 1991. Effect Of The Spreading Coefficient On Gas/Oil Capillary Pressure Curves In Presence Of Connate Water. SCA Conference Paper Number 9106, presented at the 5th SCA (Soc. Core Anal.) Annual Technical Conference, San Antonio, TX, Aug. 20-22, 1991.

Klute, A., 1986. Water retention: laboratory methods. In: A. Klute (ed.), Methods of Soil Analysis: Part 1. Physical and Mineralogical Methods. ASA (Am. Soc. Agron.), Madison, WI, ASA monogr. No. 9, 2nd ed., 635-662.

Klute, A. and C. Dirksen, 1986. Hydraulic conductivity and diffusivity: laboratory methods. In: A. Klute (ed.), Methods of Soil Analysis: Part 1. Physical and Mineralogical Methods. ASA (Am. Soc. Agron.), Madison, WI, ASA monogr. No. 9, 2nd ed., 687-734.

Kool, J.B., and J.C. Parker, 1987. Development and evaluation of closed-form expressions for hysteretic soil hydraulic properties. Water Resour. Res., 23: 105-114.

Kueper, B.H., and E.O. Frind, 1991. Two-phase flow in heterogeneous porous media, 2, Model application, Water Resour. Res., 27, 1059-1070.

Kung, K-J. S., 1990a. Preferential flow in a sandy vadose zone:, 1, Field observation, Geoderma, 46, 51-58.

Kung, K-J. S., 1990b. Preferential flow in a sandy vadose zone:, 2, Mechanism and implications, Geoderma, 46, 59-71.

Lenhard, R.J., 1992. Measurement and modeling of three-phase saturation-pressure hysteresis. Journal of Contam. Hydrol., 9: 243-269.

Lenhard, R.J., 1994. Scaling fluid content - pressure relations of different fluid systems in porous media, in Proc. 14th Annual AGU Hydrology Days, ed. H.J. Morel-Seytoux, Hydrology Days Publ., Atherton, CA.

Lenhard, R.J., and J.C. Parker, 1987. A Model for Hysteretic Constitutive Relations Governing Multiphase Flow 2. Permeability-Saturation Relations. Water Resour. Res., 23: 2197-2206.

Lenhard, R.J., and J.C. Parker. 1988. Experimental validation of the theory of extending two-phase saturation-pressure relations to three-fluid phase systems for monotonic drainage paths. Water Resour. Res., 24: 373-380.

Lenhard, R.J., and J.C. Parker, 1990. Estimation of Free Hydrocarbon Volume from Fluid Levels in Monitoring Wells. Ground Water, 28: 57-67.

Miller, E.E., and R.D. Miller, 1956. Physical theory for capillary flow phenomena. J. Appl. Phys., 27: 324-332.

Miyazaki, T., 1988. Water flow in unsaturated soil in layered slopes, J. Hydrol., 102, 201-214.

Ng, K.M., H.T. Davis, and L.E. Scriven, 1978. Visualization Of Blob Mechanics In Flow Through Porous Media. Chem. Eng. Sci., 33: 1009-1017.

Oldenburg, C.M., and K. Pruess, 1993. On Numerical Modeling of Capillary Barriers, Water Resour. Res., 29, 1045-1056.

Osborne, M., and J. Sykes, 1986. Numerical modeling of immiscible organic transport at the Hyde Park landfill, Water Resour. Res., 22, 25-33.

Ostendorf, D.W., R.J. Richards, and F.P. Beck, 1993. LNAPL Retention in Sandy Soils. Ground Water, 31: 285-292.

Page, A.L., R.H. Miller, and D.R. Keeney. 1982. Methods of Soil Analysis: Part 2. Chemical and Microbiological Properties. ASA (Am. Soc. Agron.), Madison, WI, ASA monogr. No. 9, 2nd ed., 1159p.

Pantazidou, M., and N. Sitar, 1993. Emplacement of Nonaqueous Liquids in the Vadose Zone. Water Resour. Res., 29: 705-722.

Parker, J.C., and R.J. Lenhard, 1987. A model for hysteretic constitutive relations governing multiphase flow, 1. Saturation-pressure relations. Water Resour. Res., 23: 2187-2196.

Parker, J.C, R.J. Lenhard, and T. Kuppusamy, 1987. A parametric model for constitutive properties governing multiphase flow in porous media, Water Resour. Res., 23, 618-624.

Poulsen, M.M., and B.H. Kueper, 1992. A field experiment to study the behavior of tetrachloroethylene in unsaturated porous media, Environ. Sci. Technol., 26, 889-895.

Ross, B., 1990. The diversion capacity of capillary barriers, Water Resour. Res., 26, 2625-2629.

Schroth, M.H., J.D. Istok, S.J. Ahearn, and J.S. Selker, 1995. Geometry and position of light nonaqueous-phase liquid lenses in water-wetted porous media, J. Contain. Hydrol., 19, 269-287.

Schroth, M.H., S.J. Ahearn, J.S. Selker, and J.D. Istok, 1996. Characterization of Miller-similar silica sands for laboratory subsurface hydrologic studies, in press, Soil Sci. Soc. Am. J., February 1996.

Steenhuis, T.S., K-J. S. Kung, J.-Y. Parlange, J. S. Selker, and X-X. Chen, 1990. Flow regimes in sandy soils with inclined layers, presented at the Tenth Annual Hydrology Days, AGU, Fort Collins, CO, April 10-12.

Steenhuis, T.S., J.-Y. Parlange, and K.-J. S. Kung, 1991. Comment on "The diversion capacity of capillary barriers" by Benjamin Ross, Water Resour. Res., 27, 2155-2156.

Stormont, J.C., 1995. The effect of constant anisotropy on capillary barrier performance, Water Resour. Res., 31, 783-785.

U.S. Coast Guard, 1984. Chemical Hazard Response Information System, (CHRIS), Vol. 2, Hazardous Chemical Data, U.S. Department of Transportation, Washington, D.C.

U.S. EPA. 1986. Method EPA 6010 in: Methods of Analysis of Hazardous Solid Wastes. SW-846. Third Ed. U.S. Environmental Protection Agency, Office of Solid Waste. Washington, DC, 20460.

van Genuchten, M. Th., 1980. A closed-form equation for predicting the hydraulic conductivity of unsaturated soils. Soil Sci. Soc. Am. J., 44: 892-898.